Design, Synthesis and Biological Evaluation of Novel Adamantane Derivatives as Potential Treatments for Alzheimer's Disease

by

Arash Shakeri

A thesis

presented to University of Waterloo

in fulfillment of the

thesis requirement for the degree of

Master of Science

in

Pharmacy

Waterloo, Ontario, Canada, 2017

Author’s Declaration

I hereby declare that I am the sole author of this thesis. This is the true copy of the thesis, including any required final revisions, as accepted by my examiners.

I understand that my thesis may be made electronically available to the public.

Abstract

Alzheimer's disease (AD) is a complex, multifactorial, and rapidly neurodegenerative disorder characterized by cognitive impairment and progressive dementia. Its pathology was first characterized by Alois Alzheimer as "a peculiar disease of cerebral cortex" in 1907. Amyloid beta, tau and cholinergic hypotheses are at the forefront of AD research. The currently available treatments that follow the traditional approach of "one target, one drug" are insufficient to treat AD and with the growing number of patients and an aging population developing novel derivatives as potential treatment for AD is critical. We believe that aminoadamantane derivatives can be used as suitable scaffold for developing treatments that can inhibit the aggregation of Aβ due to their favorable lipophilicity, safety profile and ease of chemical modifications. The goal of this project was to develop a library of novel aminoadamantane derivatives with suitable pharmacophores that exhibit Aβ aggregation inhibition properties. A total of 48 derivatives were synthesized and biologically evaluated in vitro for their potential Aβ anti-aggregation activity and structure-activity relationship (SAR) data was analyzed. The molecular docking studies of the lead candidates were investigated to gain insight into their mode of action. The most potent Aβ40 inhibitor was **2n** (4-amino-*N*-(3,5-dimethyladamantan-1-yl)benzamide; (Aβ40 IC_{50} = 0.4 μM)), closely followed by **2l** (*N*-(4-bromobenzyl)-3,5-dimethyladamantan-1-amine; (Aβ40 IC_{50} = 1.8 μM)) and **3m** (*N*-(1-(adamantan-1-yl)ethyl)-3-aminobenzamide; (Aβ40 IC_{50} = 1.8 μM)). In conclusion, this project provides a new class of novel aminoadamantane derivatives as potential treatments for AD.

Acknowledgements

I would like to express my gratitude to School of Pharmacy at the university of waterloo for supporting this project and also to the graduate studies office for funding the conference expenses.

I would also like to acknowledge Tarek Mohammed for his guidance and support during this project and mentoring me along the way. I would like to extend my acknowledgement to my committee members, Dr. Michael Beazely and Dr. Hyock Ju Kwon for their advice and support over the past two years.

Dedication

I would like to dedicate the work presented here to my parents, Saeed Shakeri and Maryam Yazdani and my brother Aria Shakeri for their unconditional support throughout my master's degree. I would also like to thanks all my friends and colleagues who assisted me on this wonderful journey. Lastly, I would like to express my gratitude to my supervisor, Dr. Praveen N. Rao, for not only giving me the opportunity to work on this project but also for his knowledge, support, understanding and motivation throughout my project.

Table of Contents

List of Figures

Chapter 1

List of Figures – cont'd

List of Figures – cont'd

List of Figures – cont'd

List of Figures – cont'd

List of Figures – cont'd

List of Tables

List of schemes

Chapter 6

List of Abbreviations

Aβ = Amyloid beta

ACh = Acetylcholine

AChE = Acetylcholinesterase

ACN = Acetonitrile

AICD = APP intracellular domain

AD = Alzheimer's Disease

ADAM = A disintegrin and metalloprotease

ALS = Amyotrophic lateral sclerosis

AMPA = α-Amino-3-hydroxy-5-methyl-4- isoxazolepropionic acid

APOE4 = Apolipoprotein e4

APP = Amyloid precursor protein

ATP = Adenosine triphosphate

β = Beta

BACE = Beta-site APP cleaving enzyme

BBB = Blood-brain barrier

BuChE = Butyrylcholinesterase

n-BuOH = Butanol

CDK-5 = Cyclin-dependent kinase 5

ClogP = Partition coefficient

CNS = Central nervous system

CTF = C-terminal fragment

DCM = Dichloromethane

DME = Disease-modifying effect

DMSO = Dimethylsulfoxide

ECE = Endothelin-converting enzyme

EOAD = Early onset Alzheimer's disease

EtOAc = Ethyl acetate

List of Abbreviations – cont'd

EtOH = Ethanol

FAD = Familial Alzheimer's disease

γ = Gamma

GSK-3 = Glycogen synthase kinase 3

HD = Huntington's disease

HPLC = High-performance liquid chromatography

HRMS = High-resolution mass spectrometry

IC_{50} = Concentration required for 50% inhibition

IDE = Insulin-degrading enzyme

ISF = Interstitial fluid

kDa= KiloDalton

LCMS = Liquid-chromatography mass spectrometry

LRP = Low-density lipoprotein

LTP = Long-term potentiation

MAPK = Mitogen-activated protein kinase

MCI = Mild cognitive impairment

MeOH = Methanol

$MgSO_4$ = Magnesium sulfate

MPTP = Mitochondrial permeability transition pore

µM = Micromolar

NFT = Neurofibrillary tangle

nM = Nanomolar

NMDA = N-methyl-D-aspartate

NSC = Neuronal stem cell

PD = Parkinson's disease

PHF = Paired helical filament

PSEN 1 = Presenilin 1

List of Abbreviations – cont'd

PSEN 2 = Presenilin 2

pM = Picomolar

RAGEs = Receptor for advanced glycation end products

RFUs = Relative fluorescence units

ROS = Reactive oxygen species

r.t = Room temperature

sAPPα = Soluble APP fragment α

sAPPβ = Soluble APP fragment β

SGCC = Silica gel column chromatography

τ = Tau

TEA = Triethylamine

TEM = Transmission electron microscopy

ThT = Thioflavin T

TLC = Thin-layer chromatography

Chapter 1: Introduction

1.1 Alzheimer's Disease

"I have lost myself" replied Auguste Deter to Dr. Alois Alzheimer when she was asked to write her name.[1] November 3rd 1906, more than a century ago, marks the discovery of Alzheimer's disease (AD). AD is a multifactorial neurodegenerative disorder with a complex pathophysiology, rapidly growing number of patients, and substantial socioeconomic burden on healthcare systems across the world.[2,3,4] In Canada, estimated 747,000 patients exhibited various degrees of dementia with 550,000 , almost 70% of cases, being attributed to AD. With a combined direct medical and indirect costs of 24 billion dollars in Canada and 236 billion dollars in the US in 2015, it's no surprise that AD is the most costly disease in North America. According to Alzheimer's association, by 2050 the cost of treating AD patients will rise to a staggering 1 trillion dollars in North America due to an aging population and increase life span of individuals.[5,6,7] AD pathophysiology mainly affects elderly population; however, genome-wide associated studies have identified APP, PSEN1, PSEN2 and APOE4 genes as genetic risk factors associated with early-onset of AD (EOAD).[8]

The neuropathology of AD is mainly characterized by the abnormal deposits of extracellular amyloid beta (Aβ) and intraneuronal hyperphosphorylated tau (τ) proteins. Although substantial effort was focused on these two proteins, various hypotheses have been put forward to describe the complex pathophysiology of AD. Among those, cholinergic, Aβ, tau and oxidative stress hypotheses were on the center of AD research focus (Figure 1.1).[9,10] However over the past decade a number of new mechanisms have emerged expanding the complexity of AD such as neuroinflammation, diabetes, N-methyl-D-aspartate (NMDA) excitotoxicity and receptor for advanced glycation end products (RAGEs).[11,12]

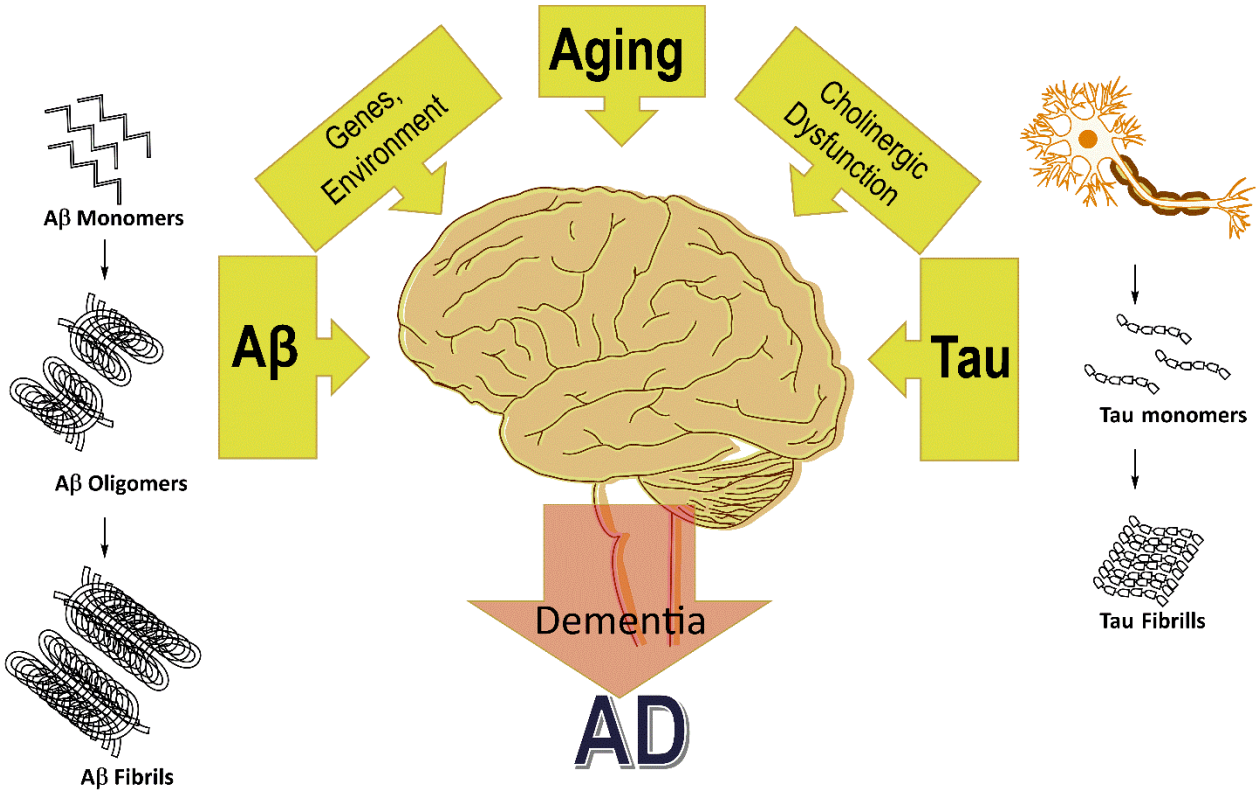

Figure 1.1: Schematic outline of AD pathophysiology with respect to major hypotheses: Aβ, tau and cholinergic dysfunction.

Currently available pharmacotherapy options for AD is only limited to three cholinesterase inhibitors, donepezil, galantamine and rivastigmine and one NMDA antagonist; memantine (Figure 1.2).[13] The aforementioned pharmacotherapies only provide modest symptomatic relief for a short period of time with no disease-modifying effect (DME) except for galantamine.[14] Alarmingly, it's been more than two decades since any potential treatments have passed the clinical trials and approved in the AD pharmacotherapy.[15]

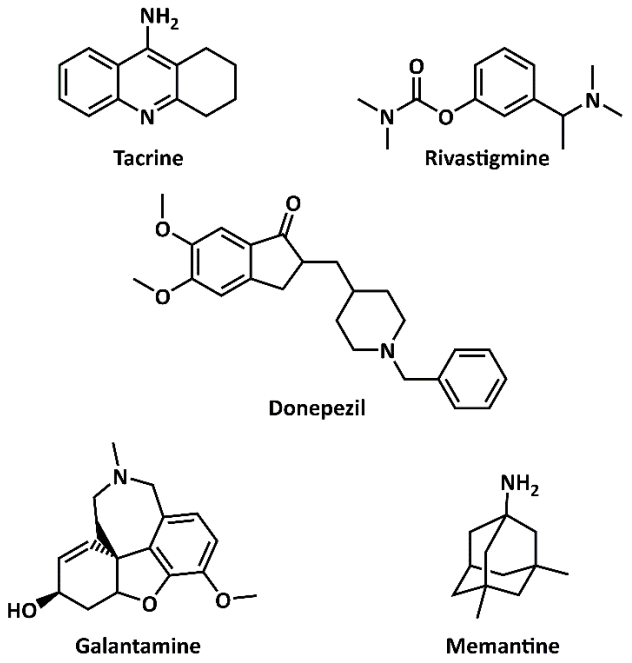

Figure 1.2: Currently approved treatments for AD.

This shortcoming is due to an age-old approach in pharmaceutical industry of "one-target, one-drug, one-disease", which begs the question of will this approach eventually lead to the development of a cure for AD? The short answer is NO! With such an intricate disorder and many layers of complexity, growing list of genetics and environmental risk factors and lack of early detection, developing multitargeting treatments seems to be the only logical approach in tackling AD as evident in the recent focus of scientific community on developing such treatments.[16]

1.2 Amyloid hypothesis

Aβ peptide was first identified in 1984 as the major component of Aβ plaques by Glenner and Wong who demonstrated that it's a 4.2-kDa peptide primarily 40 to 42 amino acids in length.[17,18] Its role in pathophysiology of AD eluded the scientists until 1992, when Hardy and Higgins postulated that the aggregation of Aβ peptide into Aβ plaques is the causative agent in AD.[19,20]

Although more than two decades of research have added more layers of complexity to the pathophysiology of the disease, the main body of the hypothesis is still accepted within the scientific community. It is noteworthy that the formation of Aβ plaques have been linked to many medical complications such as Parkinson's disease (PD), type 2 diabetes and a number of cancers.[21,22] AD is not an all or nothing phenomena, its pathophysiology takes years, in some cases decades to develop. Interestingly, up to 40% of elderly individuals show significant load of Aβ without any signs of cognitive impairment. This observation is in direct conflict with Aβ hypothesis and to address this conundrum it is essential to examine various stages of AD as summarized in Figure 1.3.

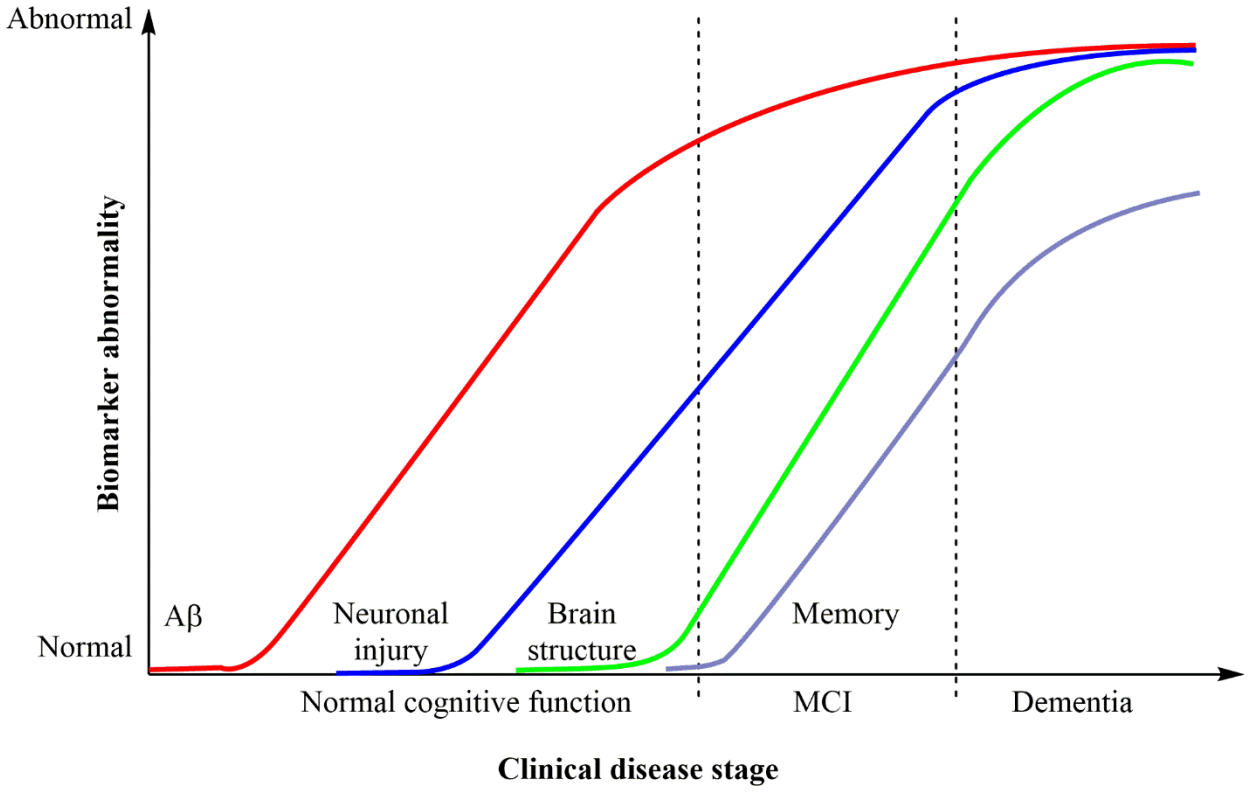

Figure 1.3: Various clinical stages of AD and its progression. Mild cognitive impairment (MCI).

As Figure 1.3 indicates, the Aβ pathology starts while the patients experience a long asymptomatic phase with normal cognitive functions while AD pathology is well underway and a

symptomatic phase where patients exhibit rapid decline in global cognitive functions, changes in personality, mode, behavior, motor apraxia and eventual death.[23,24,25] The pathology of Aβ by itself is incapable to lead to the development of AD by patients, it's rather than the conjunction of Aβ and tauopathy that leads to the diagnosis of AD.

1.3 Amyloid Precursor Protein (APP)

Aβ originates from Amyloid Precursor Protein, a family of type 1 transmembrane proteins that is mainly expressed in synapses of neurons. The primary function of APP is not fully understood however, various studies have linked APP with cell health and growth, signaling, metal homeostasis, neuronal plasticity and synapse formation.[26,27] The APP gene is located on the long arm of chromosome 21 containing 18 exons and spanning approximately 240 kb. Through alternative splicing eight isoforms are generated ranging from 365 to 770 amino acids in length, three of which, 695, 751 and 770 isoforms are more ubiquitously expressed. The biological incorporation of APP in the synapse and neuronal cellular membrane consists of a large N-terminal extracellular domain, ~600 amino acids, and a short hydrophobic C-terminal intracellular domain (Figure 1.4).[28,29] A number of point mutations and duplications of APP have been identified to impact the metabolic pathway of APP and lead to familial Alzheimer's disease (FAD), 5-10% of AD cases, which co-segregate with autosomal dominant inheritance of APP, presenilin 1 (PSEN 1) and presenilin 2 (PSEN2). These mutations lead to over production of Aβ peptides promoting the development of AD.[8,30,31]

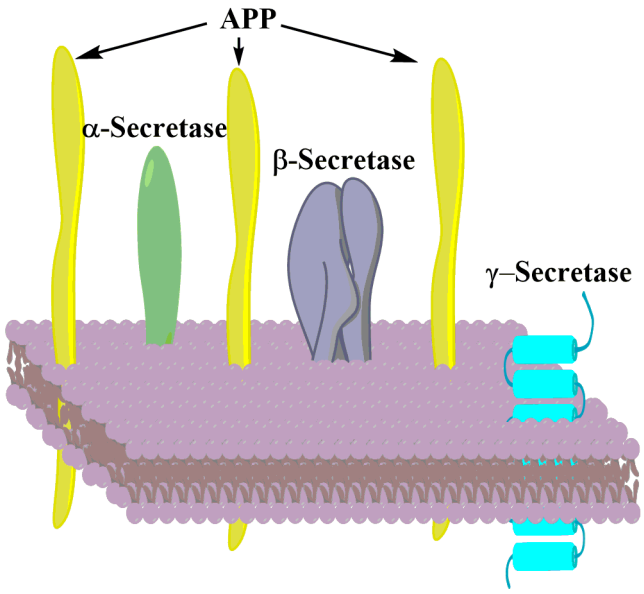

Figure 1.4: Schematic representation of APP and three secretases.

1.4 APP metabolism and processing

APP metabolic routes lead to two pathways, non-amyloidogenic pathway which refers to the formation of Aβ peptides incapable of aggregating and amyloidogenic pathway.[29,32,33] APP is processed via alpha (α), beta (β) and gamma (γ) secretases where the sequential cleavage by α- and γ-secretases lead to non-amyloidogenic route, however the sequential cleavage by β- and γ-secretases give rise to amyloidogenic route (Figures 1.5 and 1.7).

The non-amyloidogenic pathway is mediated by α-secretase within the extracellular domain very close to the cell membrane, cleaving APP between lysine-16 and leucine-17 (based on the Aβ peptide numbering) results in the shedding of a large soluble APP fragment, α-APPs and a membrane-tethered intracellular C-terminal fragment, CTF-83.[34,35] It is noteworthy, that there is no single α-secretase, rather a large family of proteolytic proteins referred to as ADAM (a disintegrin

and metalloprotease), with ADAM 9, ADAM 10 and ADAM 17 are of greater importance in AD pathology.[36,37]

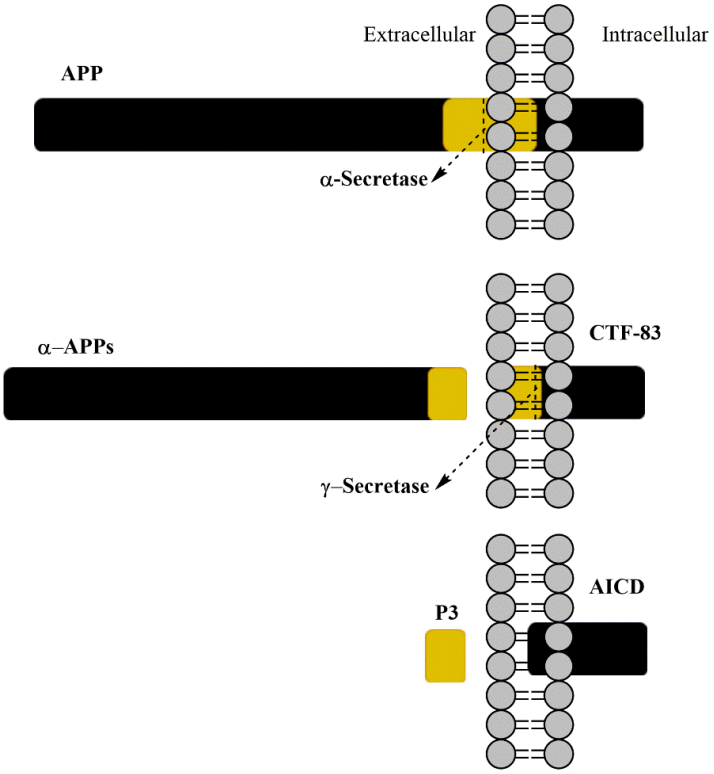

Figure 1.5: Schematic of APP processing via non-amyloidogenic pathway.

The CTF-83 is further processed by γ-secretase producing an amyloid intracellular domain (AICD) fragment and a 3-kDa peptide referred to as p3 or Aβ 17-40/42, although the exact biological impacts of these fragments remains enigmatic, recent studies suggest Aβ 17-40/42 can also deposit in brains of AD and Down Syndrome patients.[38]

The biological functions of α-APPs is extensively researched and well understood and broadly speaking, α-APPs exhibits neurotrophic and neuroprotective effects.[39,40] α-APPs is present early in brain development and stimulates the neural-progenitor proliferation and has potent neuroprotective effect against glutamate neurotoxicity. It can also modulate the APP processing by

directly interacting with β-secretase and disrupts the interaction between β-secretase and APP, lowering the production of Aβ peptides. The neuroprotective effects of APP has been observed *in vitro* studies and attributed to the C-terminal segment of the fragment, residues 591-612, which is absent in β-APPs.[41,42]

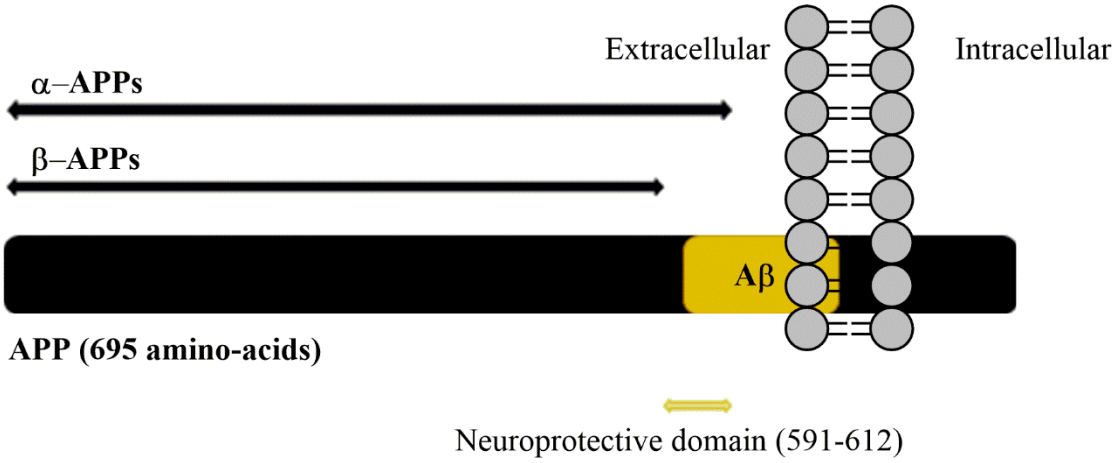

Figure 1.6: Schematic representation of various domains of APPs.

In the amyloidogenic pathway APP is first processed by β-secretase, also known as β-site APP cleaving enzyme 1 (BACE1), generating a membrane-tethered intracellular C-terminal APP fragment (CTF-99) and a large soluble N-terminal fragment β-APPs. It is worth mentioning that developing inhibitors of β-secretase is considered a desirable therapeutic option for AD.[43] The β-APPs fragment is not subjected to further processing and shares the same amino acid sequence as α-APPs apart from the last 16 C-terminal amino acids, known for its neuroprotective properties. Although β-APPs exhibits some degrees of neuroprotective effects, it's up to 100-fold less potent than α-APPs for hippocampal neuronal excitotoxicity, glucose deprivation and Aβ-induced toxicity.[44,45]

The CTF-99 contains Aβ fragment and similarly like CTF-83 is processed by γ-secretase and cleaves between Valine 711 and Isoleucine 712 or Alanine 713 and Tryptophan 714 releasing a full length 4.2 kDa Aβ40 and 42 respectively alongside with AICD fragment.[46,47] It is noteworthy that both amyloidogenic and non-amyloidogenic pathways are part of normal physiology in brain although the non-amyloidogenic pathway is more dominant and there are mechanisms in place in healthy brain to handle the various fragments mentioned before.[48] In AD patients the delicate balance between these two pathways is disrupted resulting in a shift towards amyloidogenic pathway, leading to the higher rate of production of Aβ40 and 42.

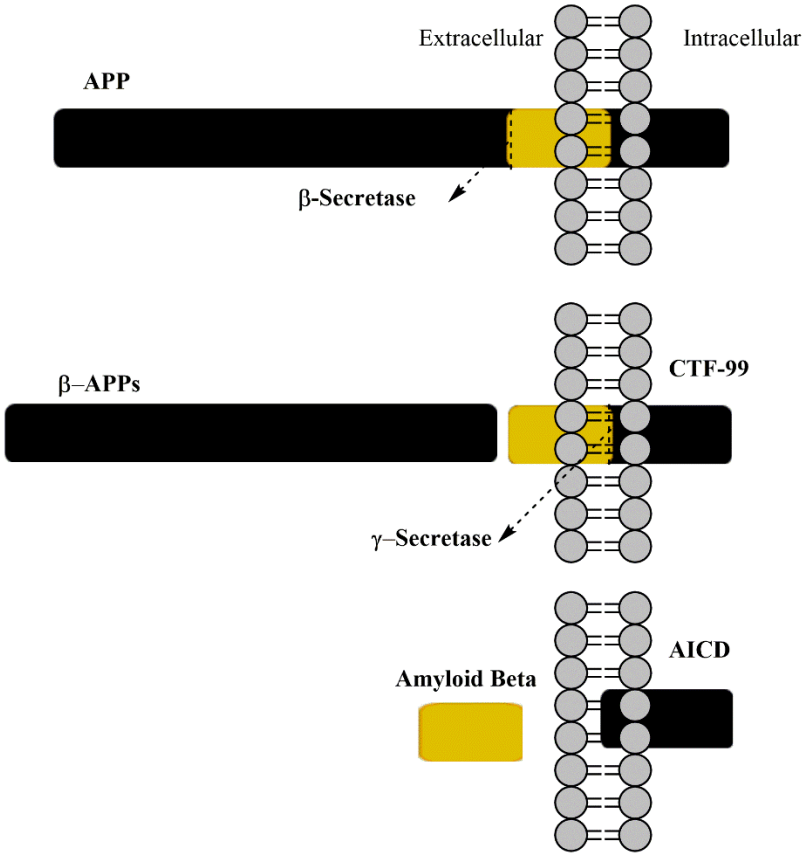

Figure 1.7: Schematic of APP processing via amyloidogenic pathway.

1.5 Aβ Structure, Function, Aggregation and Clearance

Although Aβ40 and 42 are the most common forms of this peptide, Aβ peptides vary in length from 36 to 43 amino acids as APP processed by γ-secretase. Aβ40 and Aβ42 peptides are among the most common variations of the peptide with Aβ40 being the most common product of APP cleavage by γ-secretase and Aβ42 being the more toxic form and more susceptible to aggregate into plaques due to its greater hydrophobicity (Figure 1.8).[49,50]

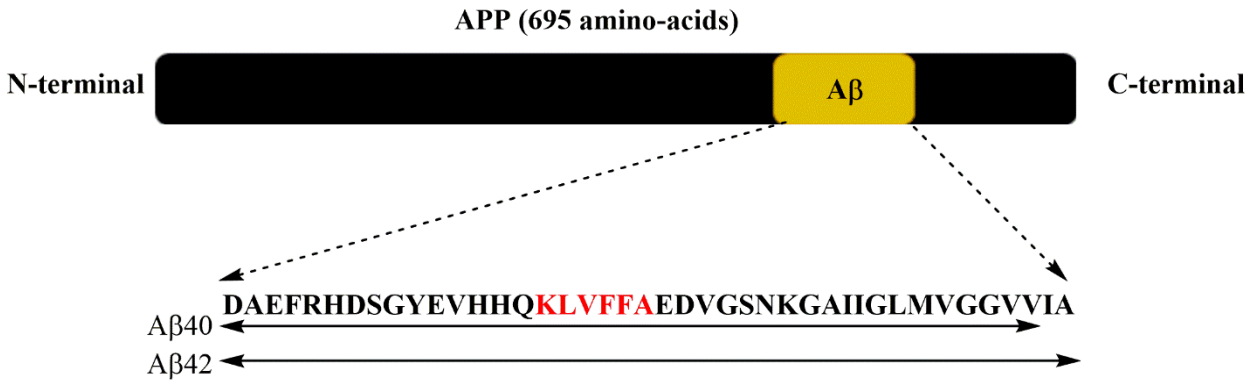

Figure 1.8: Aβ peptide sequence.

Native Aβ peptides at monomeric state are nontoxic and presumably unfolded with unordered structures (Figure 1.9).[51] The main driving forces in the aggregation of Aβ peptides into higher ordered assemblies such as dimers, trimers, oligomers and fibrils are only partially understood, however concentration of the peptide, temperature and the pH can drastically impact the rate of aggregation process of Aβ as presented in Figure 1.9.[52,53] The transition from unordered structures into misfolded peptides enriched in β-sheets initiate the aggregation process. This transition step is mainly associated with the exposure of hydrophobic segment of Aβ, the KLVFFA domain (amino acid residues of 16 to 21), however acetylcholinesterase (AChE) and certain metal ions can also facilitate the misfolding and aggregation process.[54] The misfolded monomers aggregate to each other via hydrophobic interactions and hydrogen bonding in order to form higher

order structures ranging from dimers to heptamers, eventually grow into soluble oligomers. Protofibrils are assembled from oligomers and through elongation mechanism form mature Aβ fibrils. In the elongation phase, Aβ monomers interact with the N-terminal of Aβ protofibrils via hydrogen bonding, resulting in the formation of the bent β-hairpin structure which eventually associates into Aβ fibrils.[55,56] Interestingly, the severity of the disease and synaptic loss correlates more closely with the Aβ oligomers load rather than with the Aβ fibrils (Figures 1.9 and 1.10).

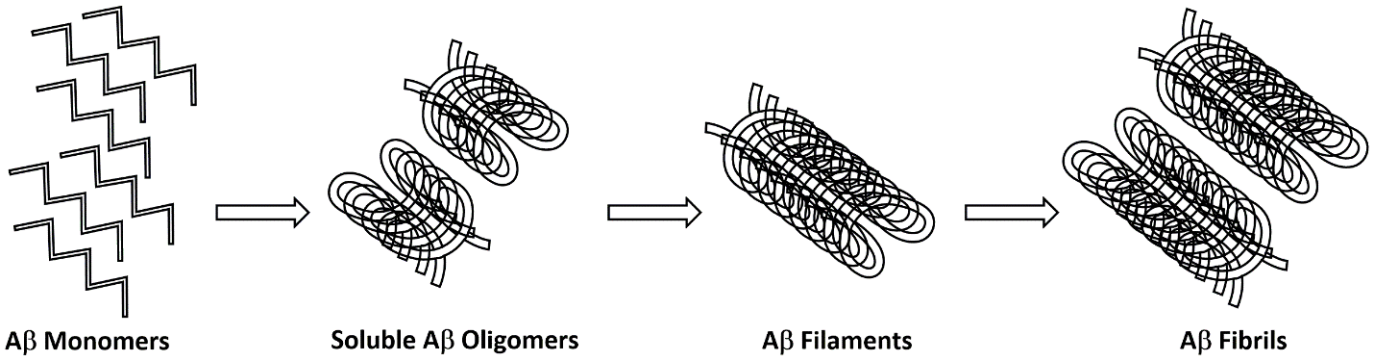

Figure 1.9: Illustration of self-induced Aβ Aggregation pathway.

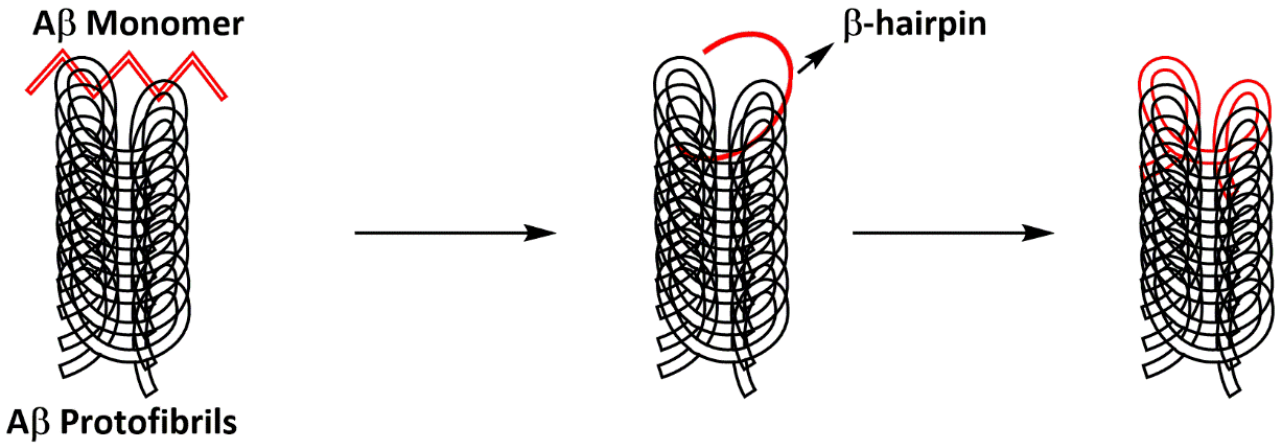

Figure 1.10: Schematic representation of elongation phase and the interaction of Aβ monomer with Aβ aggregates.

Although the aggregation of Aβ pose a variety of issues in brain, there are a number of mechanisms in place to deal with the post production of Aβ. Receptor-mediated transport of Aβ across BBB and enzymatic degradation are the first line of defense in body to maintain the Aβ level at its physiological concentration.[57,58] However, recent studies point to the presence of endogenous autoantibodies against Aβ in AD patients and healthy individuals at very low concentration. The interstitial fluid (ISF) bulk flow is responsible for the removal of soluble Aβ across BBB into the bloodstream while receptor-mediated clearance is the primary route of Aβ transport across BBB, bulk flow transport accounts for up to 15% removal of Aβ.[59]

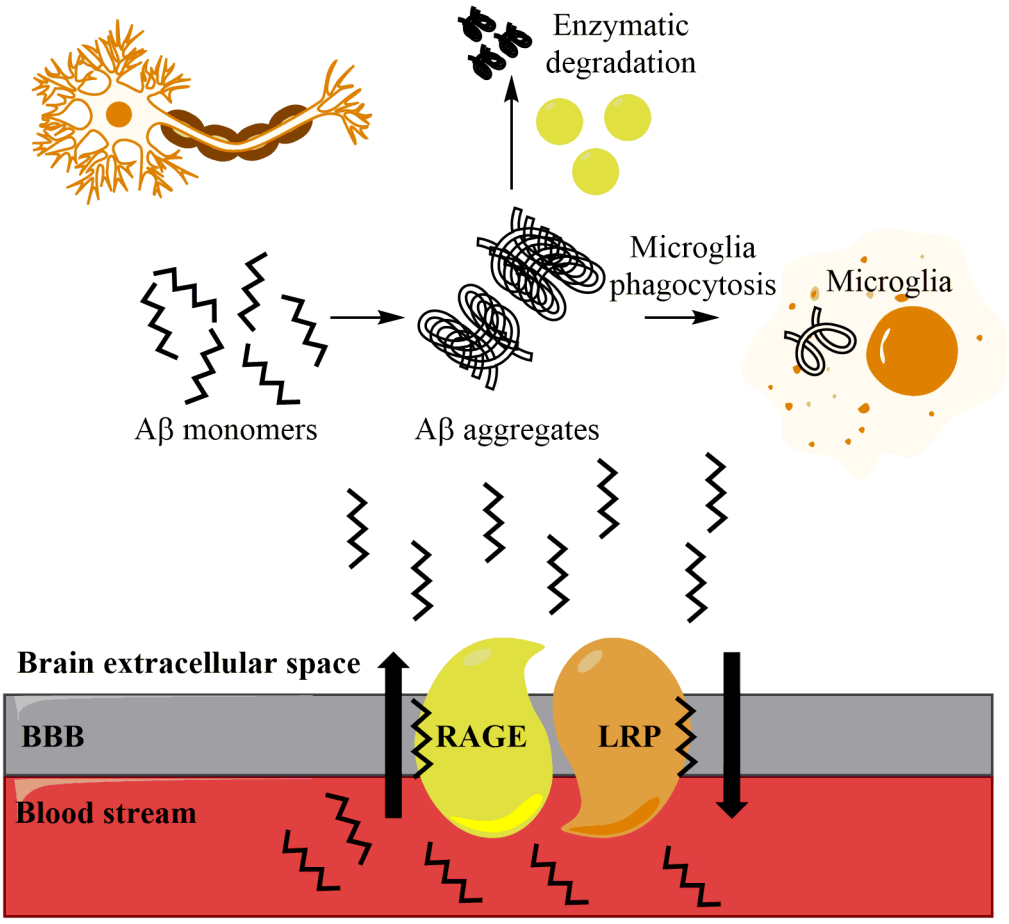

Figure 1.11: Schematic representation of Aβ removal/degradation in body. LRP and RAGE are implicated influx of Aβ across BBB while the major degradation of Aβ is fostered by NEP, IDE and ECE.

Low-density lipoprotein (LRP) and RAGE are the primary receptors involved in the flux of Aβ and a number of other proteins across BBB.[60,61] While LRP mediates Aβ efflux from brain interestingly, RAGE has been implicated in influx of Aβ into the CNS. The expression of LRP is suppressed in Aβ rich environment while RAGE expression is unregulated in such an environment completing a positive-feedback cycle, eventually diminishing the Aβ clearance via mentioned receptors. It is noteworthy that Aβ clearance in brain diminishes with age regardless of the health status of individuals. Aβ degradation via enzymes is mediated by a few zinc-bound peptidases, neprilysin (NEP), insulin-degrading enzyme (IDE) and endothelin-converting enzyme (ECE) (Figure 1.11).[62,63,64]

1.6 Aβ Pathology and physiology

The tissue degeneration in AD is associated with the formation of Aβ fibrils 7-10 nm in diameter, the Aβ toxicity is mediated via several mechanisms including, oxidative stress, mitochondrial dysfunction, inflammation, synaptic dysfunction, excitotoxicity and alteration in membrane permeability are among such mechanisms.[21,65]

The neurodegenerative effects of oxidative stress as a major contributor to neuronal loss is not limited to AD and is observed in a number of other diseases such as Parkinson's disease (PD), Huntington's disease (HD) and amyotrophic lateral sclerosis (ALS).[66,67] Oxidative stress is caused by the imbalance in the production and elimination of reactive oxygen species (ROS), a group of

oxygen-containing free radicals such as hydrogen peroxide (H_2O_2) and superoxide (O_2^-). ROS is mainly generated by mitochondria, organelle responsible for providing the energy for cells in the form of adenosine triphosphate (ATP) during oxidative phosphorylation.[68] ROS also links amyloid hypothesis to mitochondrial dysfunction, where the overproduction of Aβ decreases the activity of electron transport chain enzymes by causing deficiency in both complex 1 (NADH dehydrogenase) and complex 4 (cytochrome c oxidase) leading to ROS overproduction and ATP depletion (Figure 1.12).[67,69,70]

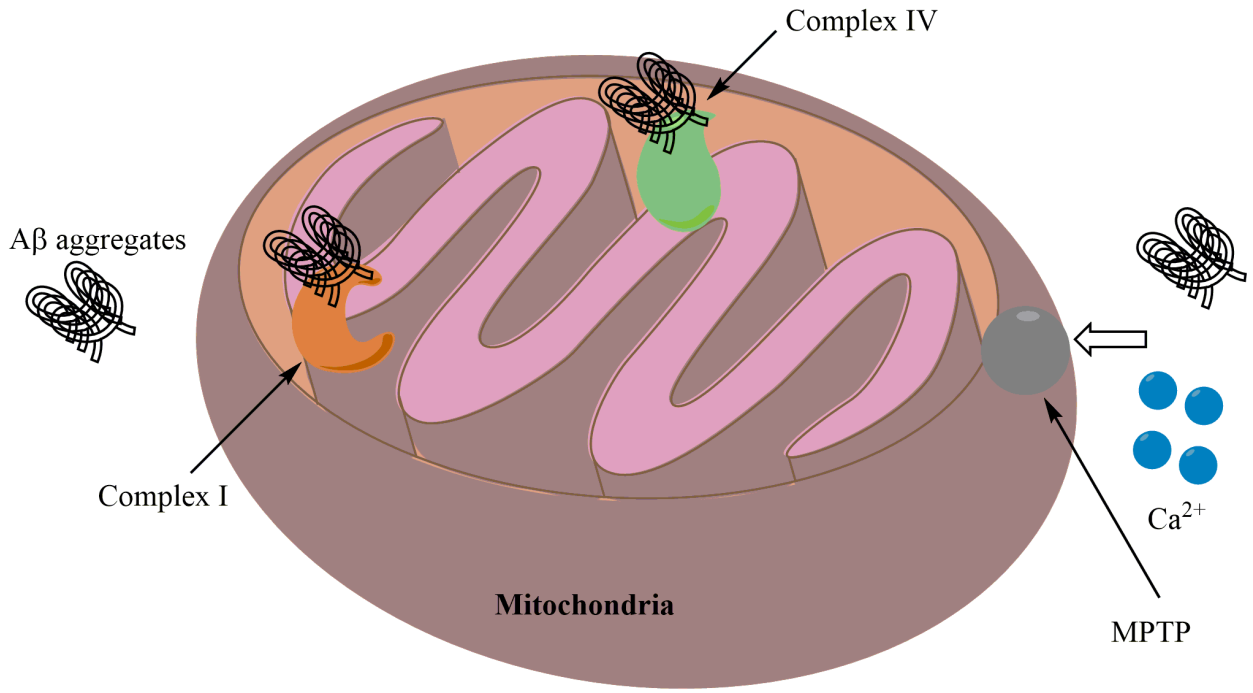

Figure 1.12: Mitochondrial dysfunction in AD. Aβ aggregation causes to oxidative stress, ATP depletion and MPTP aperture leading to mitochondrial dysfunction.

ATP depletion disrupts neurotransmission, alters axonal transport and metal ion homeostasis especially calcium (Ca^{2+}) and sodium (Na^+) in neurons which is essential to maintain the membrane potential. The other negative impact of ROS upon mitochondria is by stimulating an opening of the mitochondrial permeability transition pore (MPTP), a protein channel that passes through both inner

and outer mitochondrial membranes resulting in influx of Ca^{2+} and oxidative stress.[70,71,72] Mitochondrial dysfunction also trigger apoptosis of neuronal cells, the process of programmed cell death, although the mechanism behind this is still open to debate.

Copper and iron metal ions have the ability to form complexes with Aβ plaques and acts as catalyst to generate ROS. The ability of Aβ to reduce Cu^{2+} and Fe^{3+} to Cu^{1+} and Fe^{2+} respectively via Fenton cycle is mediated by sulfur atom of methionine amino acid (M35) which can easily donate electrons.[73,74] This ability is further facilitated considering Aβ contains a metal binding domain at the N-terminal segment. The tri-histidines (H6, H13, and H14) and aspartic acid (D1) domain chelate to copper, iron and zinc, stabilizing the Aβ oligomers, elongate the lag phase and prolong the ROS generation cycle specifically H_2O_2.

The physiological inflammatory response is a self-protection secondary response of body to an initial harmful event, like infections. However inflammation has been linked to a number of diseases either as the initiation mechanism or progression mechanism such as cancer, heart disease and not surprisingly neurodegenerative disorders.[75,76] With respect to AD, neuroinflammation is viewed as a double-edged blade, where it is beneficial in degrading Aβ, however overstimulation can eventually lead to neuronal death. It is mainly associated as a secondary response to Aβ deposition, however there are few studies suggesting that neuroinflammation is an ever-present driving force in AD pathology. In AD patients, soluble Aβ oligomers and fibrils are able to attach to microglia, a highly motile phagocytic macrophage in the CNS, triggering an immune response in body by producing pro-inflammatory cytokines and chemokines.[77,78] The impaired Aβ clearance due to higher concentration of Aβ in AD patients causes the “stimulus” to remains persistent and developing into the chronic inflammatory response, leading to neuronal damage (Figure 1.13).

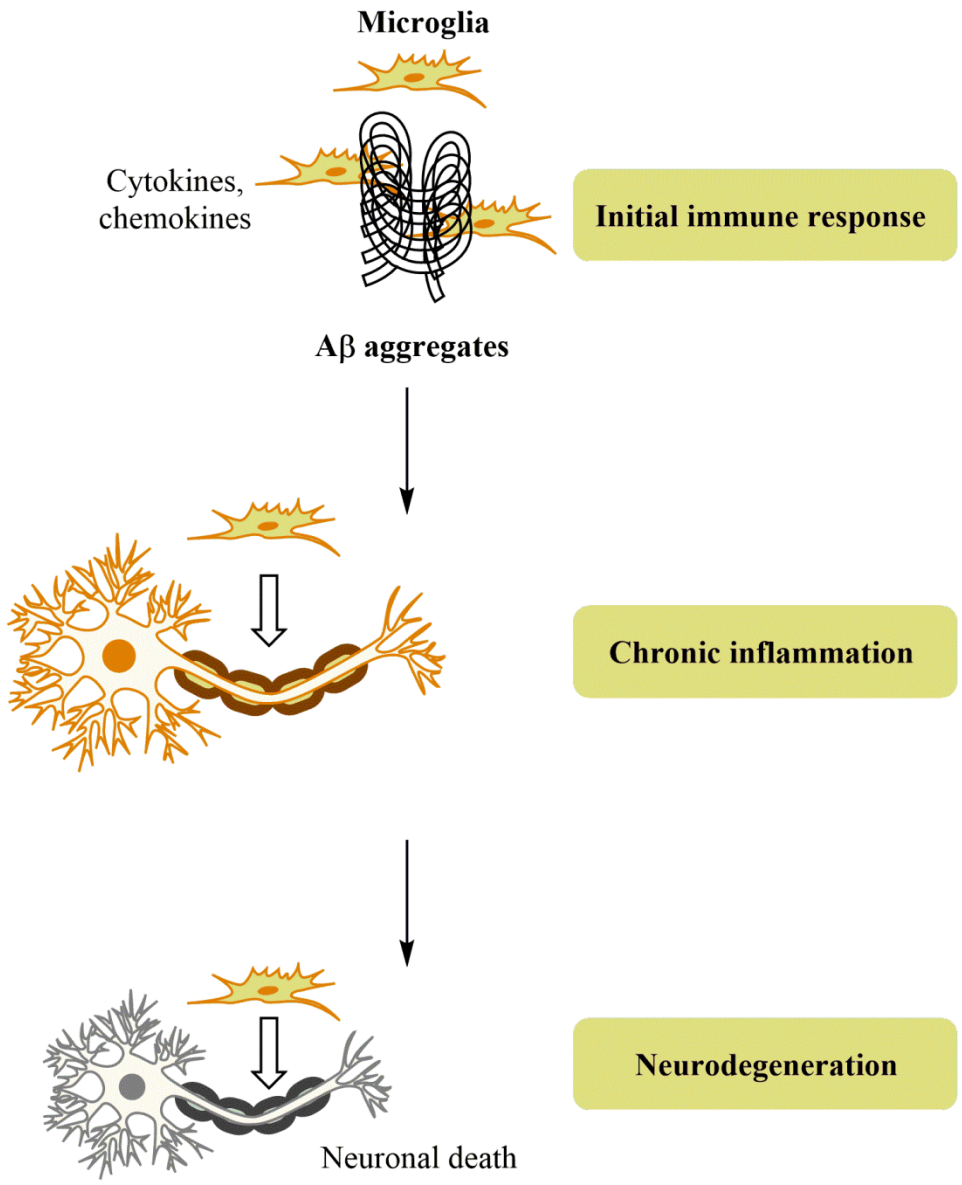

Figure 1.13: Schematic representation of neuroinflammation response to Aβ aggregates. Initial response helps with the clearance of Aβ however the sustained exposure and overstimulation leads to chronic neuroinflammation.

Synaptic plasticity, the ability to strengthen and weaken in response to neurotransmitters, is vital in global cognitive function. The loss of synaptic plasticity and long-term potentiation (LTP), enhanced level of neuronal transmission, are frequently observed in late stage of AD.[79,80] It's been

postulated that synaptic dysfunction in AD patients is due to Aβ oligomer's ability to bind to neuronal receptors on the synaptic cleft and hindering their function. Glutamate (GluR), NMDA, AMPA (α-amino-3-hydroxy-5-methyl-4-isoxazolepropionic acid) and α7-nicotinic receptors are among such receptors.[81]

Aβ is also known to interact with the cellular membrane to form channels in the neuronal membrane leading to abnormal flow of metal ions inside and outside the cells.[82] It's been postulated that the mechanism behind the formation of these channels are similar to that observed in antibacterial agents killing bacteria.

Finally, there is growing evidence that telomere shortening, a hexanucleotide (TTAGGG) repeats located at the 3` end of DNA strands, can play an important part in pathology of AD.[83,84] Telomeres play a vital role in maintaining the stability of genes and during DNA replication, after every cell division this segment become shorter and serves as a marker to the history of cell replication. In general, the shorter the telomere segment the higher the risk for AD where Aβ aggregates inhibit the activity of telomerase, a ribonucleoprotein enzyme that adds the TTAGGG segment to the DNA. Recent *in vivo* and *in vitro* studies suggest that Aβ oligomers interact with DNA-telomerase complex, blocking the elongation of telomere segment (Figure 1.14).[85,86,87]

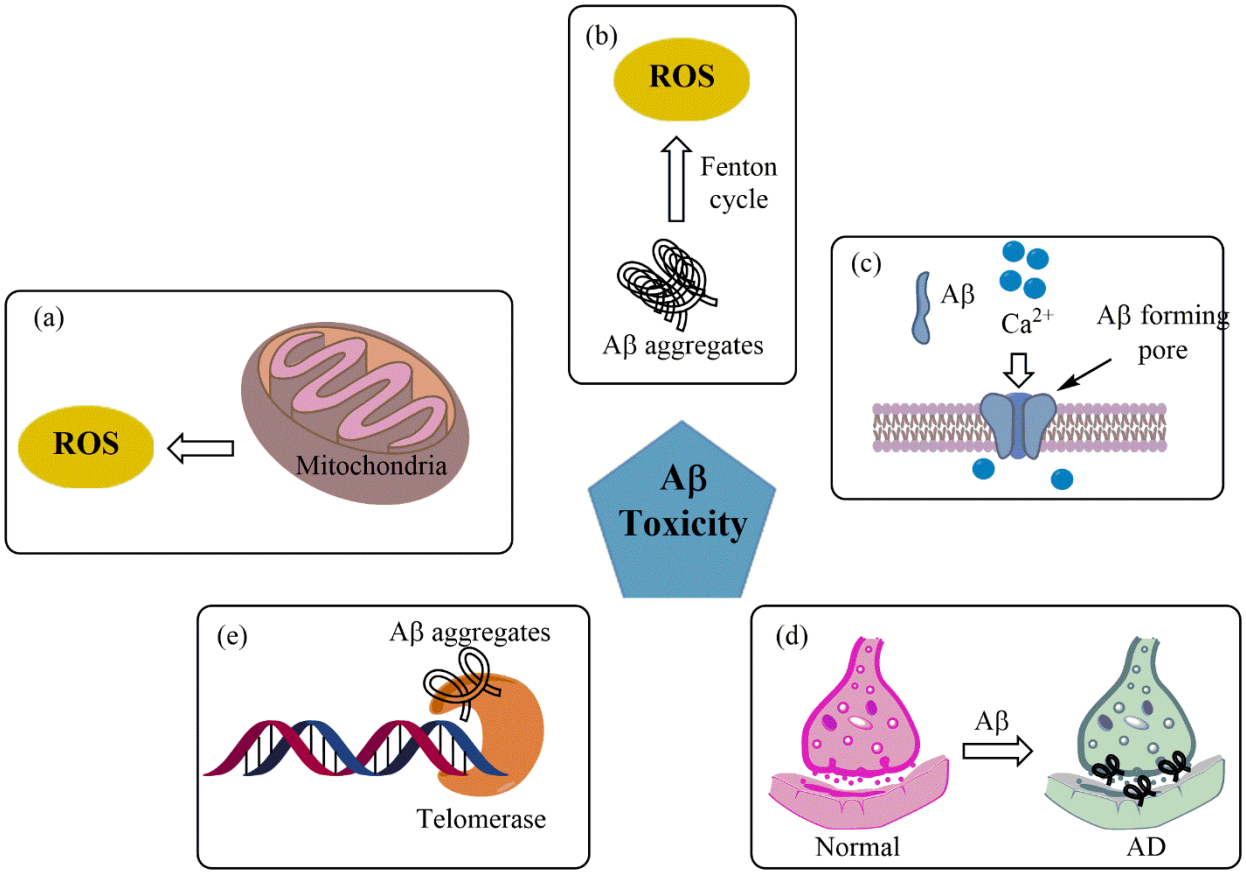

Figure 1.14: The summary of Aβ toxicity mechanims: (a) mitochondrial dysfunction, (b) oxidative stress, (c) cell membrane disruption, (d) synaptic dysfunction/toxicity (e) telomerase dysfunction.

After discussing the Aβ toxicity in great details, it is just fair to explore the positive physiological functions of Aβ in maintaining a healthy central nervous system (CNS) mainly neurogenesis, synaptic plasticity, antioxidant activity, memory formation, calcium homeostasis and metal chelation.[88,89] Although at the first glance, Aβ pathological and physiological properties appears to be at odds with each other, its crucial to keep in mind that the production of Aβ at the basal level serves a physiological purpose, however under certain circumstances this balance tips towards Aβ pathology (Figure 1.15). The fate of this balance is mainly decided by the concentration of Aβ peptide, where at picomolar (pM) concentration, Aβ exhibits physiological roles however at

nanomolar (nM) to micromolar (µM) coupled with aging effects, it shifts towards pathological roles.[90]

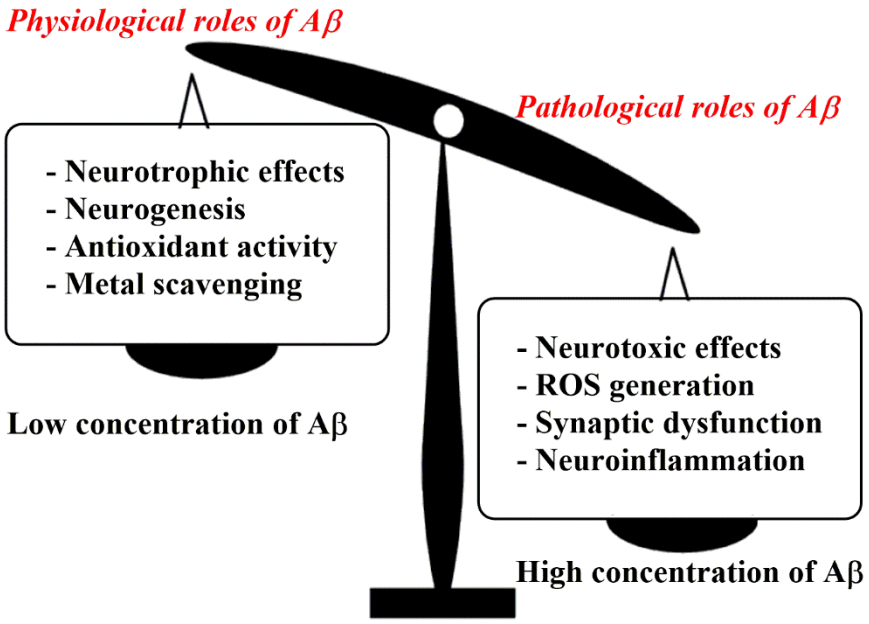

Figure 1.15: The balance between pathological and physiological roles of Aβ. Physiological effects of Aβ is observed at low concentration (pM) however in AD, elevated concentration of Aβ (nM to µM) the balance shifts to pathological effects.

Recent studies have strongly linked Aβ oligomers to neurogenesis, the process of generation and differentiation of neurons and glial cells from neuronal stem cells (NSCs). Aβ40 promotes NSC proliferation and neurogenesis whereas Aβ42 is more selective towards gliogenesis of NSCs.[88,91] Growing interest in the use of NSCs in cell therapy opens the possibility to combat the effects of neurodegenerative disorders by replacing the damaged or dead neurons. Recent efforts to identify the Aβ induced neurogenesis indicates that Aβ isoforms increase the proliferation of NSCs via the

activation of PI3K-Akt pathway, an intracellular signaling pathway critical in regulating diverse cellular functions such as growth, proliferation and survival.[92]

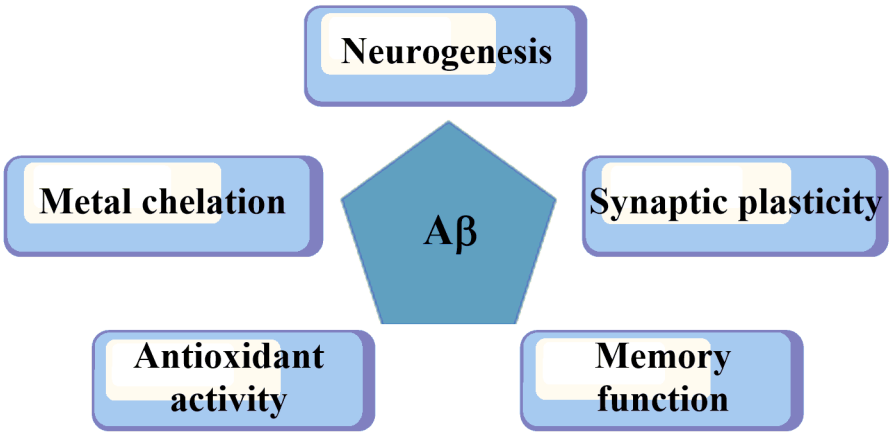

Figure 1.16: Schematic representation of physiological effects of Aβ, synaptic plasticity, neurogenesis, memory function, metal chelation and antioxidant activity.

As discussed before, transition metals especially copper and iron play a vital role in the production of ROS. Among the many mechanisms in the body to keep the concentration of these ion metals in balance, mounting evidence suggest that Aβ acts as metal scavenging agent at lower concentrations.[93,94] The tri-histidines (H6, H13, and H14) and aspartic acid (D1) domain chelates to metal ions and prevents them from participating in redox cycle, acting as a metal chelator and antioxidant in healthy neurons and a number of other cells such as neuroblastoma and hepatoma cells. In this context, it appears that the Aβ release in response to head injury or disease is a neuroprotection response against oxidative stress after which the Aβ is removed from the brain. However, the insufficient Aβ clearance in AD patients coupled with the progressive accumulation of Aβ complexes with the mentioned metal ions overwhelms the antioxidant defense systems in body, indirectly leading to the overproduction of ROS and oxidative damage that follows (Figure 1.16).[95,96,97]

1.7 Aβ Therapy

At this point it's obvious that there are many layers of complexity to Aβ hypothesis and Aβ plays a prominent role in pathophysiology of AD, however this complexity affords us many insights into a diverse potential intervention targets. Preventing the formation of Aβ, blocking Aβ aggregation process or even accelerating the clearance rate of Aβ are among these potential targets.[16,98,99,100] Several therapeutic options are currently being developed mainly focused on the reduction of Aβ load in the brain. These options can be broadly categorized in the following approaches:

1. Prevention or reduction of Aβ production
2. Modulate the Aβ aggregation process
3. Enhancing Aβ degradation or clearance from brain
4. Tackle the Aβ neurotoxicity

Recalling from APP processing, BACE 1 has emerged as a viable pharmacological target to reduce the production of Aβ by development of BACE 1 inhibitors (Figure 1.17). The BACE 1 inhibition has been identified as a potential therapeutic option in the recent years and led to the development of a number of promising candidates.[101,102] The early designed BACE 1 inhibitors proved to be inefficient due to their inability to cross blood-brain barrier (BBB). However, recently developed treatments managed to overcome this challenge. The majority of these treatments however dropped out of the clinical trials due to toxicity although a few were well tolerated in patients. Considering that BACE has two isoforms, BACE 1 and BACE 2, the possibility exists that selective BACE 1 inhibitors can cause side effects due to weak or lack of BACE 2 inhibition. The hope is to design BACE 1 inhibitors that balance safety and efficacy. In this regard, some *in vivo* studies suggest at least 50% efficacy is necessary to circumvent Aβ level sufficiently.[41,103] It is

noteworthy that BACE 1 also cleaves a number other substrate proteins, which means inhibition of the enzyme can lead to unforeseen side effects. That said, BACE 1 inhibitors still hold a substantial promise in developing a treatment for AD.[102]

The other approach in lowering the Aβ production is the up-regulation of non-amyloidogenic pathway, as α-secretase competes with BACE 1 in APP processing pathway. The benefit to this approach apart from the obvious reduction in Aβ production, is taking advantage of neuroprotective properties of α-APPs released in the non-amyloidogenic pathway.[104,105] The up-regulation of non-amyloidogenic pathway can be achieved by promoting α-secretase activity, enhancing the α-secretase transduction or by modulation of hormones, statins and other neurotransmitters.

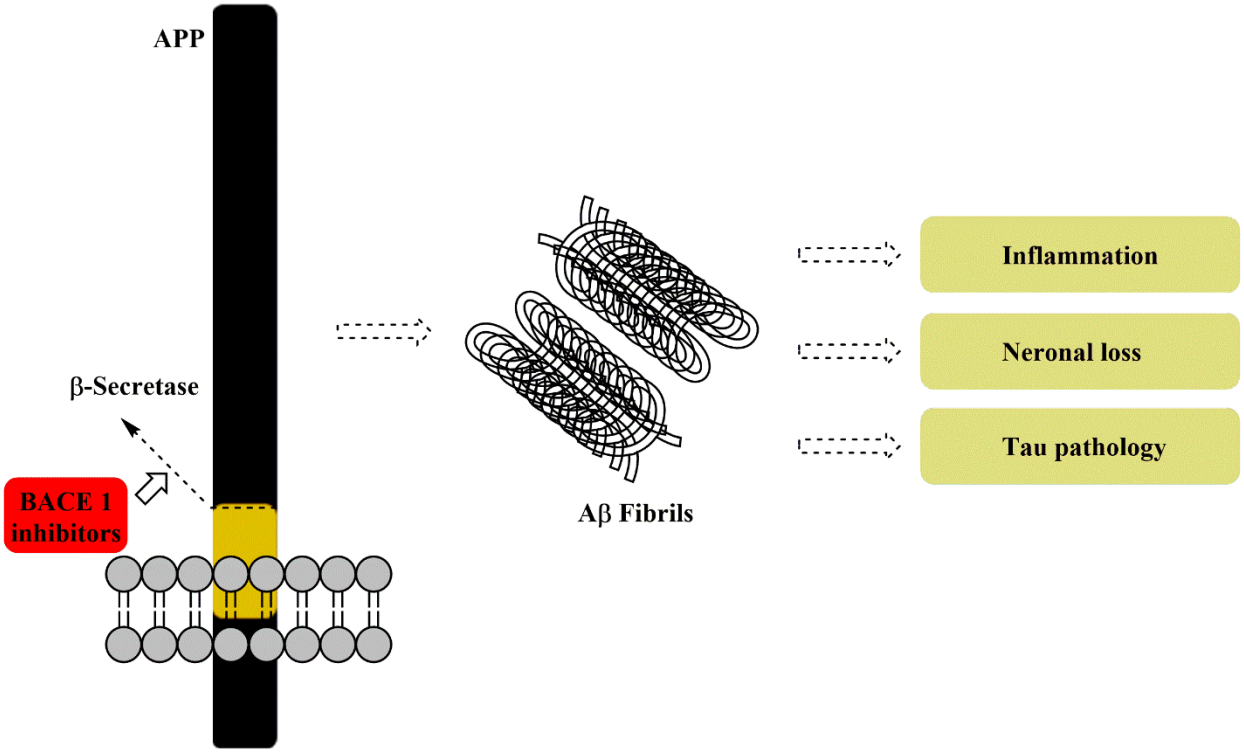

Figure 1.17: BACE 1 inhibitors and their impact on downstream pathology of AD.

Although halting or reducing the production of Aβ is an attractive approach to say the least, by the time the majority of AD patients diagnosed with the disease, there is a considerable Aβ load

already present in their brains. So what is the best therapeutic approach for these patients? Arguably, modulation of Aβ aggregation is the best option for the treatment of these patients as it can provide beneficial DME. The surge in the discovery of small molecules as Aβ aggregation modulators in recent years is a testament to the popularity of this approach. This strategy can be categorized into two groups, anti-aggregation and pro-aggregation of Aβ peptide, with the pro-aggregation approach still at its infancy compared to the well-studied anti-aggregation approach.[13,106,107] It is important to keep in mind that neither of these approaches are perfect stand-alone strategy and they should be used in co-therapy with other treatments to maximize the efficacy of the treatment. In anti-aggregation approach the main purpose is to minimize the conversion of Aβ monomers into Aβ oligomers by stabilizing the early formed intermediates, reducing the exposure time of neurons to Aβ oligomers and also reduce the rate of Aβ plaques formation.

Great number of natural and synthetic compounds have been known to modulate Aβ aggregation.[108] The anti-aggregation approach is based on stabilizing Aβ monomers and early formed intermediates to halt or slow down the aggregation process. Curcumin, congo red and orange G are known to have anti-aggregation properties towards Aβ (Figure 1.18). Congo red inhibits the formation of Aβ fibrils by binding and stabilizing the monomers and early formed intermediates and as a result reduces the concentration of toxic, soluble oligomers.[109] Curcumin, a naturally occurring compound, inhibits the aggregation of Aβ by destabilizing the protein-protein interactions while stabilizing Aβ monomers.[110,111]

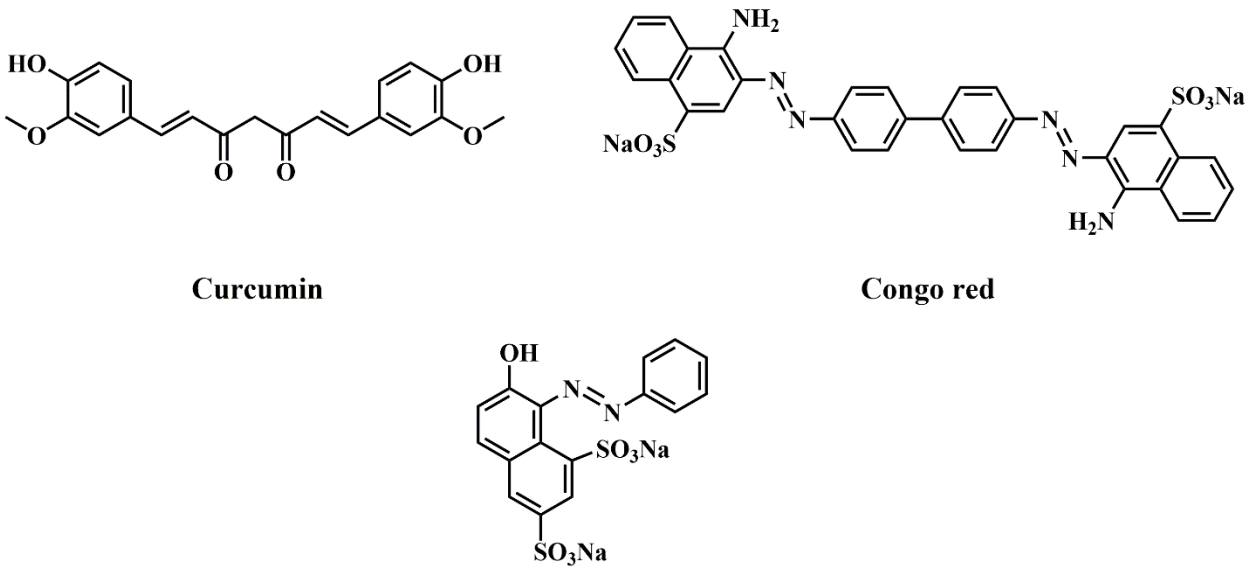

Curcumin **Congo red**

Orange G

Figure 1.18: Compounds with anti-aggregation properties.

Orange G inhibits the aggregation of Aβ protein by stabilizing the KLVFFA ($A\beta_{16-21}$) segment. Hydrophobic interactions between aromatic rings of orange G and KLVFFA, ionic interactions between negatively charged sulfonic groups of orange G and positively charged lysine amino acids leads to further stabilization of β-sheet structure of Aβ.[112] Along natural and synthetic small molecules capable of modulating Aβ aggregation process, peptide-based inhibitors has started to thrive in recent years. A 5 to 15 amino acids in length designed to interact with the KLVFFA segment have shown to inhibit the aggregation process with high degree of selectivity however the poor bioavailability of these peptides pose a major challenge in their use as therapeutic agents.

The pro-aggregation approach as the name suggests is based on facilitating the conversion of Aβ oligomers to its less toxic form; mature Aβ fibrils (Figure 1.19). The main goal in this approach is to minimize the exposure of neurons to Aβ oligomers and using Aβ plaques anti-bodies to reduce the Aβ load by triggering immune response from body.[113,114]

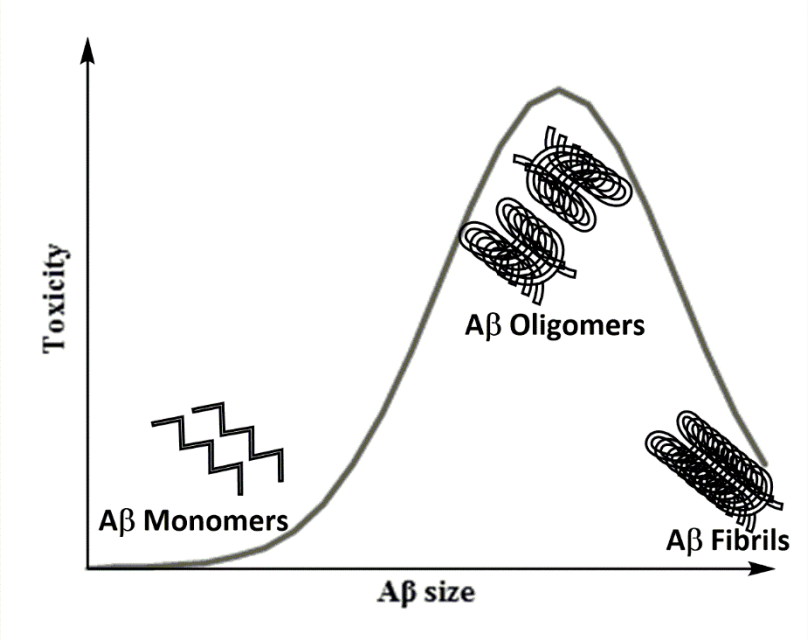

Figure 1.19: Schematic representation of Aβ toxicity and its correlation with Aβ aggregation process.

Facilitating Aβ clearance is another approach in Aβ therapy, however it's more complicated compared to the previous approaches. That said, a number of immune-mediated mechanisms have been tested to induce active or passive immune response to reduce Aβ load in the test subjects with relative success.[115,116] In immunotherapy for AD, Aβ-antibodies are raised with high selectivity toward various forms of Aβ. Passive immunization via immunoglobulins against Aβ has been more successful with Bapineuzumab and Solanezumab reaching phase III with good tolerability. However, in neither cases no significant cognitive improvement was observed despite lowering Aβ load.[117]

As discussed in previous section, certain metal ions have the ability to form complexes with Aβ oligomers and fibrils facilitating the aggregation process and enhance their toxicity. Design and

development of small molecules capable of scavenging these metal ions and therefore disrupting the formation of Aβ-metal complexes in order to minimize the neurotoxicity and restore the metal ion homeostasis have gained tremendous popularity. Small molecules with metal scavenging properties have been used for decades to deplete overloaded tissues and facilitate their excretion in diseases such as Wilson's disease or hemochromatosis.[118,119] In the context of AD, disruption of metal homeostasis is a consequence of the disease rather than the cause and simply removing them from brain can lead to undesirable side effects.[120] As such, development of multitarget compounds with Aβ inhibitory and metal scavenging properties may have potential DME, with clioquinol derivatives, a small hydrophobic family of molecules, exhibiting moderate affinity for metal ions and inhibition of Aβ aggregation (Figure 1.20).

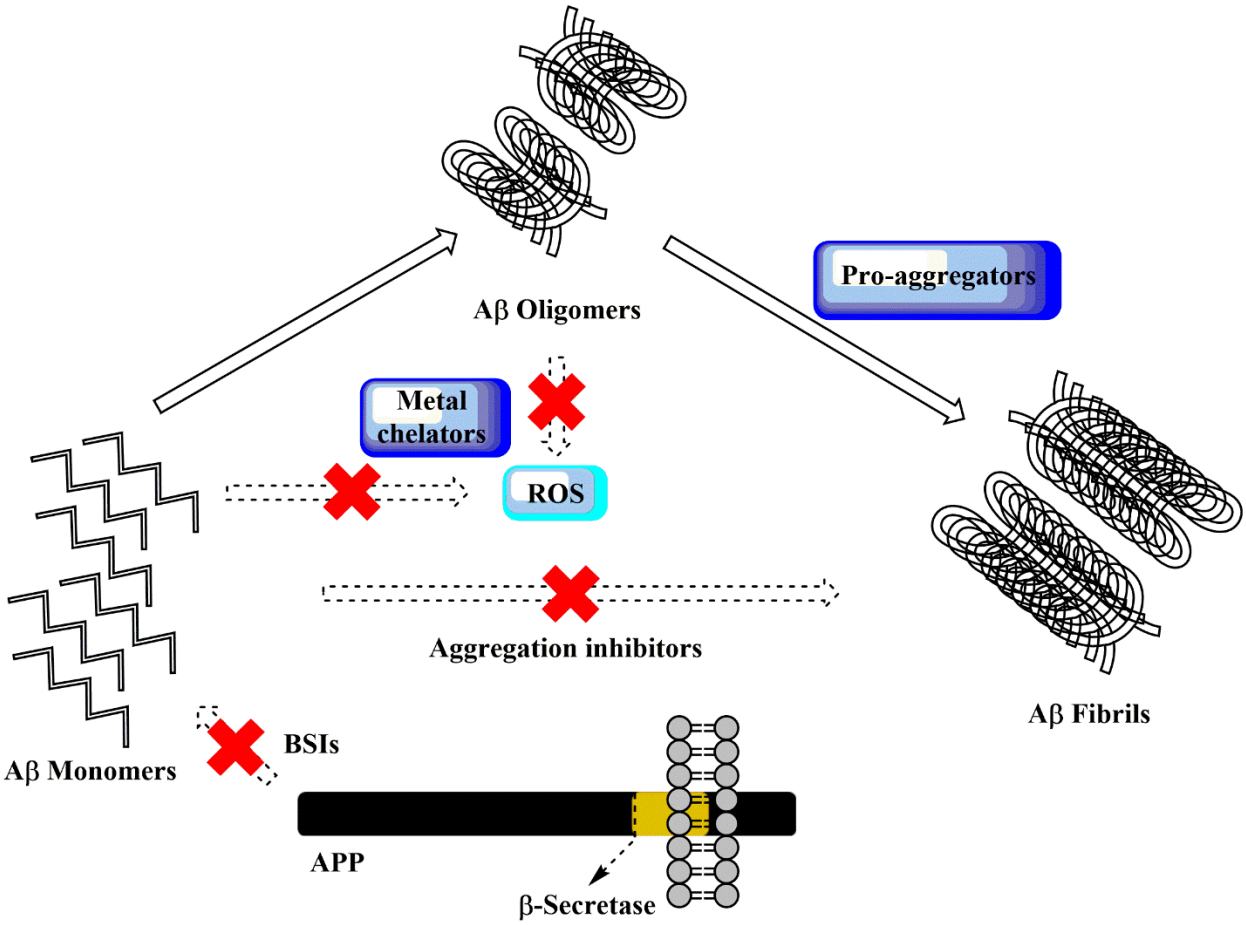

Figure 1.20: Schematic representation of various therapeutic targets in Aβ therapy. BACE 1 inhibitors (BSIs).

1.8 Other Factors in AD pathology

Although the Aβ hypothesis is the main focus of this project, it is essential to address other major hypotheses to paint a better picture of AD pathology. Cholinergic hypothesis, the oldest and most studied hypothesis with respect to AD, has been the star player in dementia and neurodegenerative disorders for many decades.[121,74] The hypothesis suggests that the loss of cholinergic function and the subsequent decline in the concentration of acetylcholine (ACh) contributes to the deterioration of cognitive functions observed in AD. Cholinergic function is

mainly rests upon ACh, a neurotransmitter in brain, acetylcholinesterase (AChE) and butyrylcholinesterase (BuChE), enzymes in charge of degrading ACh. The importance of cholinergic function in learning and memory function has provided a rationale for therapeutic interventions that increase the concentration of ACh or inhibit the activity of AChE and BuChE.[122] Although the main body of the hypothesis is still valid, the poor efficacy of available treatments for moderate to severe cases of AD points to the fact that merely targeting cholinergic hypothesis is not sufficient and any potential treatment should be a part of multitargeting platform to efficiently combat the pathology of AD.[123]

The tauopathy is of great interest in AD research as growing evidence strongly links it with neurodegenerative disorders.[124] The tau hypothesis is centered around the aggregation of hyperphosphorylated tau protein into neurofibrillary tangles (NFTs) and the subsequent neuronal damage/death. Tau protein binds to and promotes the assembly of microtubules which is vital to maintain the cytoskeletal structure and integrity of neurons.[125,126] The activity of tau protein is regulated through phosphorylation sites present on the protein via various phosphatases and kinases such as glycogen synthase kinase 3 (GSK-3), cyclin-dependent kinase 5 (CDK-5) and mitogen-activated protein kinase (MAPK).[127] In healthy individuals, there is a delicate balance between phosphorylated and non-phosphorylated species of the protein. However, in Alzheimer's patients, this balance is disrupted. This disruption leads to formation of abnormally hyperphosphorylated tau species which results in the protein losing its structural integrity, hence its function. The hyperphosphorylated tau then becomes insoluble due to the conformational changes and dissociates from the microtubules, leading to impairment of axonal transport and formation of paired helical filaments (PHF) which aggregates to NFTs as shown in Figure 1.21.[128,129]

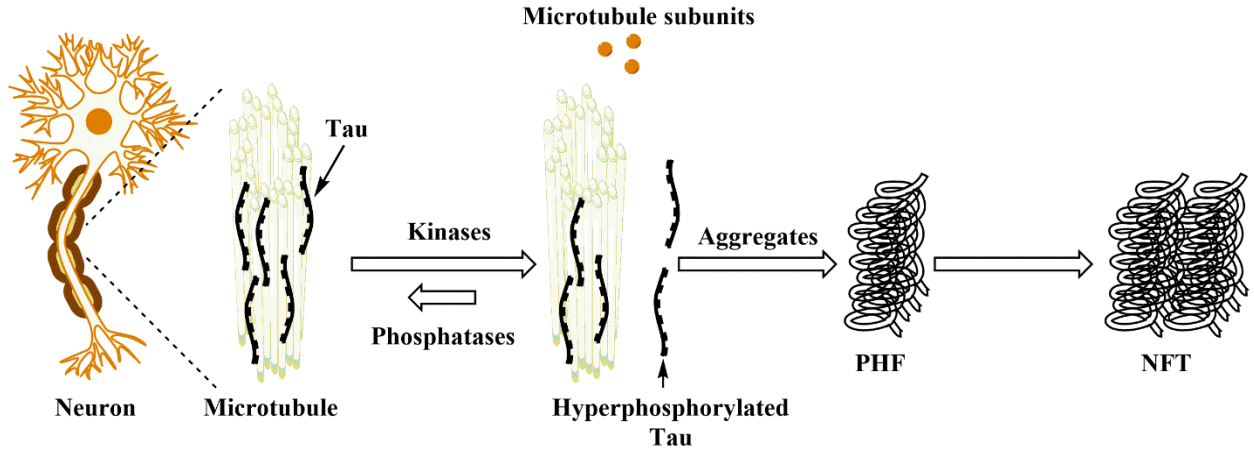

Figure 1.21: Schematic representation of tau cascade hypothesis and the aggregation process of tau protein.

The therapeutic intervention strategies for tauopathy closely mirror those from amyloid hypothesis. The inhibition of GSK-3 and CDK-5 to reduce the phosphorylation of tau, modulation of tau aggregation and immunotherapy options to remove tau aggregates from CNS.[130,131] Among these approaches, tau aggregation modulators are less desirable due to high degree of neurotoxicity at this stage of the disease. Microtubule-stabilizing strategy is a new approach in tau therapy where microtubule-stabilizing agents counteract the functional loss of hyperphosphorylated or aggregated tau.[132,133]

The impact of NMDA excitotoxicity in pathophysiology of AD is well established. NMDA receptor is carried by neurons and is essential in the optimal physiological function of brain and overall cognitive functions.[134,135] NMDA receptors are highly concentrated in hippocampus where activation of the receptor induces LTP and neuronal plasticity as the result. Elevated level of glutamate, an amino acid and neurotransmitter in CNS, results in chronic activation of NMDA receptor causing excessive amount of Ca^{2+} influx into neuron and ultimately neurodegeneration known as excitotoxicity. Under physiological condition, glutamate is responsible for 70% of

excitatory synapses in the CNS where largely postsynaptic AMPA receptors exhibit very fast activation/de-activation kinetics. In contrast, NMDA receptors are normally synaptic activated and permeable to Ca^{2+} with slow ligand gated kinetics.[136,137] Normally, NMDA receptor is blocked by Mg^{2+} allowing small influx of Ca^{2+} into neurons for a brief period of time when activated. However in AD, due to impaired glutamate uptake/recycling mechanisms, this barrier is removed causing excessive amount of Ca^{2+} influx leading to synaptic dysfunction and ultimate neuronal death.

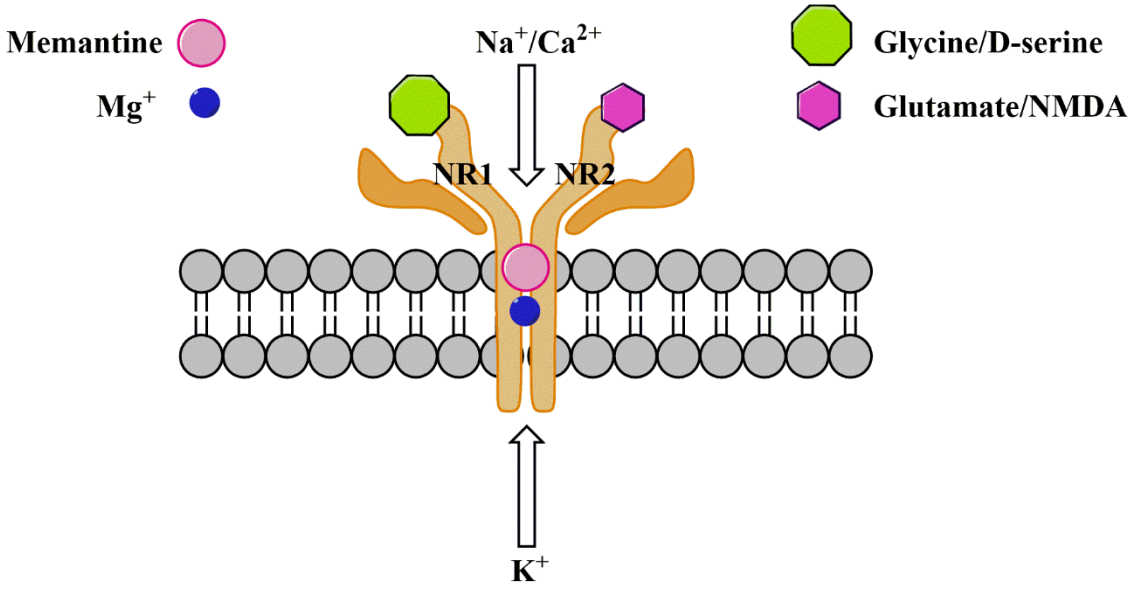

Figure 1.22: NR1 and NR2 are the two major subunits of NMDA receptor. The activation of receptor is triggered when glycine/D-serine and glutamate/NMDA bind to NR1 and NR2 respectively. Memantine, an NMDA receptor antagonist, can block the receptor and inhibit the influx of Ca^{2+} into the neurons.

1.9 Adamantane Derivatives

Organic polycyclic cage compounds such as adamantane derivatives (Figure 1.23) have attracted the interested of medicinal chemists in the past 50 years with their applications ranging from anti-viral agents such as human immunodeficiency virus (HIV) and influenza to symptomatic treatment of neurodegenerative diseases such as AD and PD.[138] Interestingly, unlike many common scaffolds such as indole, quinazoline and quinolone, aminoadamantanes are synthetic in nature with a very few naturel sources.

Discovery of anti-viral activity of amantadine sparked an interest in adamantane derivatives in 1960s where amantadine, marketed under trade name of Symmetrel, exhibited strong activity against Influenza A.[139,140] Amantadine has been used as a treatment for Parkinson's disease in the past three decades.[141] Amantadine increases the extracellular dopamine levels which results in anti-Parkinson activity although not all patients exhibit positive response to the treatment and a number of patients develop tolerance to its effects.

Further modification of adamantane and subsequent synthesis of closely related rimantadine, marketed under trade name of Flumadine, which displayed even stronger antiviral activity and fewer side effects in comparison to amantadine.[142] Food and drug administration (FDA) approved both these treatments as anti-Influenza agents, however neither one of them are the common choice in treatment of Influenza. Since then, a wide range of drugs have been introduced to the market incorporating adamantane moiety as illustrated in Figure 23.

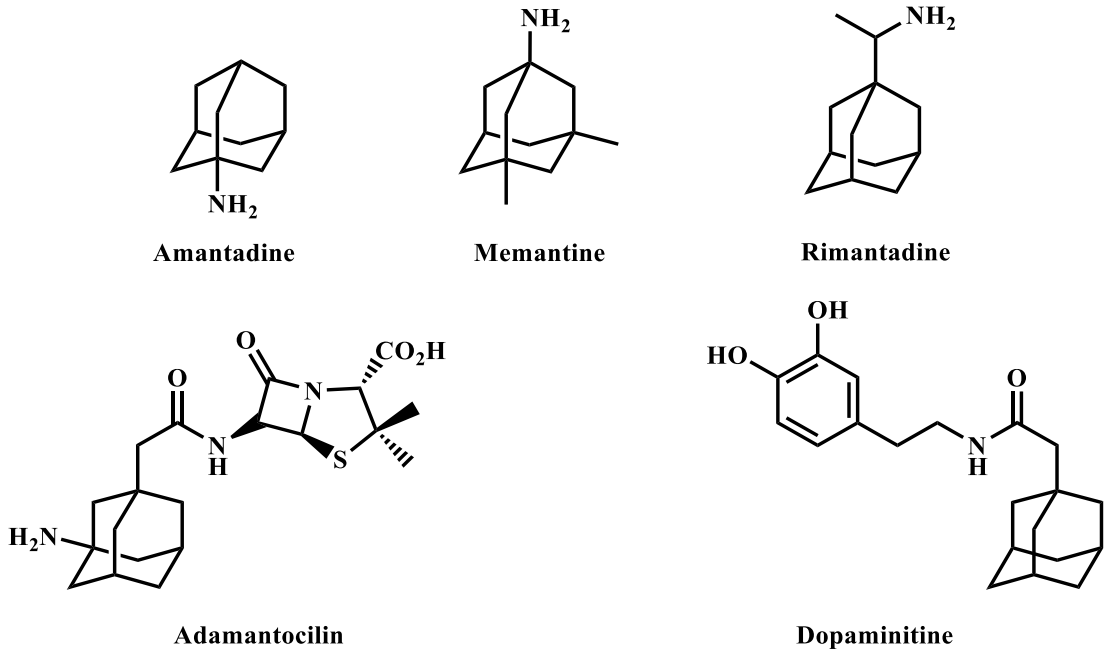

Figure 1.23: Examples of drugs and drug candidates incorporating adamantane moiety.

Memantine was designed and synthesized by Eli Lilly and Company, currently marketed under name of Namenda, is approved by FDA as a treatment for Alzheimer's patients with moderate to severe dementia.[136,143] It is a NMDA-receptor antagonist that blocks the influx of excessive calcium induced by overstimulation of the NMDA receptor. Although it has been approved as a treatment for AD, overstimulation of NMDA receptor is a common pathway to neuronal damage in a number of other diseases such as PD, HIV-associated dementia, Huntington's disease (HD), multiple sclerosis and amyotrophic lateral sclerosis (ALS) making memantine a potential treatment candidate for the mentioned diseases.

Adamantane derivatives as an example of polycyclic cage compounds, present a viable scaffold to design and develop treatments for a wide range of disorders not only as a stand-alone treatments but also as an add-on to improve the stability and lipophilicity of existing treatments.

Chapter 2: Hypothesis and Design Rationale

2.1 Hypothesis

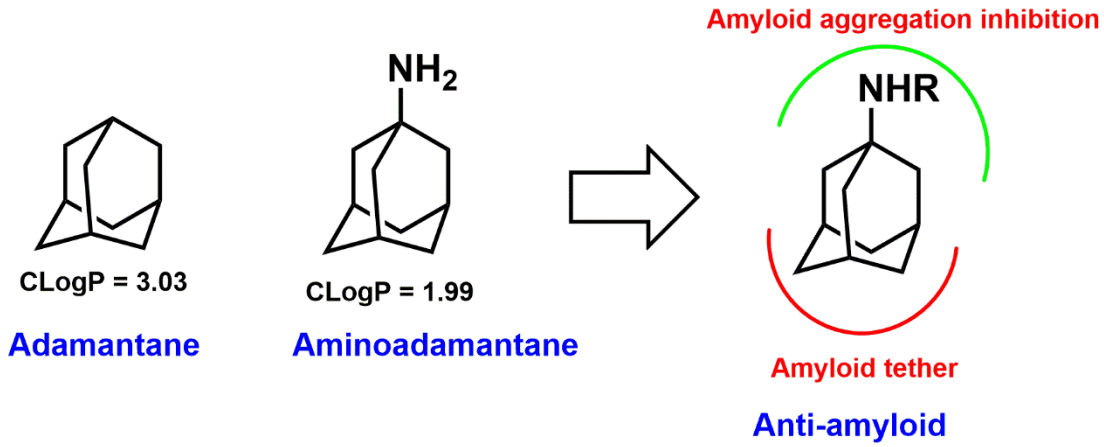

Figure 2.1: Aminoadamantane derivatives as anti-amyloid aggregation agents.

The polycyclic cage structure adamantane (tricyclo[3.3.1.1]decane) has a chemical formula $C_{10}H_{16}$ (Figure 2.1). The carbon atoms of the three cyclohexane rings in the saturated hydrocarbon adamantane are arranged in a diamond lattice structure. This tetrahedral geometry (sp^3) of the carbon framework provides a very stable conformation. Adamantane derivatives are known to exhibit a number of biological activities listed in Chapter 1 (section 1.9). The ring itself can be considered as a pharmacophore that can be incorporated in the design of potential therapeutic agents aimed toward viral disease, AD and diabetes.

The lipophilic nature of the adamantane ring provides excellent blood-brain barrier (BBB) permeability as exemplified by the aminoadamantane anti-Alzheimer's agent memantine (Figure 1.23, Chapter 1). This evidence suggests that the aminoadamantane ring can be explored to design and develop potential agents to treat CNS diseases such as AD. In this regard, Dr. Nekkar Rao's lab at the School of Pharmacy is aiming to develop novel AD therapeutics by targeting the amyloid cascade hypothesis of AD.[144,145,146] Developing therapeutic interventions that inhibit Aβ aggregation and as a result prevent the formation of toxic soluble Aβ oligomers and Aβ fibrils

appears to be a favorable approach in targeting the Aβ hypothesis. We believe that targeting the early stages of Aβ aggregation, by stabilizing the Aβ dimer, trimer or tetramer should prevent the formation of toxic Aβ oligomers and fibrils.

With this background, the *objective of this MSc proposal was to design and develop aminoadamantane based compound library as potential Aβ aggregation inhibitors.* We conducted preliminary computational studies of the aminoadamantane ring in the Aβ-dimer assembly (Figure 2.2) which suggested the potential of aminoadamantane derivatives to bind and stabilize the aggregation prone KLVFFA region of Aβ. This investigation suggested two key factors to consider; (i) the polycyclic cage compound aminoadamantane itself could provide weak inhibition of Aβ aggregation due to its smaller size and (ii) chemical modification of the primary amine to incorporate larger substituents would enhance the anti-Aβ activity.

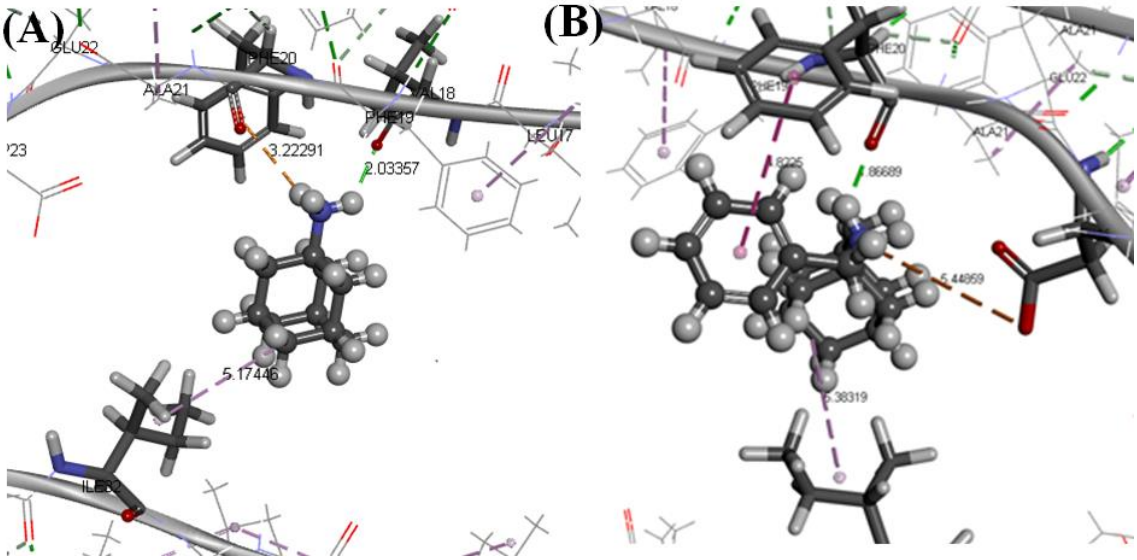

Figure 2.2: Computational modeling of aminoadamantane (A) and *N*-(adamantan-1-yl)benzamide (B) in the dimer assembly of Aβ (PDB id: 2LMN). The ligands are shown as ball and stick cartoon. Some polar and nonpolar interactions are shown.

2.2 Design Rationale

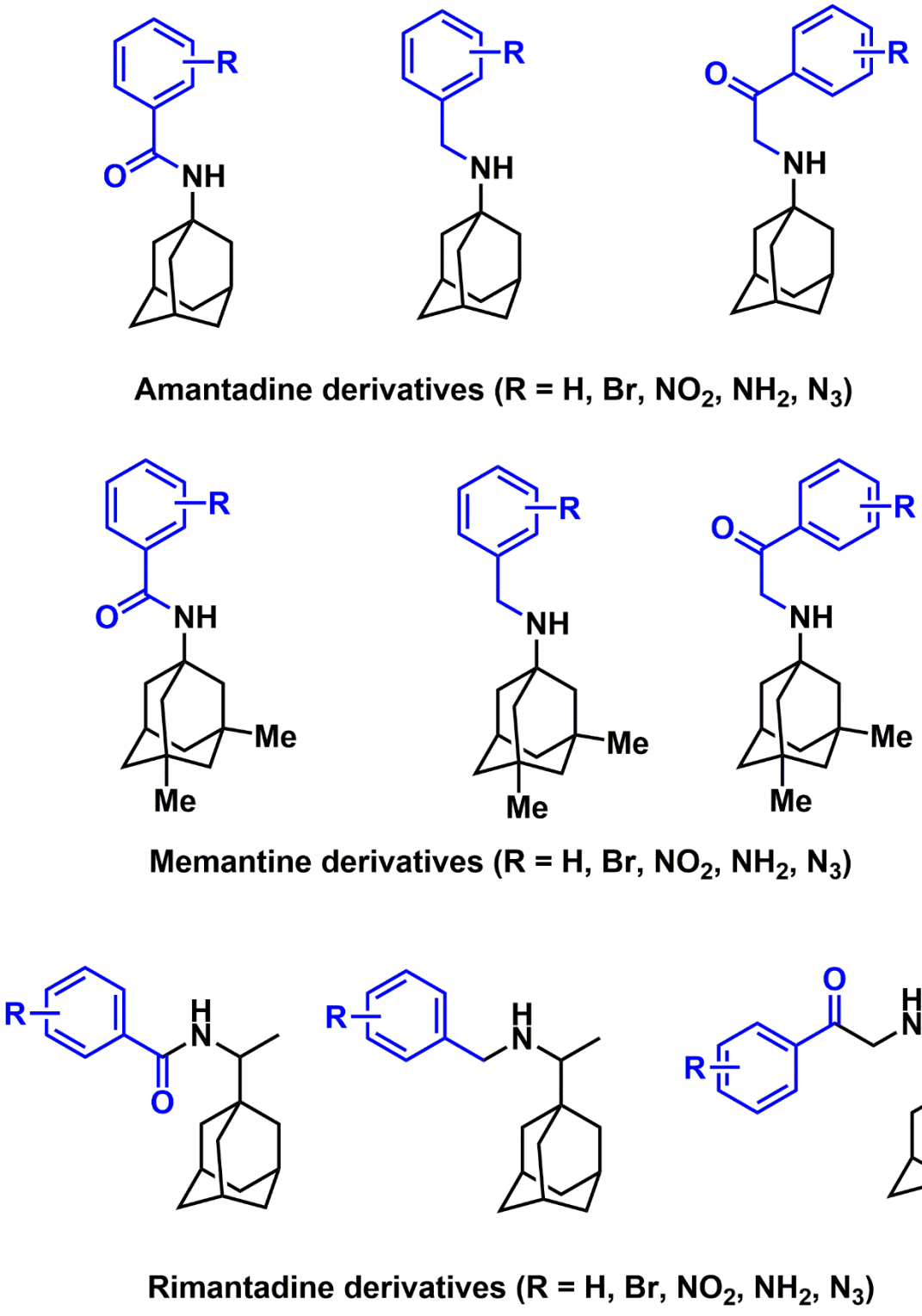

Figure 2.3: Design template of novel aminoadamantanes derivatives.

Based on computational studies, we hypothesized that the caged adamantane can act as an amyloid tether by undergoing nonpolar interactions at the C-terminal of Aβ whereas the modification of amine functionality (Figure 2.2) can increase the degree of Aβ aggregation inhibition properties. In order to study our hypothesis we aim to synthesize a library of benzamide, benzyl or phenylethan-1-one substituted derivatives of amantadine or memantine or rimantadine respectively (Figure 2.3). Furthermore, the benzamide, benzyl or phenylethan-1-one rings will be substituted at either 3- or 4-position with either a Br or NO_2 or N_3 substituent. This was based on the previous evidence which has shown that the presence of a bromobenzene substituent generally provides excellent Aβ-aggregation inhibition due to additional nonpolar contacts whereas polar substituents such as a nitro or an azide can promote electrostatic interactions with polar amino acids (eg: lysine) in the amyloid aggregates and prevent further aggregation into higher order structures.[144,146] The proposed compound library has CLogP values ranging from 3.5–6.3 which was expected to provide a diverse range of structure-activity data. The aminoadamantane library will be screened for potential anti-Aβ aggregation activity by using fluorescence based aggregation kinetics assays, transmission electron microscopy (TEM) and by computational studies.

N-substitution of aminoadamantanes with acetophenone, benzyl and benzoyl groups modulates anti-aggregation properties for Aβ due to variation in their conformation. The anti-aggregation property is sensitive to substituents at C-3 and C-4 position of either *N*-acetophenone, *N*-benzyl or *N*-benzoyl group. Key functional groups (NO_2, NH_2, N_3 and Br) as substituents were identified as suitable Aβ binding pharmacophores which can prevent Aβ aggregation.

2.3 Conclusion

The proposal aims to synthesize a library of amantadine, memantine and rimantadine based derivatives that possess a cage polycyclic adamantane ring system and evaluate their anti-amyloid aggregation properties. It is anticipated that the structure-activity relationship (SAR) studies obtained will provide a clear understanding on the ability of aminoadamantane derivatives to prevent Aβ aggregation and their mechanism of action at the molecular level.

Chapter 3: Methodology

3.1 Synthetic Chemistry

The overall synthetic routes as highlighted in the following figures were routine and relatively efficient. The majority of synthetic routes were adapted from previously published literature with various changes to optimize the synthesis and l yields.

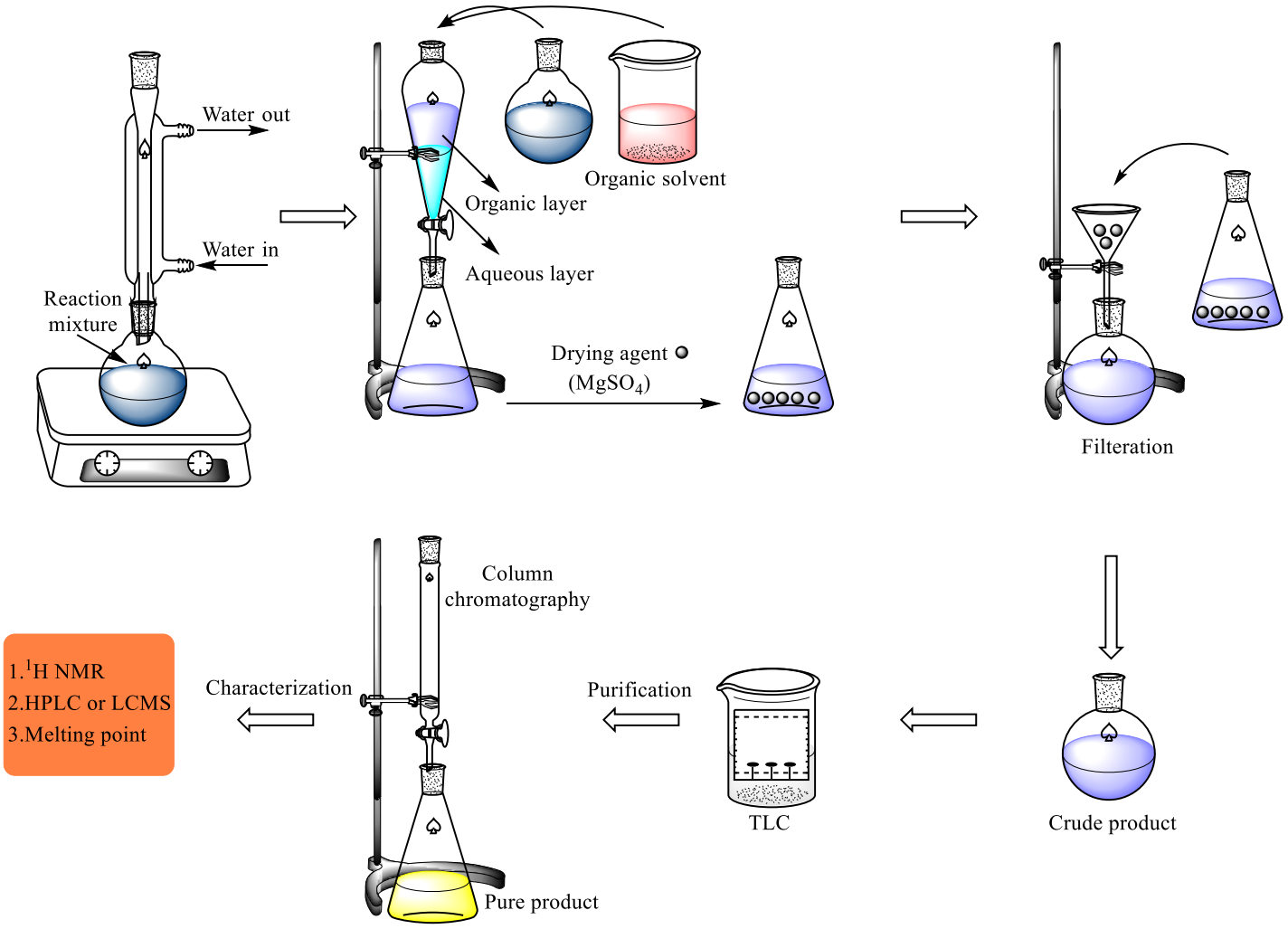

Figure 3.1: Schematic representation of overall setup to synthesize, purify and identify the target library.

Figure 3.1 illustrates the overall setup involved in the syntheses, purification and characterization of adamantane derivatives. The reactions were carried out using appropriate solvents based on the nature of reactions, solubility of reagents, and heated or refluxed for certain period of time based on the reactivity. Then the solvent was evaporated in vacuo followed by three extractions with the appropriate organic solvent (EtOAc, DCM or ether) to isolate the crude product. The organic layer was dried using $MgSO_4$ as drying agent and filtered to remove $MgSO_4$. TLC was performed to establish the solvent system suitable for the purification of the target derivatives followed by column chromatography to afford the final compounds.

The characterization of purified derivatives were carried out by proton nuclear magnetic resonance (1HNMR) spectroscopy to establish and confirm the identity of derivatives. The purity (95% or greater) of the synthesized derivatives was confirmed by using LCMS or HPLC.

3.1.1 Synthesis of benzamide, *N*-benzyl and phenylethan-1-one substituted derivatives of amantadine, memantine and rimantadine (1a-l, 2a-l and 3a-l)

The benzamide, *N*-benzyl and phenylethan-1-one substituted derivatives were synthesized via alkylation of primary amine starting from either amantadine or memantine or rimantadine by using various substrates (unsubstituted benzoyl chloride, 3-or 4-nitrobenzoyl chloride, unsubstituted benzyl bromide, 3- or 4-bromobenzyl bromide, 3-or 4-nitrobenzyl chloride, acetophenone and 1-(4-nitrophenyl)ethan-1-one) to obtain **1a-l**, **2a-l** and **3a-l**. Figure 3.2 provides the chemical structures of the synthesized derivatives. The chemistry procedures to synthesize the derivatives are provided in the experimental section (Chapter 6).

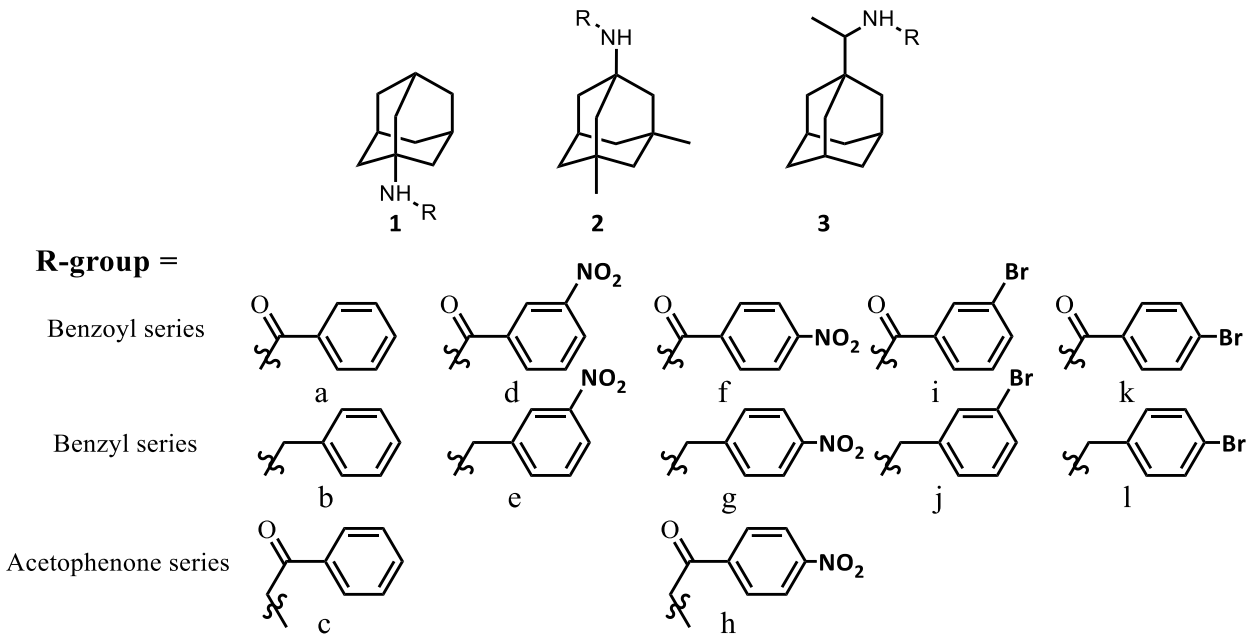

Figure 3.2: The synthesized benzamide, *N*-benzyl and phenylethan-1-one substituted derivative library.

Figure 3.3 outlines the underlying mechanism of the alkylation of amantadine with benzoyl chloride. Primary amines can react as nucleophiles with benzoyl chlorides via nucleophilic substitution (S_N2) to produce the target derivatives (benzamides). The reaction is also known as benzoylation or Schotten-Baumann reaction. The lone pair of electrons on the nitrogen (N) atom of amine attacks the electron deficient carbon (C) of benzoyl chloride as shown in Figure 3.3. In S_N2 reactions, the formation of the bond between N and C and the breaking of C-X bond occur simultaneously. These reactions generally use a base to quench the acid formed. Catalysts such as copper iodide (CuI) can enhance the reactivity of benzoyl chlorides. Figure 3.4 provides the 1HNMR spectra for amantadine (**1**) and **1a**. The addition of 5 aromatic protons (6-8 ppm) confirms the formation of the desired derivative **1a**.

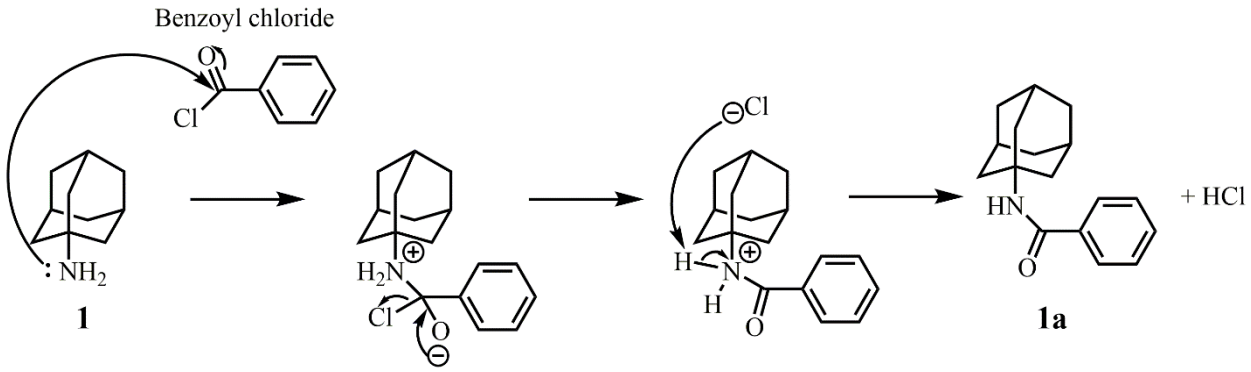

Figure 3.3: An example of mechanism used to couple various R groups to the aminoadamantane scaffold (benzoyl chloride and amantadine respectively in this example).

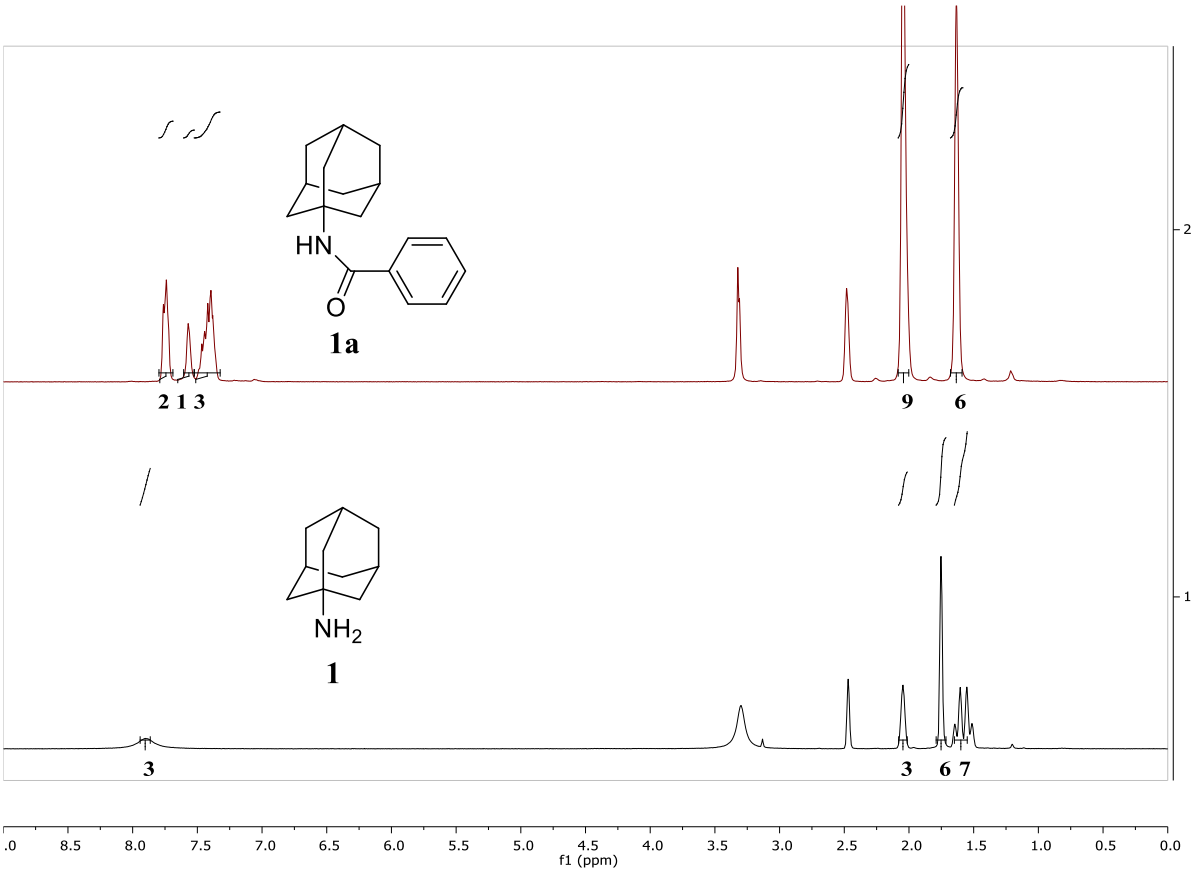

Figure 3.4: Sample 1HNMR spectra for amine alkylation of amantadine (**1**) by benzoyl chloride to obtain **1a** (in DMSO-d_6).

3.1.2 Synthesis of aminobenzamide and aminobenzyl derivatives of amantadine, memantine and rimantadine

The desired aminobenzamide and aminobenzyl derivatives were synthesized by the reduction of **1d**, **f**, **g**; **2d**, **e**, **f** and **3d**, **e**, **f** to generate **1m**, **n**, **p**; **2m**, **n**, **o** and **3m**, **n**, **o** . Figure 3.5 provides the chemical structures of the synthesized derivatives. The chemistry procedures to synthesize the derivatives are provided in Chapter 6.

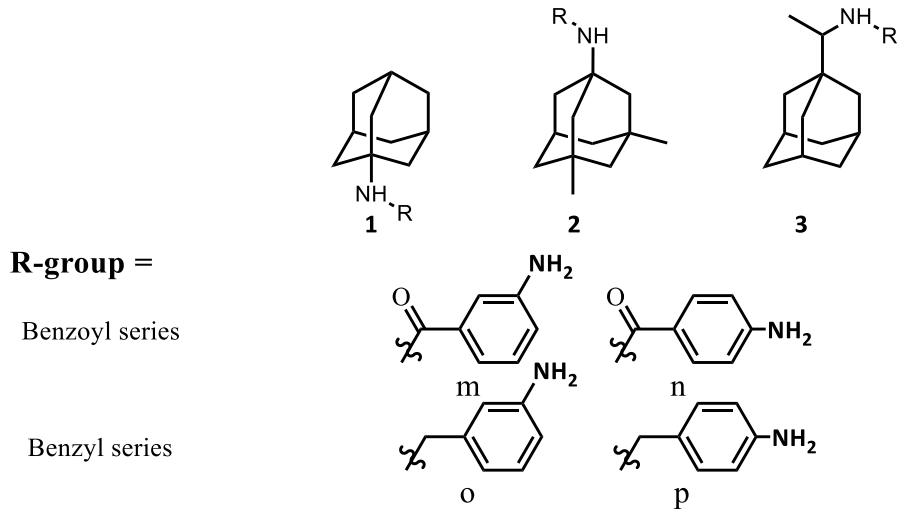

Figure 3.5: The synthesized aminobenzamide and aminobenzyl derivative of adamantane.

To obtain the desired final products carrying either an aminobenzamide or aminobenzyl substituents, the reduction of nitro functional group to amine was carried out using hydrazine hydrate ($N_2H_4.H_2O$) as reducing agent. $N_2H_4.H_2O$ can form hydrogen (H^+) and nitrogen gas (N_2) in presence of palladium (Pd/C) to facilitate the reduction process. Pd acts as the source of electrons and $N_2H_4.H_2O$ is the source of H^+, where in the first step nitro group is reduced to nitrosogroup. Hydroxylamine is generated in the second step via reductive addition of two H^+ atoms to nitroso. In final step, amine is formed from hydroxylamine (Figure 3.6). Figure 3.7 shows the 1HNMR

spectra of desired amine compound **1n** from its precursor nitro compound **1f**. The addition of 2 hydrogens at 5.5 ppm along with the shift in aromatic region confirms the formation of **1n**.

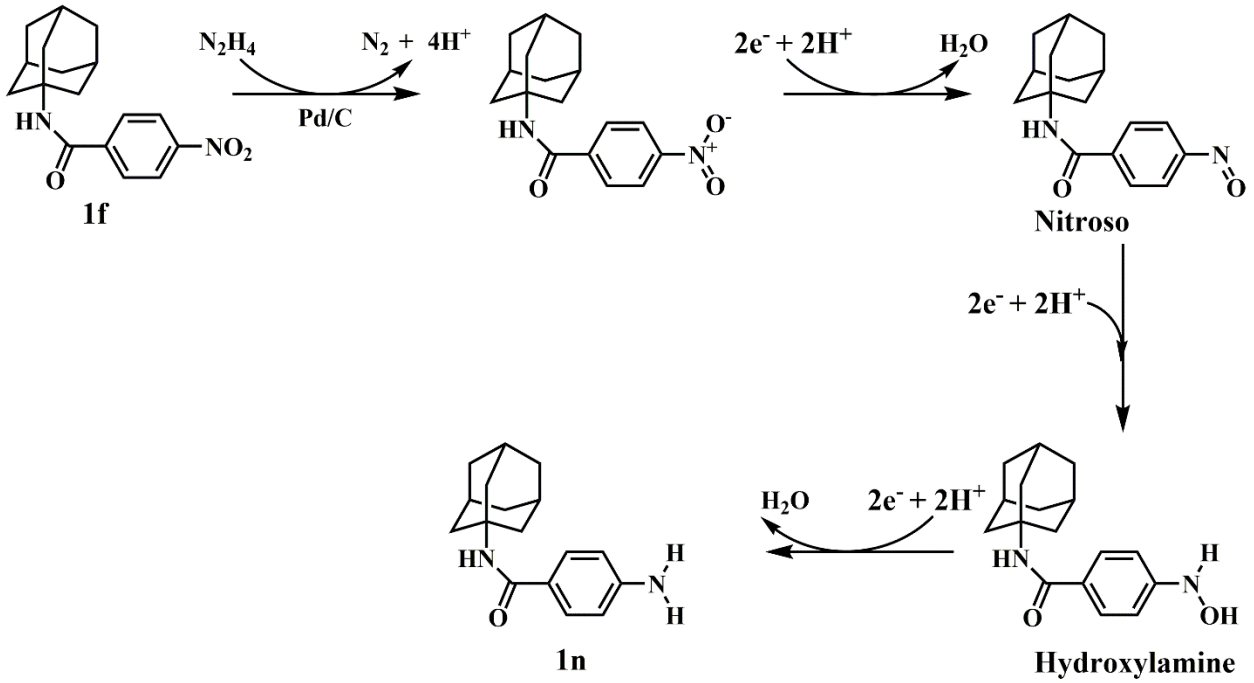

Figure 3.6: Mechanism involved in the reduction of nitro functional group on **1f** to amine **1n**.

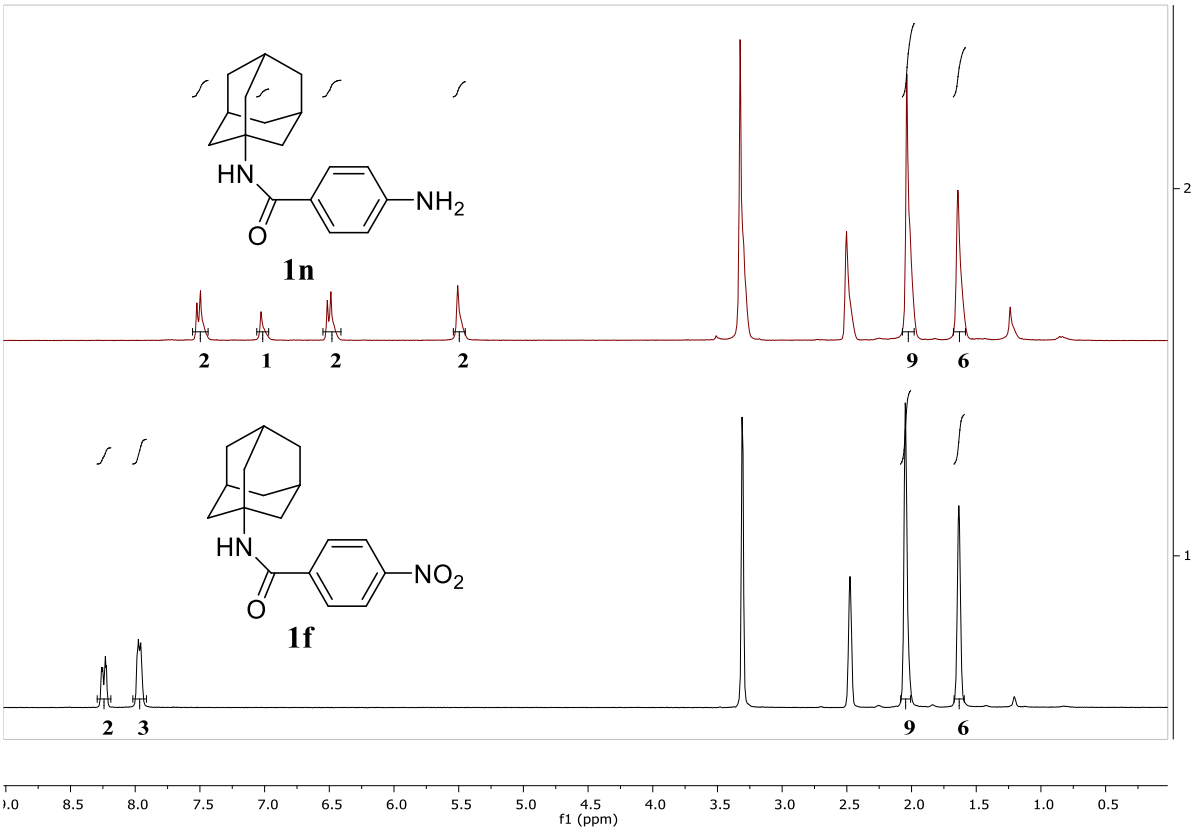

Figure 3.7: 1HNMR spectra for the reduction of nitro functional group on **1f** to amine to obtain **1n** (in DMSO-d_6).

3.1.3 Synthesis of azidobenzamide derivatives of amantadine, memantine and rimantadine

The desired azidobenzamide derivatives were synthesized by nucleophilic substitution of bromide on **1i**, **k**; **2i**, **k** and **3i**, **k** to azide to produce **1q**, **s**; **2q**, **s** and **3q**, **s**. Figure 3.8 provides the chemical structures of the synthesized derivatives. The chemistry procedures to synthesize these derivatives are provided in Chapter 6.

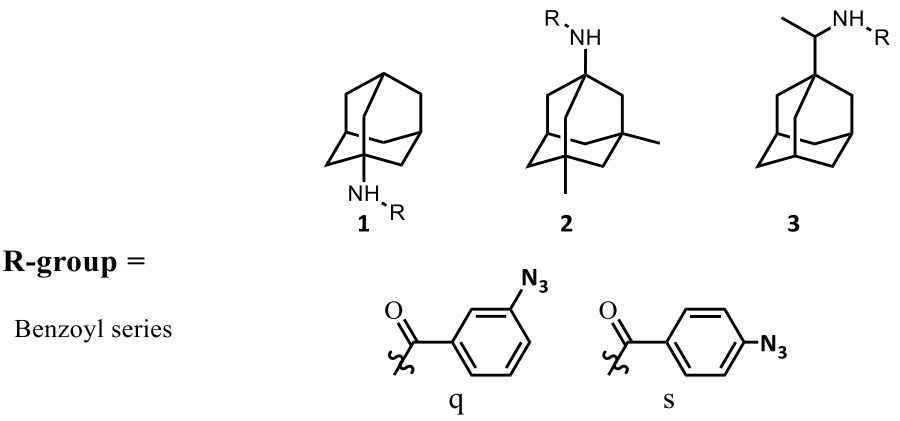

Figure 3.8: The synthesized azidobenzamide derivatives.

Synthesis of desired azide compounds from their precursor bromide compounds is a classic example of nucleophilic substitution where azide ion (N_3) acts as a nucleophile to replace bromide substituent on the aromatic ring. Sodium azide is the source of azide ion in the reaction where sodium scavenge the bromide ion (Br^-) to form sodium bromide (NaBr). The reaction proceeds in a single step where azide ion attacks the electron deficient carbon next to the bromine atom. (Figure 3.9). The ^{1}HNMR spectra of the desired azide compound **2s** from its precursor bromide compound **2k** is shown in Figure 3.10. The significant shift in the aromatic regions along with mass spectroscopy confirms the formation of **2s.**

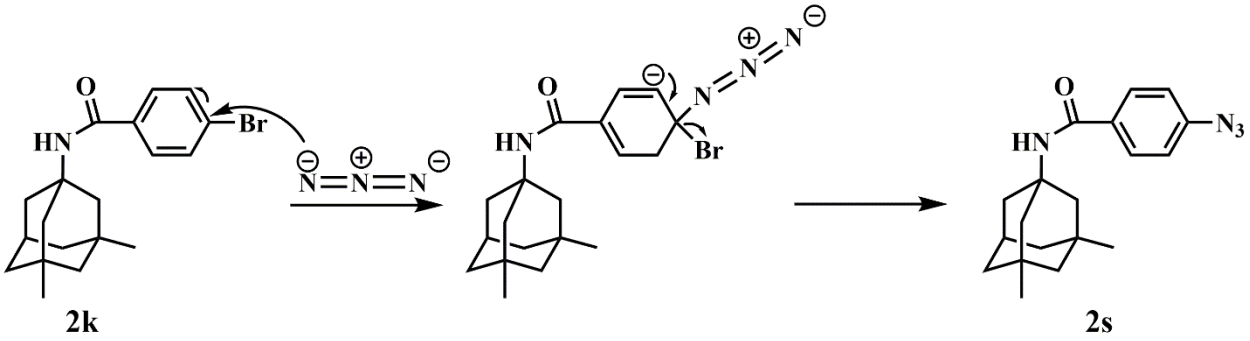

Figure 3.9: Sample 1HNMR spectra of nucleophilic substitution of bromide by azide to produce the desired derivative **2s** from **2k**.

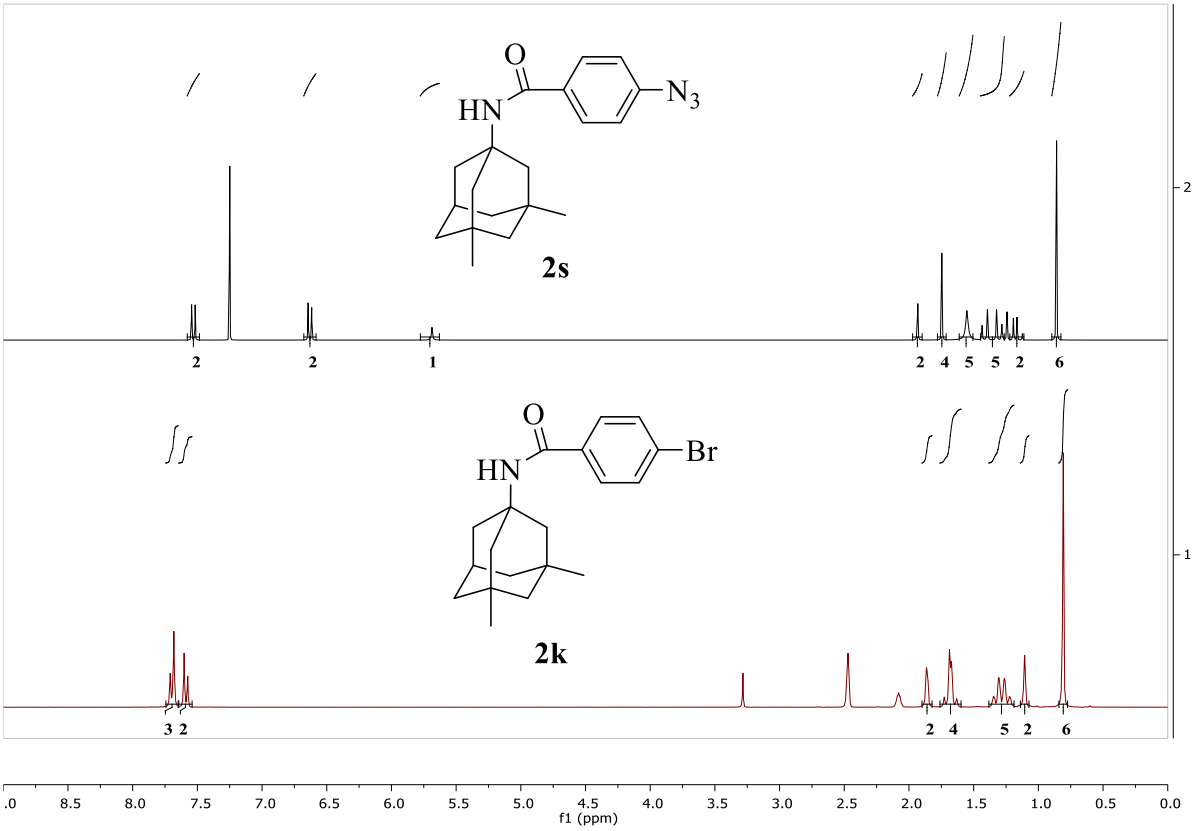

Figure 3.10: 1HNMR spectra of nucleophilic substitution of bromide by azide to produce the desired derivative **2s** from **2k (2k** in DMSO-d_6 and **2s** in $CDCl_{3)}$.

3.2 Biological Assays

3.2.1 Amyloid Aggregation Kinetics

The biological activities of synthesized compounds will be evaluated using Aβ40 and Aβ42 anti-aggregation assays. Aβ assay is a thioflavin T (ThT), based kinetic fluorescence method which is run at pH 7.4 at 37 °C. The fluorescence excitation and emission of ThT is monitored and the change in excitation-emission, due to conformational change of ThT, is detected upon interaction of ThT with β-sheet formation of Aβ oligomers and fibrils.[147] The interactions between ThT and Aβ fibrils result in a linear fluorescence shift from 385-446 nm to 450-490 nm, allowing to quantify the aggregation of Aβ monomers in real time (Figure 3.11). Compounds with anti-aggregation

properties promote free ThT which is indicated by the lower relative fluorescence units (RFU) values whereas compounds with pro-aggregation properties result in higher RFU values in comparison with Aβ control.

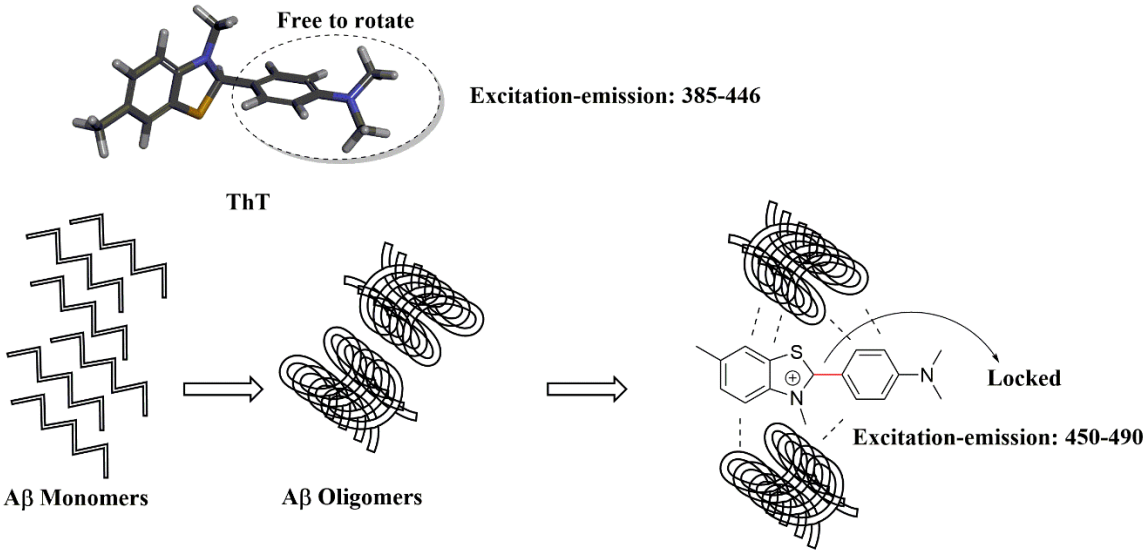

Figure 3.11: ThT-Aβ oligomers interaction in Aβ kinetic assay.

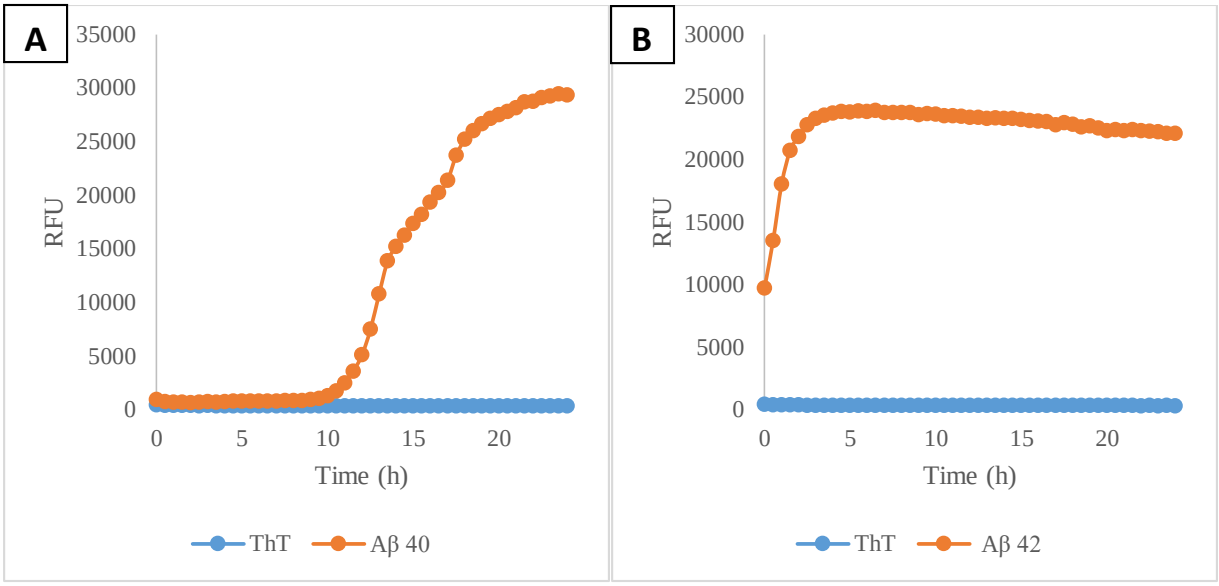

Figure 3.12: A typical ThT monitored A) Aβ40 aggregation plot, B) Aβ42 aggregation plot. The lag phase only observed in Aβ40 aggregation and ends at the start of aggregation slope. The plateau phase is observed in both Aβ40/42 aggregation plot where the peptide is mainly in the fibril form.

The following set of aggregation kinetics and imaging experiments were carried out on the synthesized adamantane derivatives:

1- Self-induced Aβ40 aggregation kinetic assay for all derivatives
2- Self-induced Aβ42 aggregation kinetic assay for selected derivatives with anti-aggregation properties toward Aβ40
3- TEM imaging to study the morphology of Aβ 40/42 for derivatives with anti-aggregation properties toward both Aβ 40/42
4- Structure-activity relationship (SAR) study on the lead derivatives

3.2.2 Transmission Electron Microscopy (TEM)

Transmission electron microscopy (TEM) is a common technique used in various fields to obtain high resolution images from a sample. In context of this research, the morphology of Aβ was studied at the conclusion of a 24 hour incubation period of the lead derivatives with Aβ 40. Derivatives with inhibitory properties against Aβ 40 decrease the density of Aβ fibrils compared to Aβ control. It also provides a quantitative method to further confirm the SAR data gathered from biological assays. The experimental setup is provided in chapter 6.

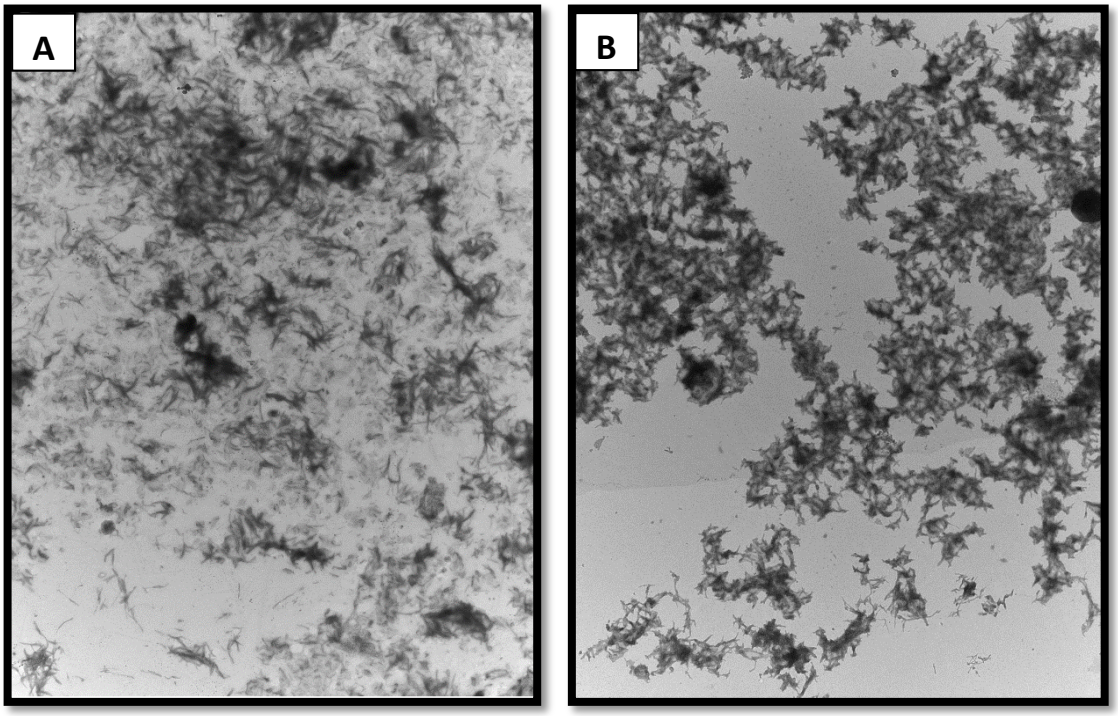

Figure 3.13: TEM imaging of : A) Aβ 40 fibrils, B) Aβ 42 fibrils.

3.3 Conclusion

The alkylation of primary of amantadine, memantine and rimantadine by benzoyl and benzyl series (Figure 28) were straightforward with relatively decent yields in general, however coupling the acetophenone series with the start materials (1, 2, 3) proved to be challenging with limited

success and low yields. The aminobenzamide and aminobenzyl derivatives (Figure 31) were synthesized with relative ease and high yields in general. Finally, the nucleophilic substitution of bromide by azide proved to be more challenging than initially anticipated with low yields and stability of the azido-substituted derivatives hindering the synthesis of the entire library. A total of 48 derivatives were synthesized, identified, characterized and assayed against Aβ 40 and 42.

Chapter 4: Results and Discussion

4.1 Structure-Activity Relationship (SAR) studies

The anti-aggregation potential of the synthesized derivatives were measured by the ThT based kinetic assay explained in the previous chapter (section 3.2). Test compounds were evaluated at 1,

5, 25 μM concentrations in triplicates in the presence of Aβ40/42 (5 μM). The obtained IC_{50} values were compared with the standard controls, orange G and resveratrol, and the adamantane scaffolds, **1**, **2** and **3**. The obtained SAR data is divided into three sections based the three adamantane scaffolds. This chapter describes the SAR data acquired and discusses the ability of synthesized derivatives to prevent Aβ aggregation.

4.1.1 Amantadine (1) based derivatives SAR

Table 4.1: Inhibition data for amantadine (**1**) based derivatives on self-induced Aβ40/42 aggregation.

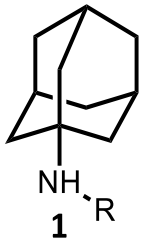

1

Compound	R	IC_{50} (μM)[a] Aβ40	Aβ42	ClogP[b]
Amantadine	-	N.A	N.A	2.00
1a	Benzoyl	P.A	-	3.52
1b	Benzyl	N.A	-	4.17
1c	Acetophenone	4.3	>50	3.54
1d	3-Nitrobenzoyl	P.A	-	3.70
1e	3-Nitrobenzyl	P.A	-	3.91
1f	4-Nitrobenzoyl	P.A	-	3.70
1g	4-Nitrobenzyl	P.A	-	3.91
1i	3-Bromobenzoyl	P.A	-	4.58

1j	3-Bromobenzyl	P.A	-	5.03
1k	4-Bromobenzoyl	P.A	-	4.58
1l	4-Bromobenzyl	P.A	-	5.03
1m	3-Aminobenzoyl	N.A	>50	2.61
1n	4-Aminobenzoyl	2.9	>50	2.61
1p	4-Aminobenzyl	N.A	N.A	2.94
1q	3-Azidobenzoyl	P.A	-	4.22
1s	4-Azidobenzoyl	P.A	-	4.22
Orange G	-	3.2	8.8	-0.63
Resveratrol	-	2.8	4.1	2.83

[a]The calculated IC_{50} values are the mean values of triplicate readings for two independent experiments. The values are based on the ThT-based fluorescence assay. N.A = Not Active (less than 10% inhibition), P.A = Promotes Aggregation. [b]The ClogP values were determined using *ChemBioDraw Ultra 14.0.* CambridgeSoft Company.

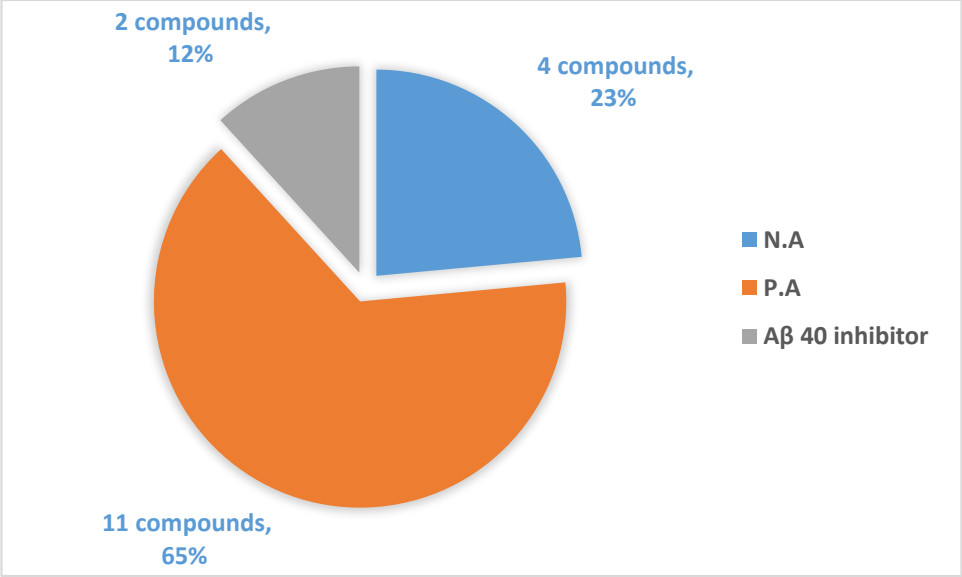

Figure 4.1: Summary of inhibition data for 17 amantadine (**1**) based derivatives on self-induced Aβ40 aggregation. N.A = Not Active, P.A = Promotes Aggregation.

Surprisingly most of the amantadine based derivatives exhibited pro-aggregation activity toward Aβ40 as presented in Table 4.1. The unsubstituted **1a** derivative promoted the aggregation of Aβ40 by 36% at 25 μM, however the **1b** derivative did not exhibit any inhibition for Aβ40. Interestingly only compounds **1c** and **1n** exhibited anti-aggregation activity toward Aβ40 where **1c** exhibited an IC_{50} value of 4.3 μM toward Aβ40 with similar potency compared to the reference agents orange G (3.2 μM) and resveratrol (2.8 μM). However it was not effective against Aβ42 (IC_{50} > 50 μM) compared to the reference agents orange G (8.8 μM) and resveratrol (4.1 μM). The addition of electron withdrawing (EWG) nitro functional group at *meta*- (3) position on **1d** promoted the aggregation of Aβ40 by more than 3 folds compared to **1a**. A similar pattern was observed for **1e**. Interestingly, moving the nitro group to *para*- (4) position in **1f** exhibited pro-aggregation activity at lower concentrations of 1 μM (60%) and 5 μM (31%). At 25 μM it was ineffective against Aβ40. Moving the nitro group to *para*- position on **1g** yielded similar results compared to **1e**. The addition of EWG bromo was detrimental to anti-aggregation activity of

derivatives **1i**, **1j**, **1k** and **1l** regardless of *meta*- or *para*- positioning where the derivatives promoted the aggregation of Aβ40 up to 5 folds at all tested concentrations as illustrated in Figure 4.2 (kinetic data is provided for **1i** as an example).

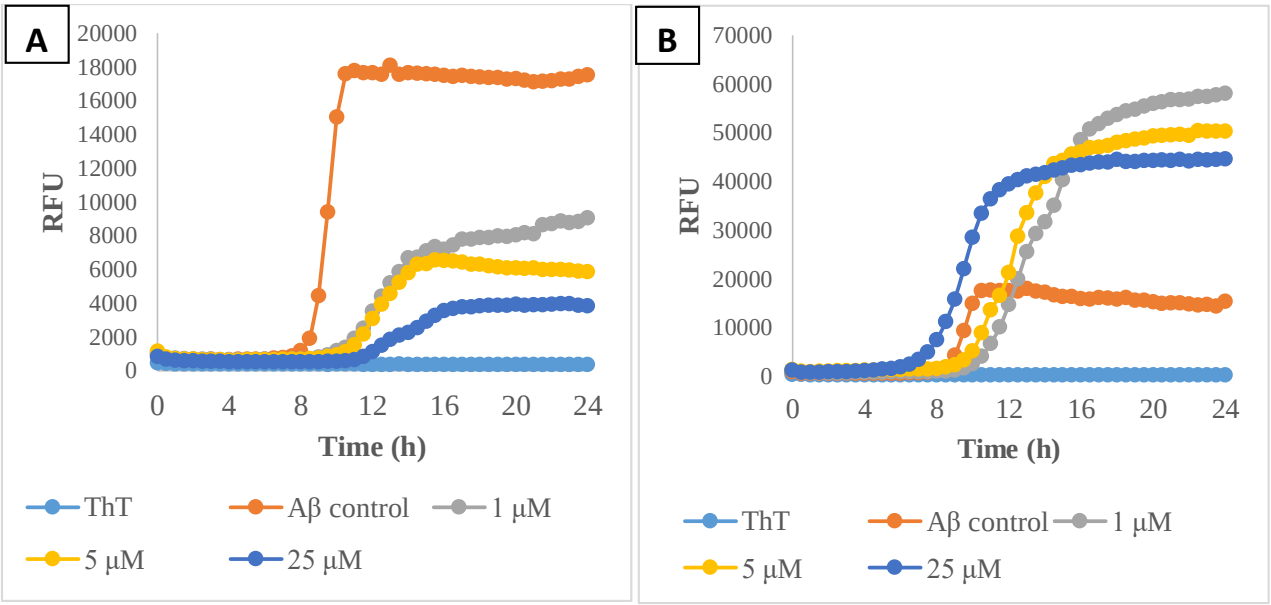

Figure 4.2: ThT-based Aβ40 aggregation kinetic data at 37 °C, at pH 7.4, 24 h. Panels: (A) Resveratrol, (B) **1i**. Results are expressed as average of two independent experiments (n =3).

The addition of amine functional group on **1m**, **1n** and **1p** yielded mixed inhibitory activity against Aβ40 aggregation. With amino group at *meta*-position in **1m** and *para*-position in **1p**, both derivatives failed to inhibit the aggregation of Aβ40 and Aβ42 at the tested concentrations. Compound **1n** was identified as the most potent Aβ40 inhibitor in the amantadine based derivatives (IC_{50} = 2.9 μM) with similar activity as reference agents. This indicates that amine group enhances the Aβ40 inhibition at *para*- position compared to **1m** and unsubstituted **1a**. The effect of electron donating group (EDG) of azide was investigated in derivatives **1q** and **1s**. The presence of azide on *meta*- or *para*- position of **1q** and **1s** respectively promoted the aggregation of Aβ40 by 42% and 98% at 25 μM. None of the compounds in this series exhibited any activity towards Aβ42.

4.1.2 Top candidates from the amantadine (1) based derivatives

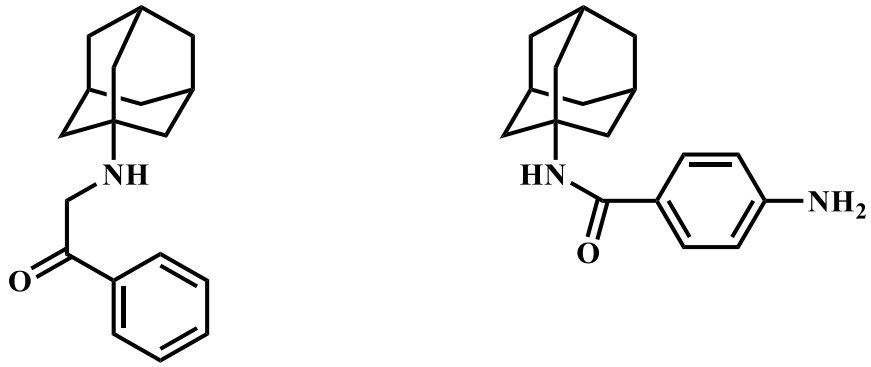

1c **1n**

Aβ40 IC_{50} = 4.3 μM **Aβ40 IC_{50} = 2.9 μM**

Figure 4.3: Compounds with anti-Aβ40 activity in the amantadine based series.

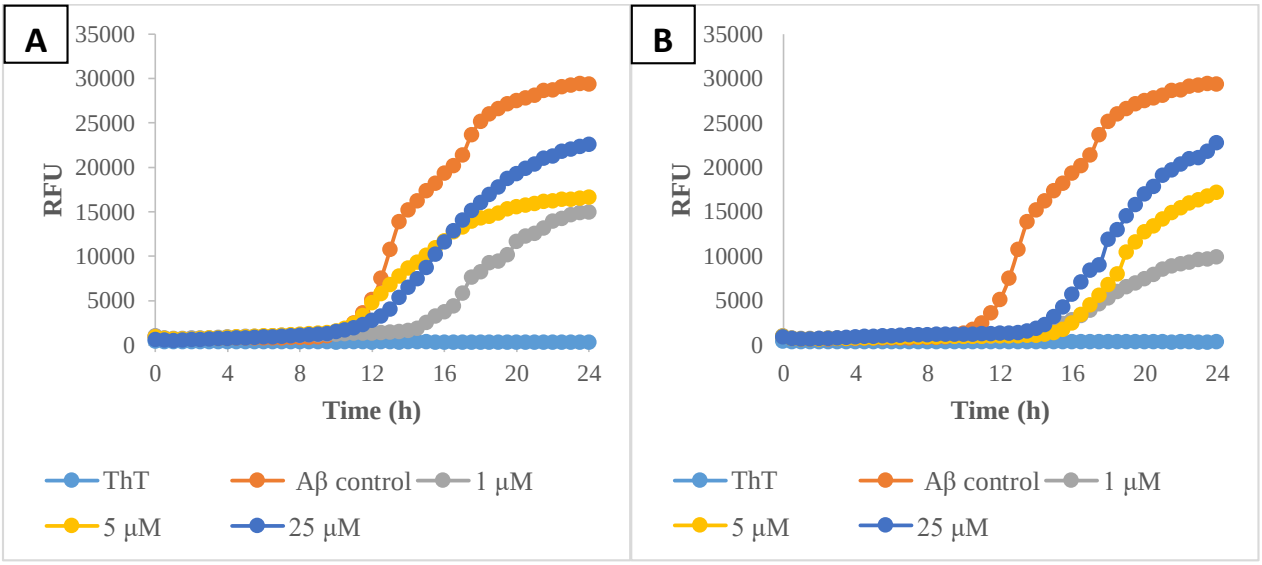

Figure 4.4: ThT-based Aβ40 aggregation kinetic data at 37 °C, at pH 7.4, 24 h. Panels: (A) **1c**, (B) **1n**. Results are expressed as average of two independent experiments (n =3).

The aggregation kinetic data for derivative **1c** (Figure 4.4 panel A) demonstrates that the compound inhibits the aggregation of Aβ40 at all tested concentrations. However its efficacy decreases as the concentration increases. Compound **1c** showed 55%, 43% and 23% inhibition at 1,

5 and 25 μM concentrations respectively. At 1 μM, **1c** was also able to delay the aggregation process by 1.5 fold, however it wasn't able to shift the lag phase at higher concentrations.

Similar pattern was observed with **1n**, where **1n** exhibited 66%, 41% and 22% inhibition at 1, 5 and 25 μM concentrations respectively. At 1 μM, **1n** showed superior anti-aggregation activity compared to reference agent resveratrol with 35% inhibition. However it was less potent at 5 and 25 μM (52% and 81% respectively). **1n** also delayed the aggregation process by 1.5 fold at all tested concentrations, shifting the lag phase to 15 hour mark compared to 10 hour with Aβ control.

4.1.3 Molecular modeling study of the lead candidate (1n)

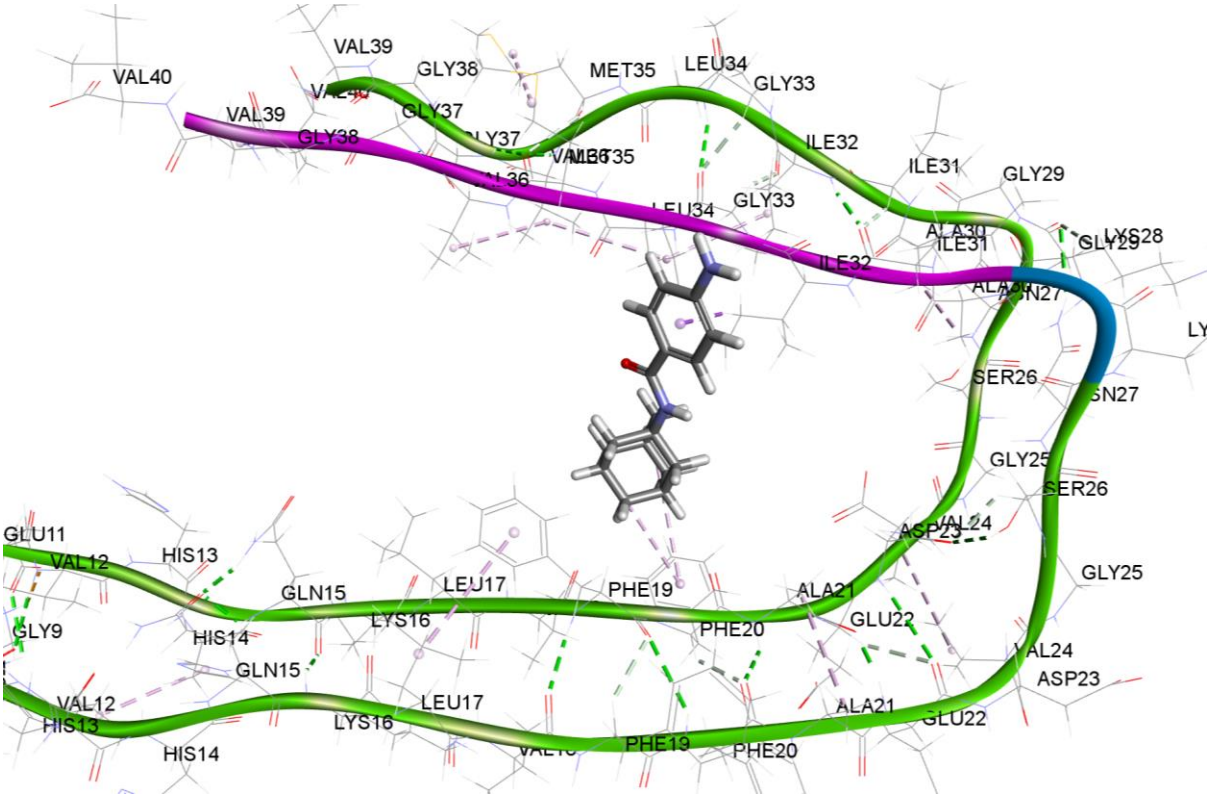

Figure 4.5: Docking of **1n** in the Aβ dimer (PDB id: 2LMN) model.

The binding mode of Aβ40 aggregation inhibitor **1n** was investigated in the Aβ dimer model. The modeling study showed that the amantadine hydrophobic core was close to KLVFFA segment of the peptide to form two hydrophobic pi-alkyl interactions with Phe20 at 4.43 Å and 5.17 Å as shown in Figure 4.5. The aromatic ring of **1n** was able to form a strong pi-sigma hydrophobic interaction with **Ile32** at 2.86 Å. The amino group at the *para*- position was also able to form two relatively strong hydrogen bondings with ile32 at 4.21 Å and 4.60 Å respectively. The hydrogen bondings of **1n** along with the other hydrophobic interactions stabilize the dimer structure and contribute to its superior anti-aggregation activity compared to **1c**.

Majority of the compounds in this series were promoting Aβ40 aggregation which proves that our hypothesis doesn't hold true. It appears that the adamantane based derivatives might

promote Aβ40 aggregation by acting as small molecule chaperones and change the conformation of Aβ40 which forces β-sheet formation and fibril assembly. This could be an advantage as Aβ fibrils are known to be less toxic compared to Aβ oligomers. In a hypothetical scenario, amantadine derivatives might in fact convert the more toxic Aβ oligomers into less toxic fibrils. The exact molecular mechanisms involved needs an in-depth study.

4.1.4 Memantine (2) based derivatives SAR

Table 4.2: Inhibition data for memantine (**2**) based derivatives against self-induced Aβ40/42 aggregation.

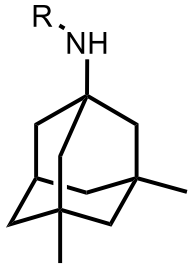

2

Compound	R	IC_{50} (μM) [a] Aβ40	Aβ42	ClogP[b]
Memantine	-	N.A	N.A	3.0
2a	Benzoyl	P.A	-	4.56
2b	Benzyl	P.A	-	5.21
2c	Acetophenone	P.A	-	4.57
2d	3-Nitrobenzoyl	P.A	-	4.73
2e	3-Nitrobenzyl	P.A	-	4.95
2f	4-Nitrobenzoyl	P.A	-	4.73

2g	4-Nitrobenzyl	P.A	-	4.95
2i	3-Bromobenzoyl	P.A	-	5.62
2j	3-Bromobenzyl	23.8	N.A	6.07
2k	4-Bromobenzoyl	P.A	-	5.62
2l	4-Bromobenzyl	1.8	>50	6.07
2m	3-Aminobenzoyl	5.5	N.A	3.65
2n	4-Aminobenzoyl	0.4	N.A	3.65
2o	3-Aminobenzyl	P.A	-	3.98
2q	3-Azidobenzoyl	P.A	-	5.26
2s	4-Azidobenzoyl	P.A	-	5.26
Orange G	-	3.2	8.8	-0.63
Resveratrol	-	2.8	4.1	2.83

[a]The calculated IC_{50} values are the mean values of triplicate readings for two independent experiments. The values are based on the ThT-based fluorescence assay. n.a = not active, P.A = promotes aggregation. [b]The ClogP values were determined using *ChemBioDraw Ultra 14.0.* CambridgeSoft Company.

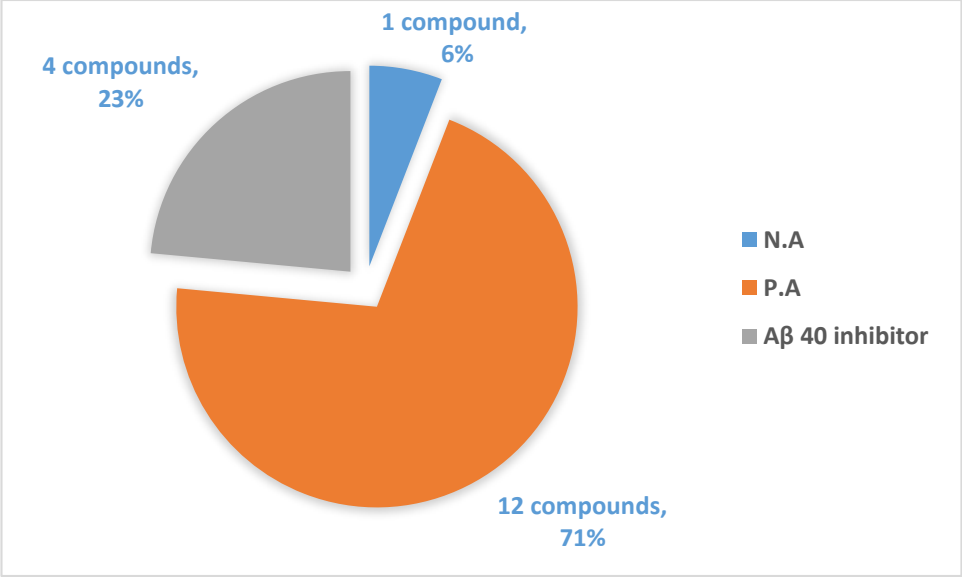

Figure 4.6: Summary of inhibition data for 17 memantine (**2**) based derivatives against self-induced Aβ 40. N.A = Not Active, P.A = Promotes Aggregation.

Memantine based derivatives inhibitory activity against Aβ aggregation ranges from anti- to pro-aggregation as summarized by Table 4.2. The unsubstituted **2a**, **2b** and **2c** derivatives promoted the aggregation of Aβ40 in a concentration dependent manner especially in case of **2a** by 2.5 folds. The addition of nitro substituent in **2d**, **2e**, **2f** and **2g** derivatives also promoted the aggregation of Aβ40 in a concentration dependent manner. This observation was further investigated and confirmed by molecular modeling studies of the derivatives where they de-stabilized the Aβ40 dimer structure, facilitating the aggregation process.

Interestingly unlike amantadine based derivatives, the addition of bromo in **2j** and **2l** exhibited inhibitory properties with IC_{50} values of 23.8 µM and 1.8 µM respectively. Compound **2l** significantly more potent (13.2 folds) compared to **2j** suggesting that the *para*- position of bromo compared to *meta*- position enhances the inhibitory activity. Compound **2l** also exhibited superior IC_{50} value compared to both references compounds orange G and resveratrol (IC_{50} = 3.2 µM and

2.8 μM respectively). Surprisingly, both **2i** and **2k** promoted the aggregation at all tested concentrations.

Compound **2n** (IC_{50} = 0.4 μM) was identified as the most potent Aβ40 inhibitor in the memantine based derivatives with amino group at *para*- position, although it was not active against Aβ42. Moving the amino to *meta*- position diminished the inhibitory activity of **2m** (IC_{50} = 5.5 μM) by more than 13 folds. The **2o**, **2q** and **2s** derivatives promoted Aβ40 aggregation. None of the compounds in this series exhibited activity toward Aβ42.

4.1.5 Top candidates from the memantine (2) based derivatives

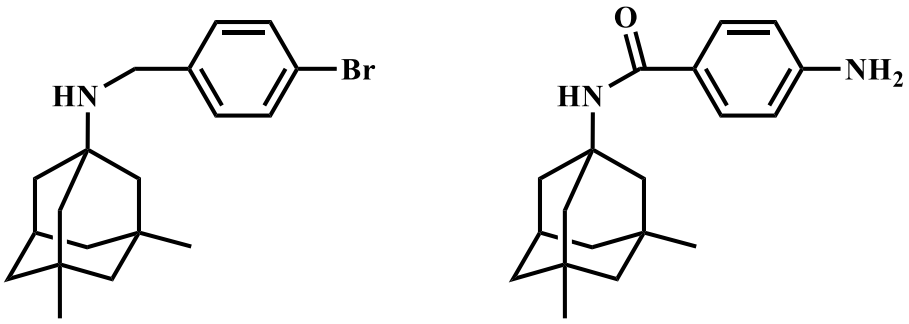

2l **2n**

Aβ40 IC_{50} = 1.8 μM **Aβ40 IC_{50} = 0.4 μM**

Figure 4.7: Compounds with anti-Aβ40 activity in the memantine based series.

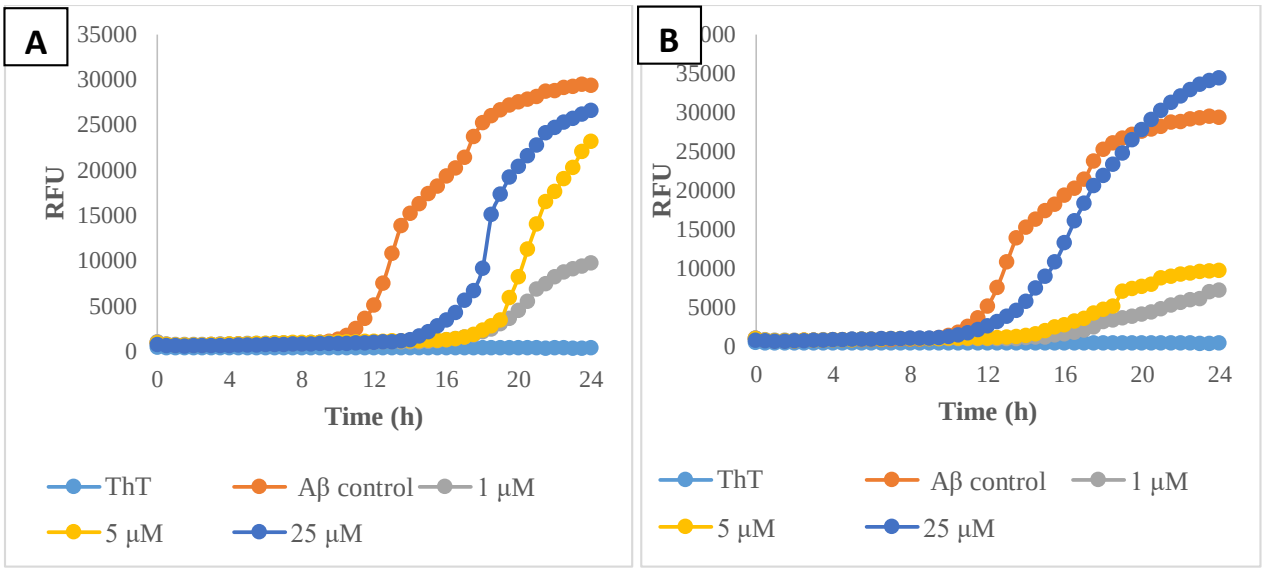

Figure 4.8: ThT-based Aβ40 aggregation kinetic data at 37 °C, at pH 7.4, 24 h. Panels: (A) **2l**, (B) **2n**. Results are expressed as average of two independent experiments (n =3).

As illustrated by Figure 4.8, the 4-bromobenzyl derivative (**2l**) inhibited the aggregation of Aβ40 and showed superior inhibition of 67% at 1 μM compared to the both references orange G and resveratrol at 21% and 35%. However it was less potent at 5 μM and 25 μM concentrations with 21% and 9% inhibition, respectively. Both the reference compounds exhibited a concentration-dependent inhibition against Aβ40 unlike **2l** and **2n** derivatives. Compound **2l** was also able to shift the lag phase to the right even at highest tested concentration delaying the aggregation by 1.6 fold.

The 4-aminobenzoyl derivative (**2n**) was even more potent than **2l**, exhibiting superior inhibition at 1 μM and 5 μM with 76% and 67% inhibition and hindering the aggregation process by stabilizing the early formed intermediates as evident by Figure 4.8 (panel B). At 5 μM, it was more potent than orange G with 53% inhibition and resveratrol with slightly weaker inhibition at 64%. Interestingly, at 25 μM **2n** promoted the aggregation of Aβ40 by 17%.

4.1.6 Molecular modeling studies of the lead candidates (2l and 2n)

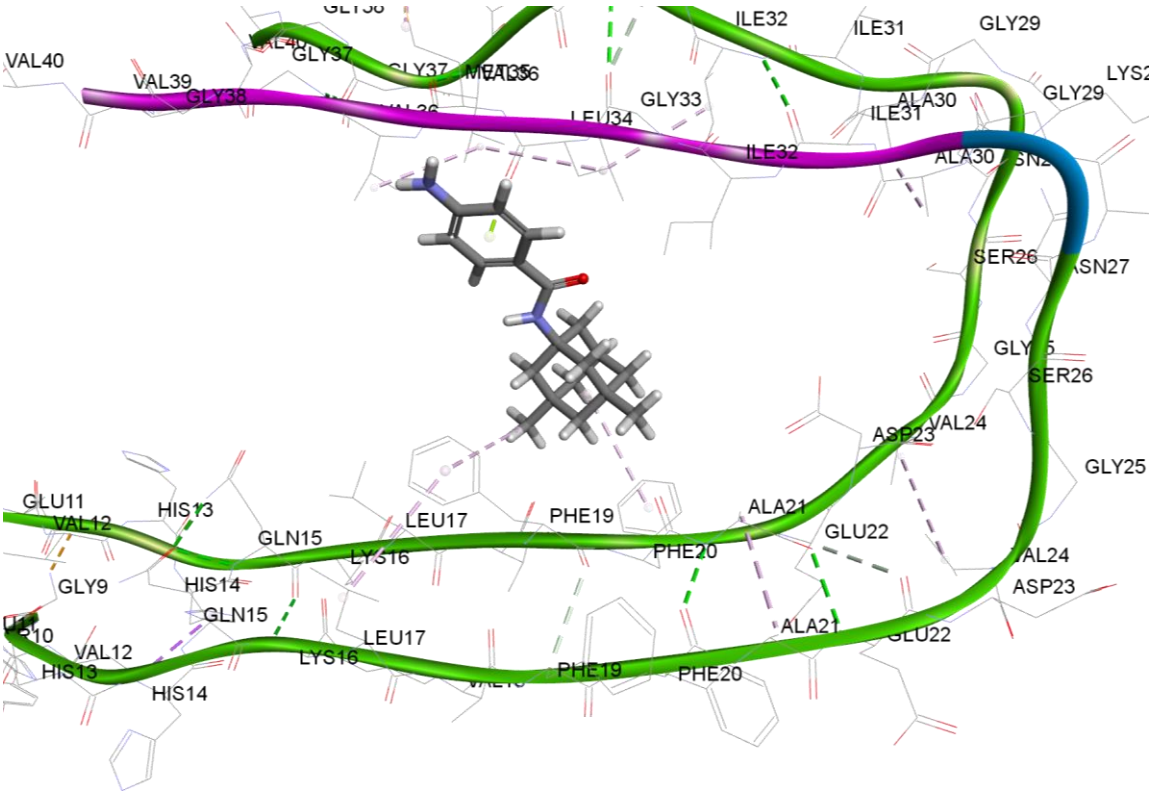

Figure 4.9: Docking of **2n** in the Aβ dimer (PDB id: 2LMN) model.

The binding mode of **2n** in Aβ dimer model demonstrates that its memantine core was oriented towards KLVFFA segment to form a relatively strong pi-alkyl hydrophobic interaction with Phe20 at 5.14 Å. One of the methyl groups attached to the core also forms a slightly weaker pi-alkyl hydrophobic interaction with Phe19 at 5.33 Å. The aromatic ring of **2n** is close to oxygen on Leu34 to provide a strong pi-lone pair interaction at 2.94 Å. The amino group at the *para*-position is also close enough to oxygen on Val36 to form two hydrogen bondings at 3.17 Å and 4.27 Å respectively. This observation is in agreement with the Aβ assay data confirming that **2n** stabilize the dimer and early formed intermediates and slows the rate of aggregation.

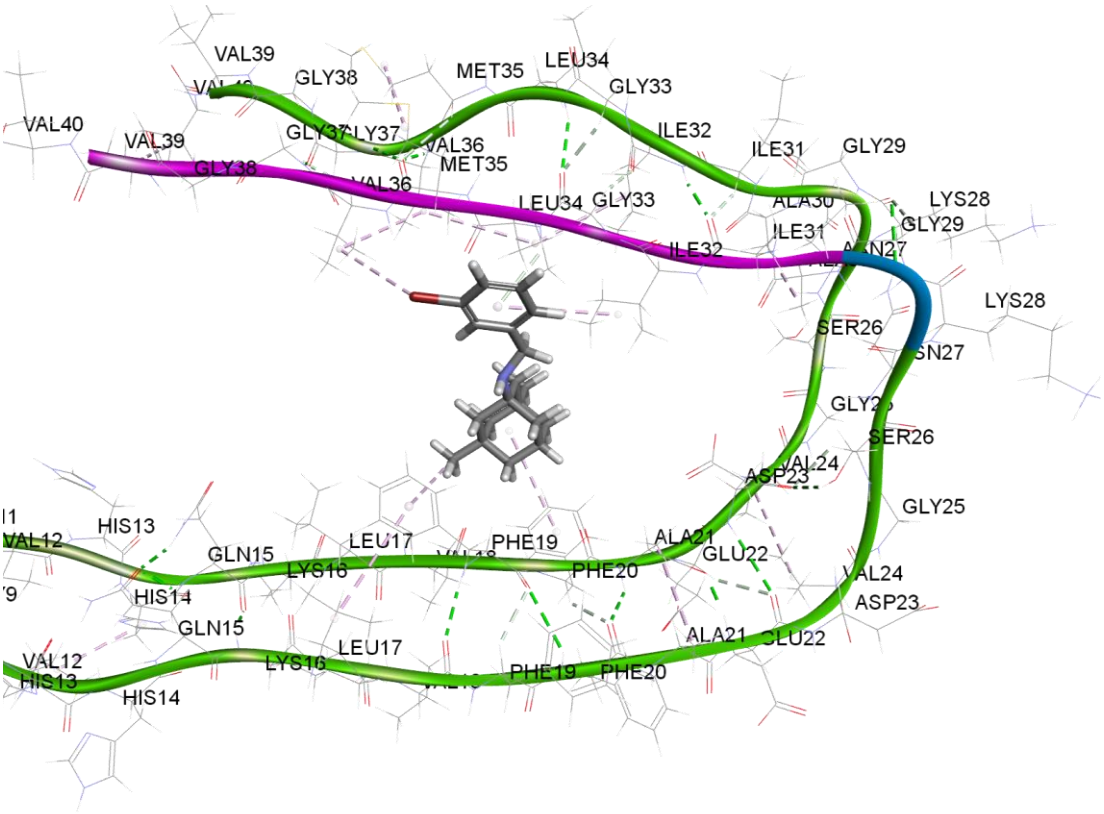

Figure 4.10: Docking of **2l** in the Aβ dimer (PDB id: 2LMN) model.

The binding mode of **2l** with Aβ dimer model is provided in Figure 4.10. Similar to **2n**, the memantine core is oriented towards KLVFAA segment, making two hydrophobic pi-alkyl interactions at 5.26 Å with Phe20 and at 4.92 Å with Phe19. The aromatic rings undergoes two hydrophobic pi-alkyl interactions at 5.50 Å with Ile32 and at 3.20 Å with Leu34. The bromo substituent at *para*- position is close to Val36 where it forms a hydrophobic interaction at 4.71 Å. Overall this derivative exhibited a number of hydrophobic interactions with the dimer structure allowing it to inhibit the aggregation of Aβ.

The aggregation kinetics and modeling studies show that memantine based derivatives predominantly are capable of promoting Aβ40 aggregation. Molecular docking studies using Aβ dimer model shows that these compounds form a high energy complex with Aβ suggesting their

inability to stabilize the dimer assembly. However four compounds in this series (**2j**, **2l**, **2m** and **2n**) were able to prevent Aβ40 aggregation with **2n** identified as a potent inhibitor which was 8-fold more potent compared to orange G.

4.1.7 Rimantadine (3) based derivatives SAR

Table 4.3: Inhibition data for rimantadine (**3**) based derivatives against self-induced Aβ40/42 aggregation.

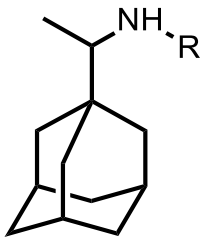

3

Compound	R	IC_{50} (μM) [a] Aβ40	Aβ42	ClogP[b]
Rimantadine	-	N.A	N.A	3.90
3a	Benzoyl	P.A	-	5.49
3b	Benzyl	P.A	-	6.14
3d	3-Nitrobenzoyl	P.A	-	5.66
3e	3-Nitrobenzyl	P.A	-	5.88
3f	4-Nitrobenzoyl	P.A	-	5.66
3g	4-Nitrobenzyl	P.A	-	5.88
3h	4-Nitroacetophenone	N.A	N.A	5.41
3i	3-Bromobenzoyl	P.A	-	6.55

3j	3-Bromobenzyl	P.A	-	7.00
3k	4-Bromobenzoyl	P.A	-	6.55
3l	4-Bromobenzyl	P.A	-	7.00
3m	3-Aminobenzoyl	5.5	N.A	4.58
3n	4-Aminobenzoyl	1.8	N.A	4.58
3o	3-Aminobenzyl	P.A	-	4.91
3p	3-Azidobenzoyl	P.A	-	6.19
3s	4-Azidobenzoyl	P.A	-	6.19
Orange G	-	3.2	8.8	-0.63
Resveratrol	-	2.8	4.1	2.83

[a]The calculated IC_{50} values are the mean values of triplicate readings for two independent experiments. The values are based on the ThT-based fluorescence assay. N.A = Not Active, P.A = Promotes Aggregation. [b]The ClogP values were determined using *ChemBioDraw Ultra 14.0.* CambridgeSoft Company.

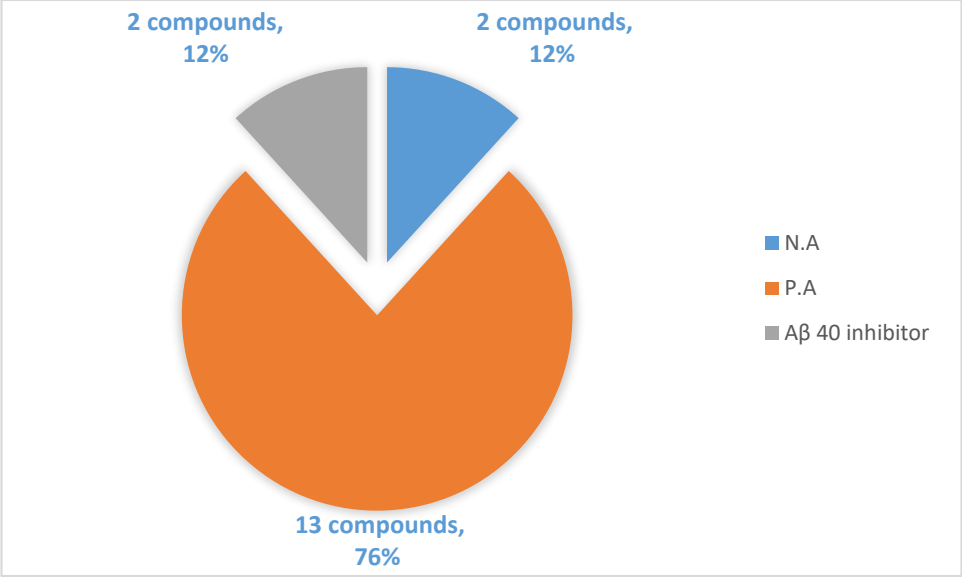

Figure 4.11: Summary of inhibition data for 17 rimantadine (**3**) based derivatives against self-induced Aβ40. N.A = Not Active, P.A = Promotes Aggregation.

Rimantadine based derivatives generally promoted Aβ40 aggregation with derivatives **3m** and **3n** exhibiting aggregation inhibition at 5.5 and 1.8 μM as provided in Table 4.3. It is worth mentioning that none of the three derivatives (**3h**, **3m** and **3n**) that passed the initial screening with Aβ40, exhibited any activity for Aβ42.

The unsubstituted benzoyl (**3a**) and benzyl (**3b**) derivatives promoted the aggregation of Aβ40 at all the concentrations, although **3b** exhibited a much weaker pro-aggregation behavior at 39% at the highest concentration compared to **3a** at 200%. The 3- and 4-nitrobenzoyl derivatives **3d** and **3f** respectively, yielded similar activity to the unsubstituted derivative (**3a**). The addition of nitro at *meta*- and *para*- position to benzyl derivatives **3e** and **3g** also proved to be detrimental to the inhibition of Aβ40.

The 3- and 4-bromobenzoyl derivatives (**3i** and **3k**) like other bromo substituted derivatives from the amantadine and memantine series, also promoted the aggregation of Aβ40 however their

pro-aggregation activity decreased as the concentration of the test compounds was increased from 1 μM to 25 μM. Interestingly, both derivatives significantly reduced the lag phase, accelerating the aggregation of Aβ40. The **3j** and **3l** derivatives, 3- and 4-bromobenzyl, also promoted the aggregation of Aβ40 at all concentrations.

The addition of amino substituent at the *meta*- and *para*- position on benzoyl yielded **3m** and **3n** derivatives. The **3m** and **3n** derivatives were identified as the lead compounds in the rimantadine series with IC_{50} values of 5.5 μM and 1.8 μM respectively for Aβ40. Compounds **3o**, **3p** and **3s** also promoted the aggregation of Aβ40 in the initial screening of the synthesized derivatives. None of the compounds in this series were able to prevent or promote Aβ40/42 aggregation.

4.1.8 Top candidates from the rimantadine (3) based derivatives

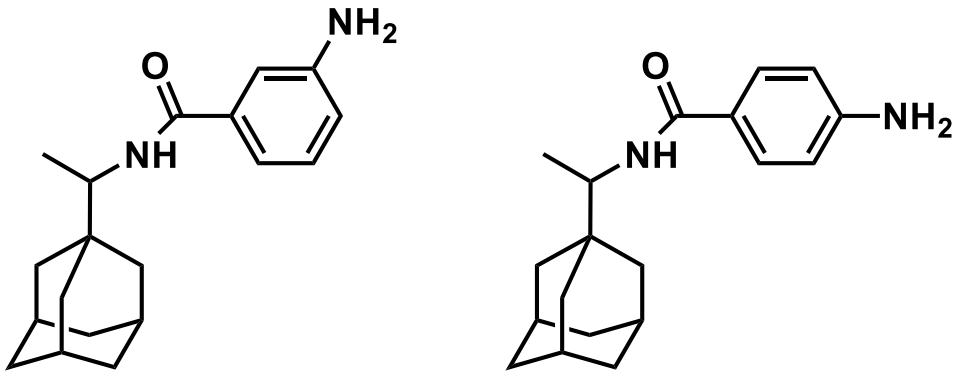

3m

Aβ40 IC_{50} = 5.5 μM

3n

Aβ40 IC_{50} = 1.8 μM

Figure 4.12: Compounds with anti-Aβ40 activity in the rimantadine series.

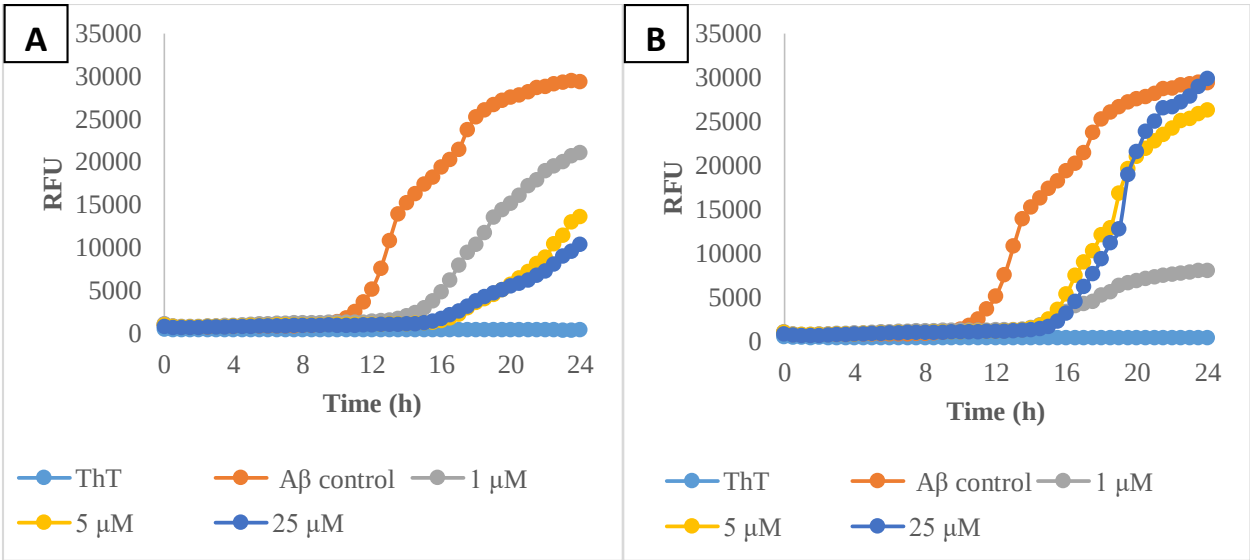

Figure 4.13: ThT-based Aβ40 aggregation kinetic data at 37 °C, at pH 7.4, 24 h. Panels: (A) **3m**, (B) **3n**. Results are expressed as average of two independent experiments (n =3).

The aggregation kinetic data of **3m** and **3n** derivatives is shown in Figure 4.13. The **3m** derivative inhibits the aggregation of Aβ40 at the tested concentrations. Interestingly, **3m** is the only derivative showing concentration dependent inhibition in the entire library. **3m** exhibited inferior inhibition at 1, 5 and 25 μM (28%, 54% and 65%) compared to resveratrol (35%, 64% and 81%). This observation was also mirrored by the IC_{50} values of **3m**, resveratrol and orange G at 5.5, 2.8 and 3.2 μM respectively. The lead derivative from this series, **3n** (IC_{50} = 1.8 μM) was ~ 1.5 fold more potent compared to resveratrol (IC_{50} = 2.8 μM). In this series none of the compounds exhibited inhibition of Aβ42 aggregation.

4.1.9 Molecular modeling studies of the lead candidates (3m and 3n)

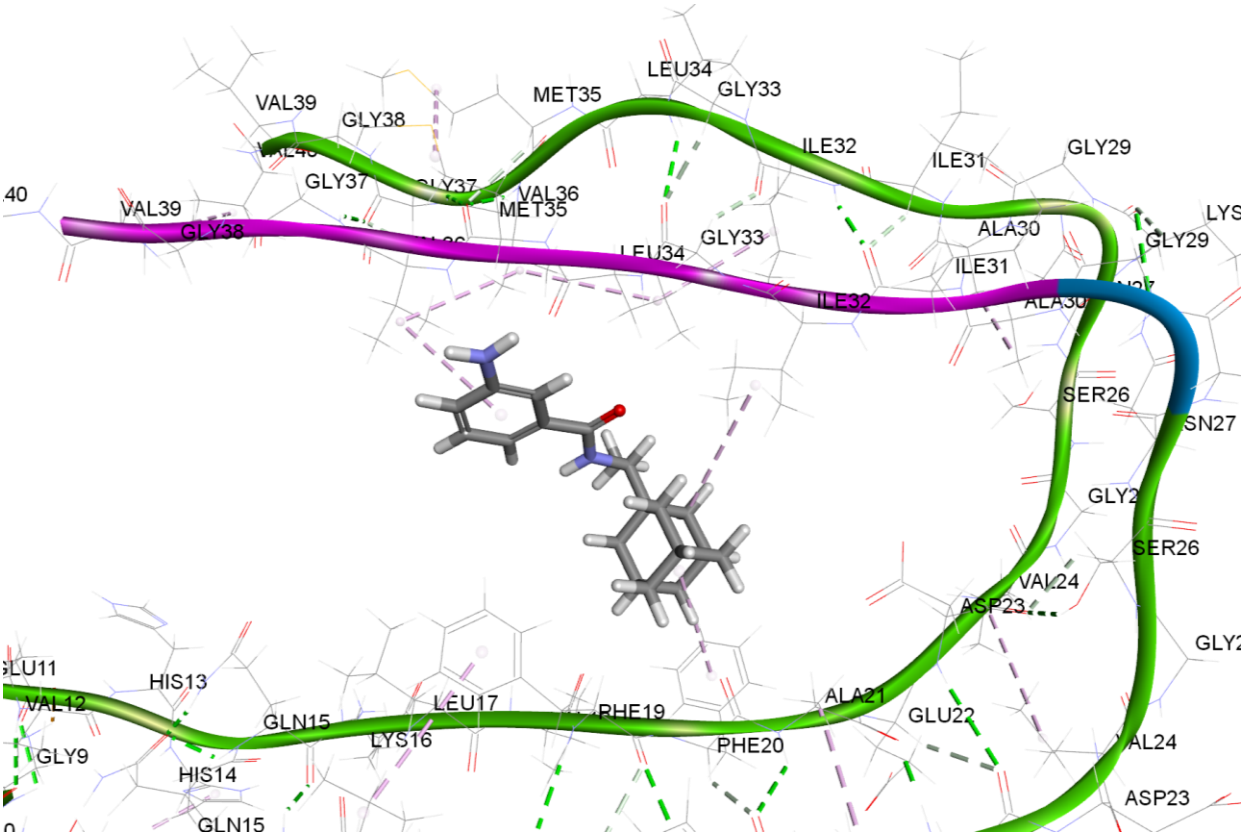

Figure 4.14: Docking of **3m** in the Aβ dimer (PDB id: 2LMN) model.

The binding mode of **3m** in Aβ40 dimer model is shown in the Figure 4.14. The rimantadine core was oriented in the center of dimer structure, allowing it to form two pi-alkyl hydrophobic interactions with the opposite sides of the loop. The interaction was made with Phe20 at 5.06 Å and the second interaction was made with Ile32 at 5.32 Å. The benzoyl aromatic ring forms pi-alkyl hydrophobic interaction with Val36 at 5.43 Å. The amino group at *para*- position is close to oxygen on Leu34 resulting in formation of two hydrogen bondings at 3.99 Å and 4.83 Å forming a stable complex with dimer structure hindering the aggregation process.

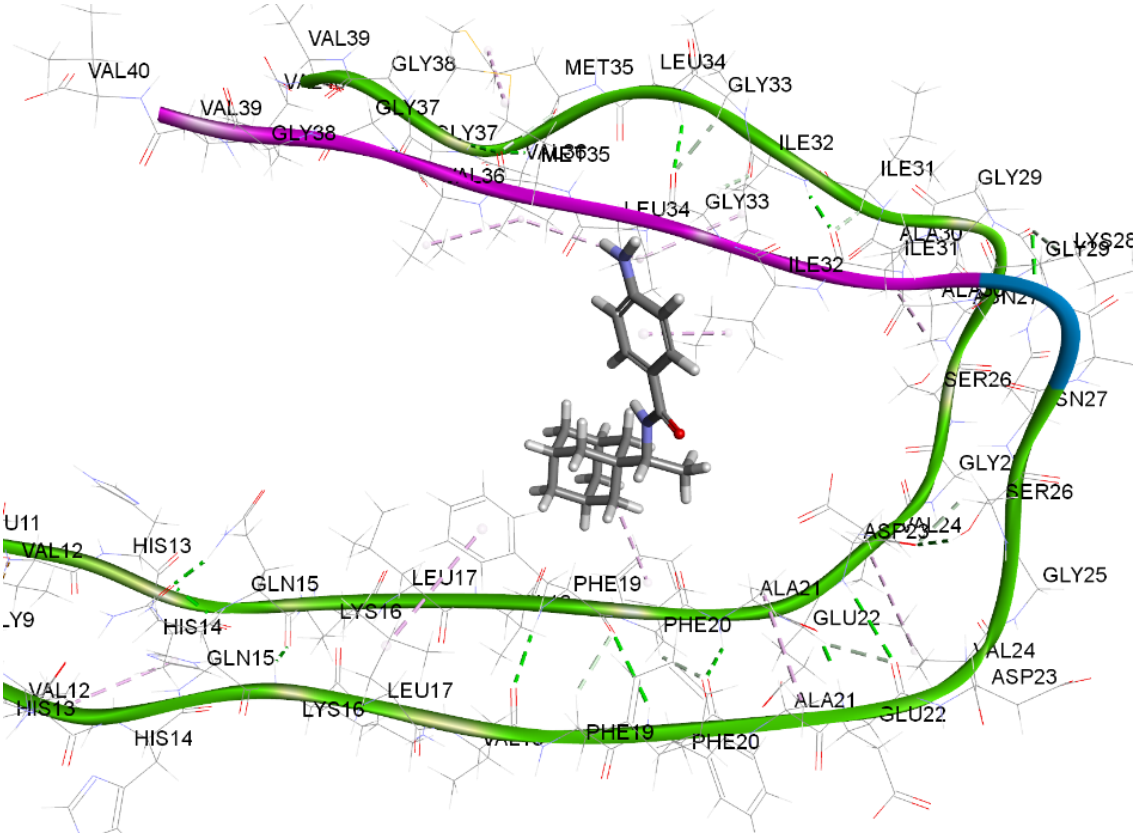

Figure 4.15: Docking of **3n** in the Aβ dimer (PDB id: 2LMN) model.

As illustrated in Figure 4.15, the rimantadine core of **3n** is much closer to KLVFAA segment compared to **3m** allowing it to form a much stronger pi-alkyl hydrophobic interaction with Phe20 at 4.15 Å. Similarly, the benzoyl aromatic ring is positioned closer to Ile32, forming a strong pi-alkyl hydrophobic interaction at 4.14 Å. As a result, the *para*- positioned amino group located closer to Leu34 compared to **3m**, forming two hydrogen bondings with the back-bone of Leu34 at 2.90 Å and 4.61 Å. Overall this derivative exhibited a number of hydrophobic interactions with the dimer structure hindering its aggregation.

4.1.10 Transmission electron microscopy (TEM) data for compounds 1n, 2n and 3n

The morphology of Aβ40 was investigated in the presence of the lead candidates from each series, compounds **1n**, **2n** and **3n**. As illustrated in Figure 4.16, all the lead candidates were able to inhibit the aggregation of Aβ40 (Panels B, C and D for **1n**, **2n** and **3n** respectively) compared to Aβ40 control (Panel A) and mirrored the obtained data from the ThT-based Aβ40 aggregation kinetic experiments (Figures 4.4, 4.8 and 4.13). The observation of Aβ40 oligomers further confirms the assay results where the lead compounds were able to stabilize the early formed Aβ40 intermidiates and delay the aggregation process.

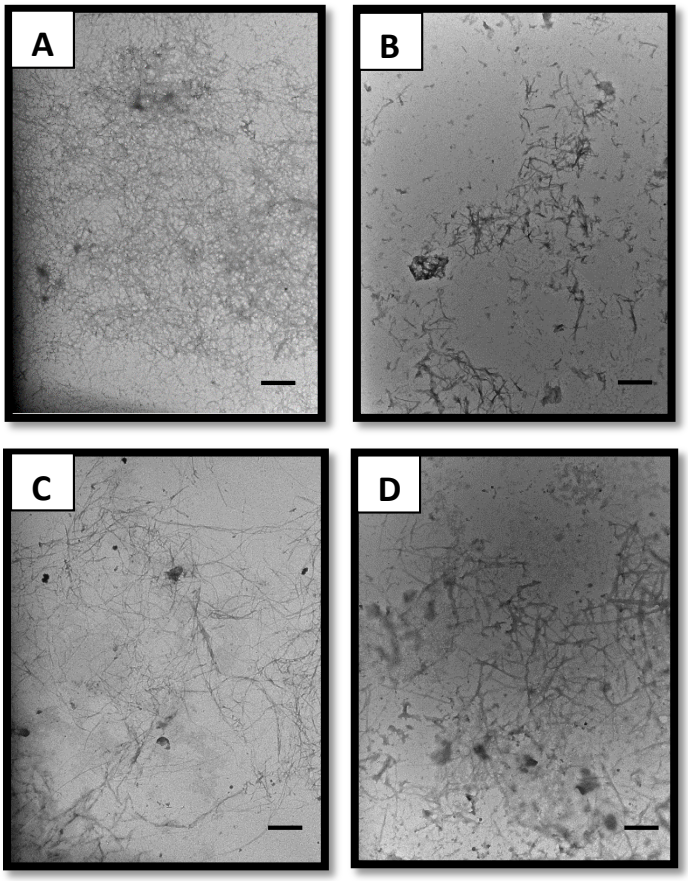

Figure 4.16: TEM assessment of Aβ40 morphalogy in presence and absence of lead compounds. Panels: (A) Aβ40 control, (B) Aβ40 incubated with **1n**, (C) Aβ40 incubated with **2n**, (D) Aβ40 incubated with **3n**.

4.1.11 Promotion of Aβ40 aggregation by aminoadamantanes

As discussed in Chapter 1 (section 1.7), developing Aβ inhibitors is one of the more favorable approaches in Aβ therapy. In recent years pro-aggregation approach has attracted considerable attention where by converting Aβ oligomers which is the most toxic form of Aβ aggregates to less toxic Aβ fibrils, can minimize the exposure of neuronal cells to Aβ oligomers and improve the cell viability as a result. Ideally, Aβ fibril specific antibodies can be used in combination with treatments capable of promoting the aggregation of Aβ to convert Aβ oligomers to mature fibrils and remove them by the antibodies, thereby reducing the Aβ load.

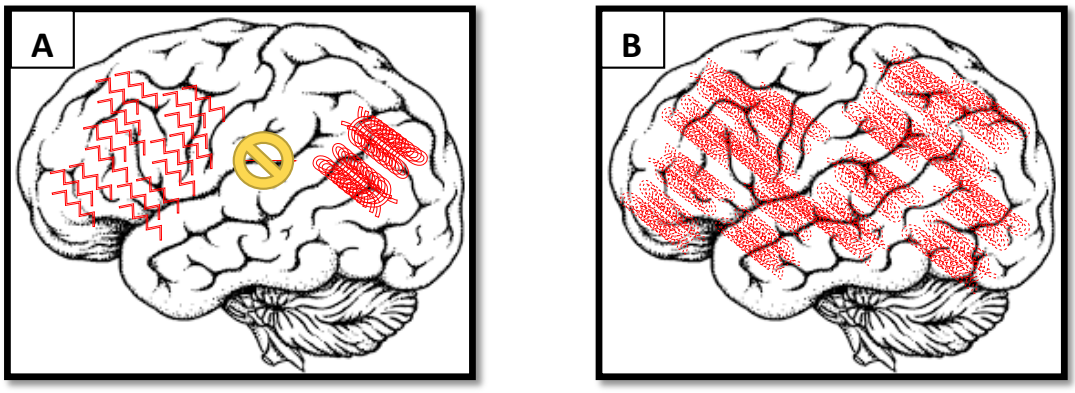

Figure 4.17: Two approaches in targeting Aβ hypothesis, Panels: (A) anti-aggregation (B) pro-aggregation.

Chapter 5: Conclusion and Future Work

5.1 Conclusion

A library of 48 aminoadamantane derivatives were designed, synthesized and characterized. They were evaluated for anti- Aβ activity against both Aβ40 and 42 aggregation. These experiments were conducted by ThT based fluorescence and TEM studies.

The adamantane scaffolds (amantadine, memantine and rimantadine) was chosen as the templates in design and development of the library based on their therapeutic application in neurodegenerative disorders including AD, review of recent literatures and preliminary molecular modeling studies. The library was synthesized utilizing a number synthetic methods described in Chapter 3 with yields ranging from 9% to 92%. The biological screenings were accomplished using previously reported methods and optimized in-house to obtain SAR data. The molecular modeling were conducted to gain some insights into and validate the SAR data for anti-aggregation properties of the lead derivatives. The following table provides a summary of various parameters of the synthesized library:

Table 5.1: Summary of various parameters of the synthesized aminoadamantane library.

➢ **Molecular weights (MWs)**	**241.2-361.1 g/mol**
➢ **Partition Coefficients (ClogPs)**	**2.61-7.00**
➢ **Aβ40 aggregation inhibition**	**0 -76%**
➢ **Aβ40 IC_{50}**	**0.4 – 23.8 µM**
➢ **Aβ42 aggregation inhibition**	**0-15%**
➢ **Aβ42 IC_{50}**	**>50 µM**

In general, the majority of the synthesized derivatives (36 out of 48) were classified as Aβ40 aggregation promoters. Only few derivatives exhibited inhibitory activity for Aβ40 with **2n** memantine derivative (IC_{50} = 0.4 μM) identified as the most potent which was 8-fold more potent compared to orange G (IC_{50} = 3.2 μM) with the other lead candidates exhibiting IC_{50} value ranging from 1.8 to 23.8 μM (chapter 4). Presence of amino group on the aromatic ring of the synthesized derivatives proved to be essential for superior inhibitory activity with the exception of **1c** and **2l**.

The molecular modeling studies of the lead derivatives showed that the hydrophobic interactions of compounds with the KLVFFA segment is necessary to inhibit the aggregation of Aβ40. Formation of relatively strong interactions such as hydrogen bonding and hydrophobic with other regions of Aβ is necessary to stabilize the Aβ dimer structure and hinder the aggregation process.

The SAR data acquired from biological screening of derivatives coupled with molecular modeling studies support the hypothesis that the aminoadamantane scaffold serves as a suitable template to design and develop potential treatments for AD.

5.2 Future directions

Based on the current SAR and biological evaluations the future studies regarding this project can be divided into two promising however opposite directions:

- Further expansion of the library by modifying the structure of lead derivatives to improve their biological profile as Aβ inhibitors.
- Further exploring and developing pro-aggregation candidates as an alternative approach in treatment of AD as discussed in Chapter 1 and Chapter 4, section 4.1.11.

In that regard, the memantine derivative **2d** was identified as the lead Aβ40 promoter, which not only promoted the aggregation of Aβ40, it also dramatically reduced the lag phase at 25 μM (Figure 5.1). As discussed in Chapter 1 and Chapter 4, pro-aggregation compounds can be used to minimize the exposure of neurons to toxic Aβ oligomers.

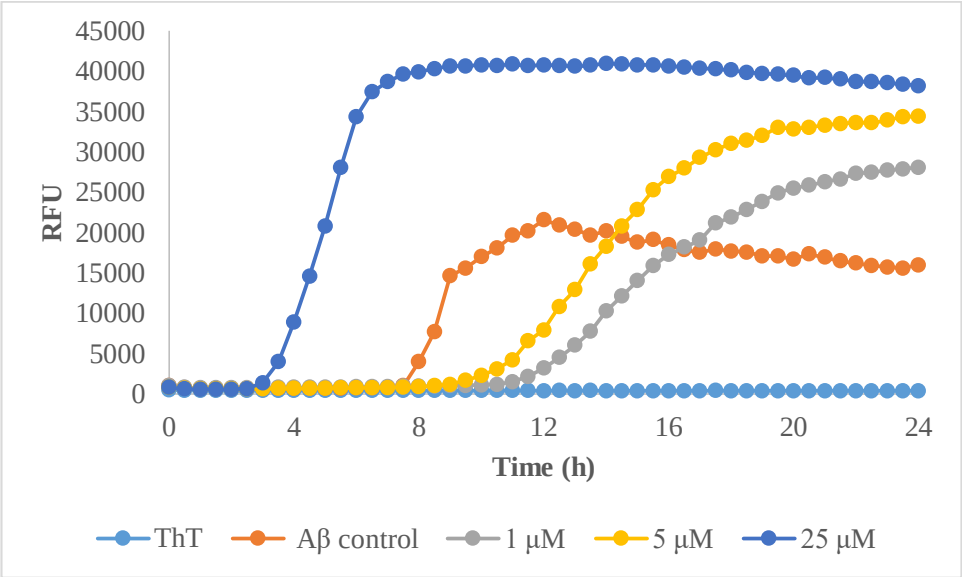

Figure 5.1: ThT-based Aβ40 aggregation kinetic data of **2d** at 37 °C, at pH 7.4, 24 h. Results are expressed as average of two independent experiments (n =3).

Screening the library for other pathological aspects of AD such as cholinergic dysfunction, NMDA excitotoxicity and metal chelation can also be considered as the next steps in this project. In that regards, selected numbers of the library was screened for AChE inhibition as listed as Appendix 2.

Chapter 6: Experimental

6.1 General Information

All necessary chemicals and reagents were obtained from commercial vendors (Acros Organics ®, Sigma-Aldrich ®, Alfa aesar ®, TCI ®) with a minimum purity of 95% and were used without further purification. Melting points were determined using a REACH Devices digital melting point apparatus and are uncorrected. ^{1}H NMR (300 MHz) spectra were recorded on a Bruker ® Avance spectrometer using $CDCl_3$ or DMSO-d_6 as reference solvents. Coupling constants (*J* values) were recorded in hertz (Hz) and the following abbreviations were used to assign multiplicity of NMR signals: s = singlet, d = doublet, t = triplet, m = multiplet, br = broad.

Compound purification was accomplished using Merck 230-400 mesh silica gel 60. All synthesized derivatives showed single spot on thin-layer chromatography (TLC) performed on Merck 60 F_{254} silica gel plates (0.2 mm) using three different solvent systems (9:1 EtOAc: MeOH; 3:1 EtOAc: hexanes and 3:1 EtOAc: DCM) and spots were visualized with UV 254 nm. Compound purity was measured using an Agilent 6100 series single quad LCMS equipped with an Agilent 1.8 µm Zorbax Eclipse Plus C18 (2.1 x 50 mm) running 90:10 MeOH/IPA at a flow rate of 0.4 mL/min with detection at 254 nm by UV.

6.2 Chemistry

6.2.1 General method to synthesize substitutedbenzamide derivatives of amantadine, memantine and rimantadine 1-, 2-, 3- (a, d, f, i, k):

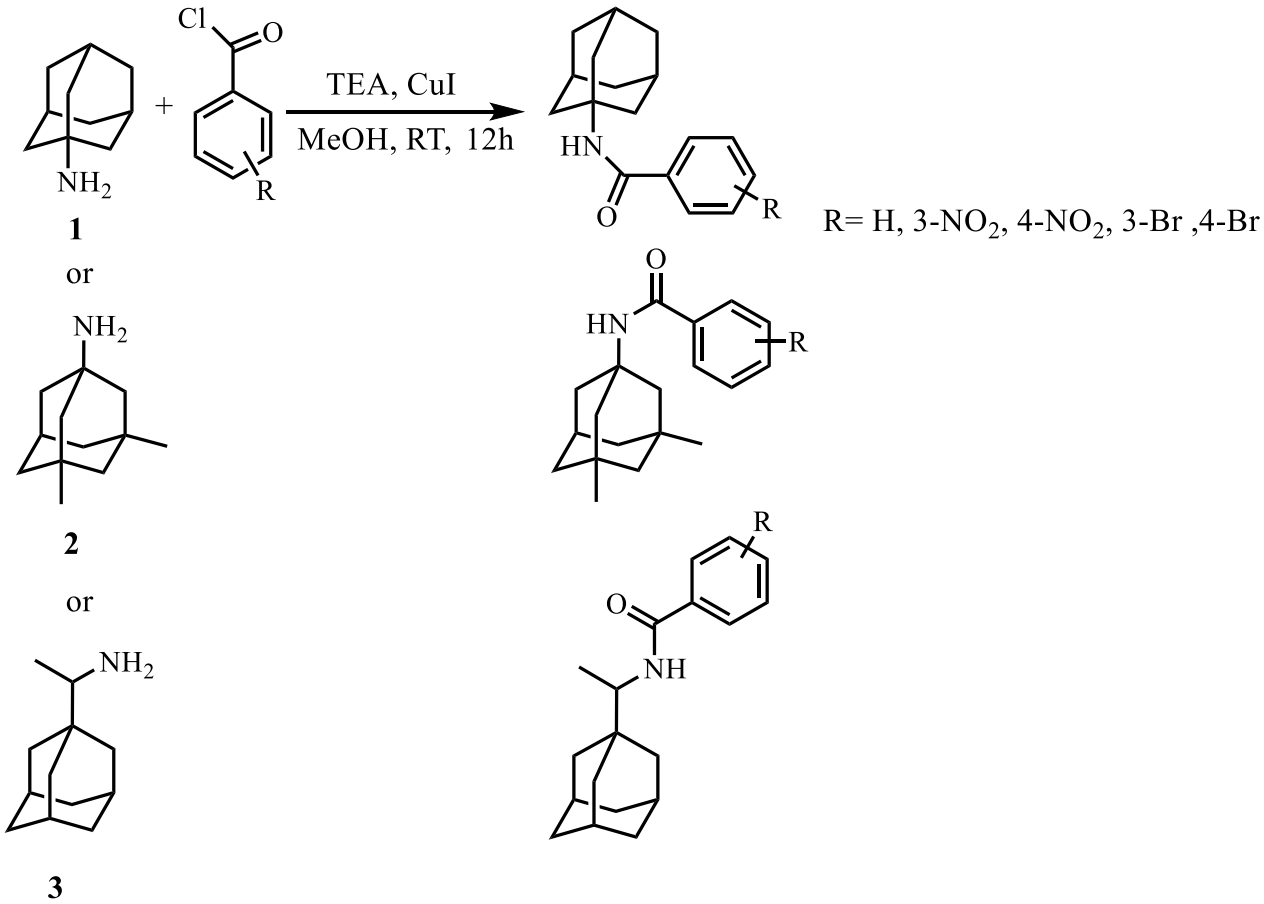

Scheme 6.1: General method to synthesize substitutedbenzamide derivatives **1-**, **2-** and **3-(a, d, f, i, k)**

0.300 g (1.6 mmol) of amantadine HCl, (1.4 mmol) or memantine HCl or (1.4 mmol) or rimantadine HCl, 0.163 mL (1.6 mmol) of benzoyl chloride and 30 mg (0.16 mmol) CuI were added to 10 mL of MeOH. The reaction mixture was stirred for 12 h at room temperature in the presence of 0.45 mL (3.2 mmol) of TEA. The mixture was concentrated and diluted with 5 mL of distilled water, followed by three extractions (3 x 15 mL) at slightly acidic conditions (pH ~ 6) with

EtOAc and dried over $MgSO_4$. Column chromatography was performed using EtOAc/MeOH (5:1) as solvent system to afford target compounds **1-**, **2-** and **3-**(**a**, **d**, **f**, **i**, **k**). (59-80%Yield)

6.2.2 General method to synthesize *N*-substitutedbenzyl derivatives of amantadine, memantine and rimantadine 1-, 2- and 3- (b, e, g, j, l):

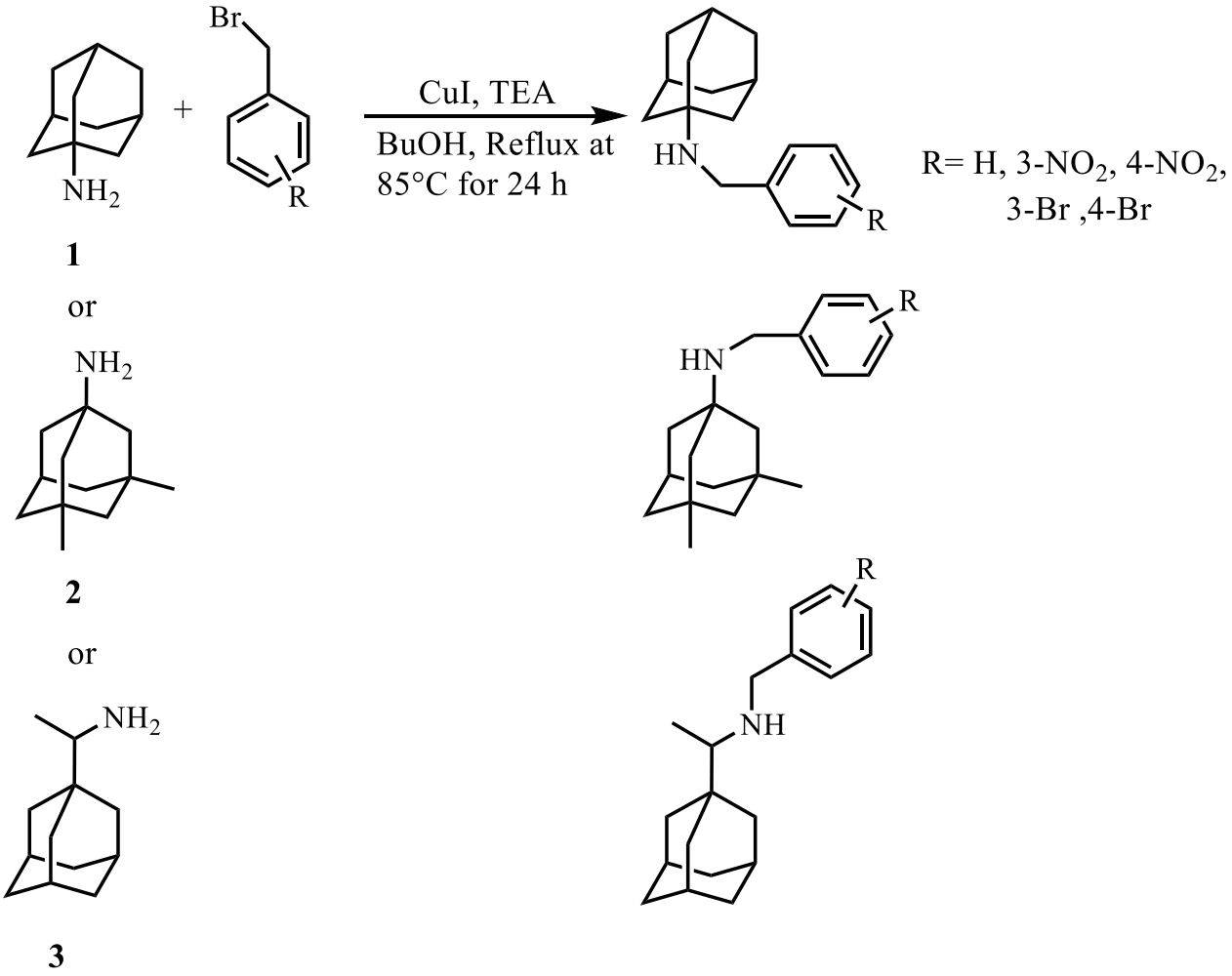

Scheme 6.2: General method to synthesize *N*-substitutedbenzyl derivatives 1-, 2- and 3-(b, e, g, j, l)

0.300 g (1.6 mmol) of amantadine HCl, (1.4 mmol) or memantine HCl or (1.4 mmol) rimantadine HCl, was added to 10 mL of *n*-BuOH and heated up to 80 °C. Then 0.45 mL (3.2 mmol) of TEA was added to quench HCl followed by the addition of 30 mg (0.16 mmol) of CuI and 0.16 mL (1.6 mmol) of benzyl bromide. The reaction mixture was refluxed at 85 °C for 24 h. The reaction mixture was concentrated and diluted with 5 mL of distilled water, followed by three extractions (3 x 15 mL) at slightly acidic conditions (pH ~ 6) with EtOAc and dried over $MgSO_4$. The crude compound was purified by carrying out column chromatography using EtOAc/MeOH (5:1) as solvent system to afford compounds **1-,2-,3-(b, e, g, j, l)**. (42-75%Yield)

6.2.3 General method to synthesize substitutedphenylethan-1-one derivatives of amantadine, memantine and rimantadine 1-, 2- and -3- (c, h):

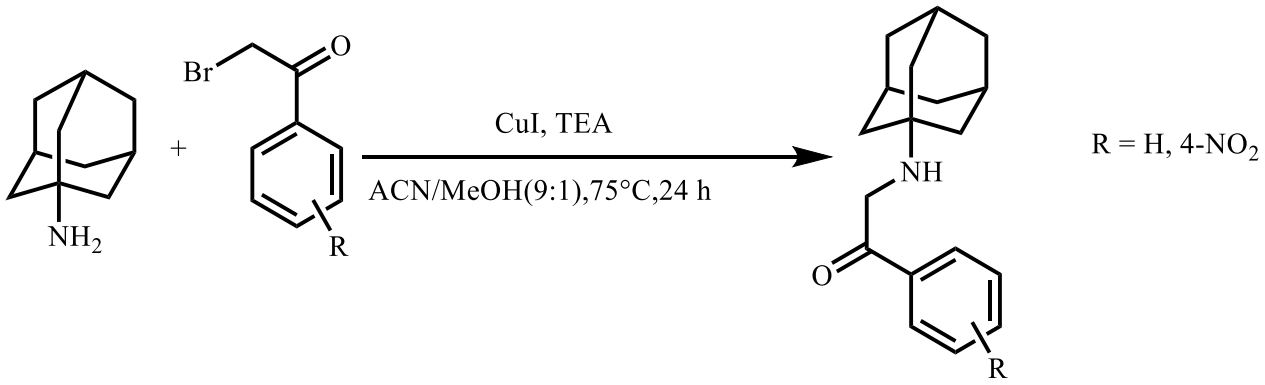

Scheme 6.3: General method to synthesize phenylethan-1-one derivatives **1-, 2-** and **3-** (**c** , **h**).

0.500 g (2.7 mmol) of amantadine HCl (2.3 mmol) or memantine HCl or (2.3 mmol) rimantadine HCl and 0.53 g (2.7 mmol) of 2-bromoacetophenone were added to 10 mL of

ACN/MeOH (9:1) solvent system. The reaction mixture was refluxed at 75 °C for 24 hours in the presence of 0.74 mL (5.3 mmol) of TEA and 51 mg (0.27 mmol) of CuI. The mixture was concentrated and diluted with 5 mL of distilled water, followed by three extractions (3 x 15 mL) at slightly acidic conditions (pH ~ 6) with EtOAc and dried over $MgSO_4$. Colum chromatography was carried out using DCM/MeOH (9:1) solvent system to afford the target compounds **1-c,2-c,3-h,**. (9-16%Yield).

6.2.4 General method of nitro reduction to synthesize aminobenzamide derivatives of amantadine, memantine and rimantadine 1-, 2- and 3- (m, n, o, p):

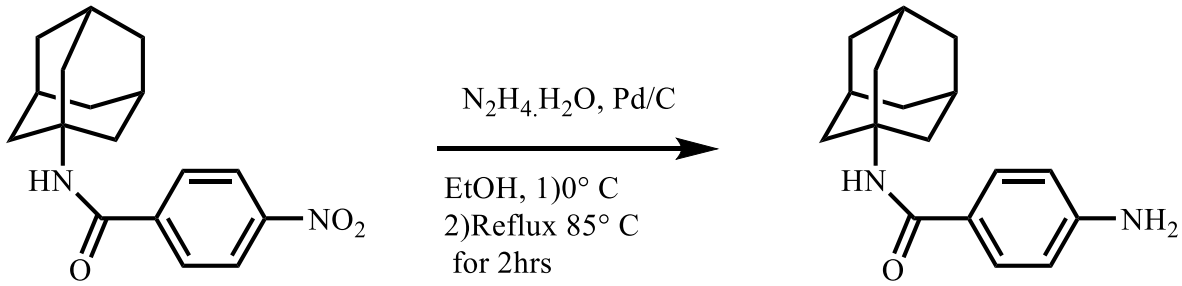

Scheme 6.4: General method of nitro reduction to synthesize aminobenzamide derivatives **1-,2-,3-(m, n, o, p)**

0.300 g (1.0 mmol) of compound **1f** was dissolved in 20 mL of EtOH. 110 mg (0.09 mmol) of 10% Pd/C and sufficient molecular sieve were added to the reaction mixture on ice bath. 0.096 g (0.093 mL) (2.99 mmol) of $N_2H_4.H_2O$ (50%) was slowly added to the reaction mixture while stirring. The reaction mixture was then refluxed for 2 hours at 85 C, then filtered to remove Pd/C and molecular sieves, was concentrated and diluted with 5 mL of distilled water, followed by three extractions (3 x 15 mL) with EtOAc and dried over $MgSO_4$. Column chromatography was carried out using hexane/acetone (5:1) solvent system to afford the target compounds **1-,2-,3- (m, n, o, p),**. (72-92%Yield).

6.2.5 General method to synthesize azidobenzamide derivatives of amantadine, memantine and rimantadine 1-, 2- and 3- (q, s):

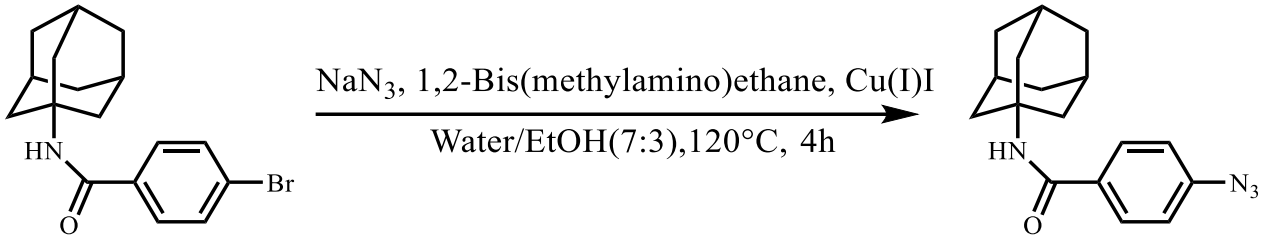

Scheme 6.5: General method of conversion of bromobenzamides to azidobenzamides.

0.2 g (0.6 mmol) of corresponding bromide precursor of **1-,2-,3- (i, k)** was dissolved in 20 mL of degassed mixture of water/EtOH (7:3). Then 78 mg (1.2 mmol) of NaN_3, 11 mg (0.06 mmol) of CuI and 0.2 mL (0.18 mmol) of *N,N*-dimethylethylenediamine was added. Then the reaction mixture was refluxed at 120˚C for 4 h under an argon atmosphere. The mixture was concentrated and diluted with 5 mL of distilled water, followed by three extractions (3 x 20 mL) with ether and dried over $MgSO_4$. Column chromatography was carried out using DCM/MeOH (5:1) solvent system to afford the target compounds **1-,2-,3-,**. (23-45%Yield).

6.2.6 ^{1}H NMR data for amantadine derivatives 1a-l

Amantadine HCl: ^{1}H NMR (300 MHz, DMSO-d_6) δ 7.90 (s, 3H), δ 2.05 (s, 3H), δ 1.75 (d, J = 2.8 Hz, 6H), δ 1.58 (q, J = 12.6 Hz, 6H).

***N*-(Adamantan-1-yl)benzamide (1a):** Yield: 0.24 g, 59%; Mp: 146-149°C. The product was obtained as a yellow solid and was purified using EtOAc/MeOH (5:1). ^{1}H NMR (300 MHz, DMSO-d_6) δ 7.74 (dd, *J* = 7.9, 4.4 Hz, 2H), δ 7.57 (d, *J* = 4.4 Hz, 1H), δ 7.42 – 7.36 (m, 3H), δ 2.04 (d, *J* = 4.5 Hz, 9H), δ 1.63 (t, *J* = 3.3 Hz, 6H). $C_{17}H_{21}NO$. Purity: 99%

***N*-Benzyladamantan-1-amine (1b):** Yield: 0.24 g, 62%; Mp: 188-191°C. The product was obtained as a dark yellow solid and was purified using EtOAc/MeOH (5:1).^{1}H NMR (300 MHz, DMSO-d_6) δ 8.59 (br, 1H), δ 7.50 – 7.37 (m, 5H), δ 4.07 (s, 2H), δ 2.13 (s, 2H), δ 1.93 – 1.88 (m, 6H), δ 1.73 – 1.57 (m, 7H). $C_{17}H_{23}N$. Purity:99%

2-((Adamantan-1-yl)amino)-1-phenylethan-1-one (1c): Yield: 0.07 g, 9%; Mp: 172-175°C. The product was obtained as a dark brown solid and was purified using DCM/MeOH (9:1). ^{1}H NMR (300 MHz, DMSO-d_6) δ 8.42 (s, 1H), δ 8.02 – 7.97 (m, 2H), δ 7.67 – 7.62 (m, 1H), δ 7.52 (dd, *J* = 8.2, 6.9 Hz, 2H), δ 4.79 (s, 2H), δ 2.05 (s, 2H), δ 1.88 (s, 7H), δ 1.61 (s, 6H). $C_{18}H_{23}NO$. Purity: 99%

***N*-(Adamantan-1-yl)-3-nitrobenzamide (1d):** Yield: 0.2 g, 42%; Mp: 163-166°C. The product was obtained as a light yellow solid and was purified using EtOAc/MeOH (5:1). ^{1}H NMR (300 MHz, DMSO-d_6) δ 8.56 (d, *J* = 2.1 Hz, 1H), δ 8.31 (d, *J* = 8.1 Hz, 1H), δ 8.19 (d, *J* = 7.8 Hz, 1H), δ 8.01 (s, 1H), δ 7.70 (t, *J* = 8.0 Hz, 1H), δ 2.06 (s, 9H), 1.64 (s, 6H). $C_{17}H_{20}N_2O_3$. Purity:99%

***N*-(3-Nitrobenzyl)adamantan-1-amine (1e):** Yield: 0.21 g, 28%; Mp: 178-180°C. The product was obtained as a brown solid and was purified using EtOAc/MeOH (5:1). ^{1}H NMR (300 MHz,

DMSO-d_6) δ 9.08 (s, 1H), δ 8.42 (s, 1H), δ 8.18 (d, *J* = 8.6 Hz, 1H), δ 7.96 (d, *J* = 7.6 Hz, 1H), δ 7.67 (t, *J* = 8.0 Hz, 1H), δ 4.14 (s, 2H), δ 2.10 (s, 2H), δ 1.95 – 1.80 (m, 6H), δ 1.61 (d, *J* = 10.7 Hz, 6H), δ 1.20 (s, 1H). $C_{17}H_{22}N_2O_2$. Purity:95%

***N*-(Adamantan-1-yl)-4-nitrobenzamide (1f):** Yield: 0.36 g, 75%; Mp: 180-182°C. The product was obtained as a white solid and was purified using EtOAc/MeOH (5:1). ^{1}H NMR (300 MHz, DMSO-d_6) δ 8.24 (dd, *J* = 8.8, 2.8 Hz, 2H), δ 8.02 – 7.91 (m, 3H), δ 2.05 (d, *J* = 3.0 Hz, 9H), δ 1.63 (d, *J* = 3.6 Hz, 6H). $C_{17}H_{20}N_2O_3$. Purity:96.7%

***N*-(Adamantan-1-yl)-3-bromobenzamide (1i):** Yield: 0.41 g, 78%; Mp: 157-159°C. The product was obtained as a light yellow solid and was purified using EtOAc/MeOH (5:1). ^{1}H NMR (300 MHz, DMSO-d_6) δ 7.92 (t, *J* = 1.8 Hz, 1H), δ 7.73 (s, 2H), δ 7.66 (d, *J* = 8.0 Hz, 1H), δ 7.36 (t, *J* = 7.8 Hz, 1H), δ 2.03 (s, 9H), δ 1.62 (s, 6H). $C_{17}H_{20}BrNO$. Purity:98%

***N*-(3-Bromobenzyl)adamantan-1-amine (1j):** Yield: 0.29 g, 66%; Mp: >250°C. The product was obtained as a light brown solid and was purified using EtOAc/MeOH (5:1). ^{1}H NMR (300 MHz, DMSO-d_6) δ 9.29 (br, 1H), δ 7.89 (s, 1H), δ 7.64 – 7.56 (m, 2H), δ 7.36 (t, *J* = 6.6 Hz, 1H), δ 4.06 (s, 2H), δ 2.12 (s, 3H), δ 1.97 (s, 6H), δ 1.63 (q, *J* = 12.5 Hz, 6H). $C_{17}H_{22}BrN$. Purity:98.6%

***N*-(Adamantan-1-yl)-4-bromobenzamide (1k):** Yield: 0.32 g, 59%; Mp: 178-180°C. The product was obtained as a white solid and was purified using EtOAc/MeOH (5:1). ^{1}H NMR (300 MHz, DMSO-d_6) δ 7.68 (t, *J* = 8.8 Hz, 3H), δ 7.59 (d, *J* = 8.2 Hz, 2H), δ 2.03 (s, 9H), δ 1.62 (s, 6H). $C_{17}H_{20}BrNO$. Purity:97%

***N*-(4-Bromobenzyl)adamantan-1-amine (1l):** Yield: 0.34 g, 43%; Mp: >250°C. The product was obtained as a brown solid and was purified using EtOAc/MeOH (5:1). ^{1}H NMR (300 MHz, Chloroform-*d*) δ 7.43 (t, *J* = 7.0 Hz, 4H), δ 3.80 (s, 2H), δ 1.86 (d, *J* = 2.9 Hz, 9H), δ 1.63 (d, *J* = 4.5 Hz, 6H). $C_{17}H_{22}BrN$. Purity:99%

***N*-(Adamantan-1-yl)-3-aminobenzamide (1m):** Yield: 0.16 g, 60%; Mp: 163-166°C. The product was obtained as a dark brown solid and was purified using hexane/acetone (5:1). ^{1}H NMR (300 MHz, DMSO-d_6) δ 7.26 (s, 1H), δ 6.99 (t, *J* = 7.8 Hz, 1H), δ 6.88 (s, 1H), δ 6.82 (d, *J* = 7.6 Hz, 1H), δ 6.61 (d, *J* = 7.8 Hz, 1H), δ 5.12 (s, 2H), δ 2.01 (s, 9H), δ 1.62 (s, 6H). $C_{17}H_{22}N_2O$. Purity:99%

***N*-(Adamantan-1-yl)-4-aminobenzamide (1n):** Yield: 0.2 g, 74%; Mp: 171-172°C. The product was obtained as a light brown solid and was purified using hexane/acetone (5:1). ^{1}H NMR (300 MHz, DMSO-d_6) δ 7.51 (d, *J* = 8.3 Hz, 2H), δ 7.01 (d, *J* = 7.9 Hz, 1H), δ 6.49 (t, *J* = 7.9 Hz, 2H), δ 5.50 (d, *J* = 7.3 Hz, 2H), δ 2.02 (d, *J* = 7.1 Hz, 9H), δ 1.63 (d, *J* = 7.7 Hz, 5H), δ 1.22 (d, *J* = 7.7 Hz, 1H). $C_{17}H_{22}N_2O$. Purity:99%

***N*-(4-Aminobenzyl)adamantan-1-amine (1p):** Yield: 0.12 g, 46%; Mp: 219-221°C. The product was obtained as a dark brown solid and was purified using hexane/acetone (5:1). ^{1}H NMR (300 MHz, DMSO-d_6) δ 8.44 (s, 1H), δ 8.26 (d, *J* = 8.4 Hz, 1H), δ 8.15 (d, *J* = 8.3 Hz, 2H), δ 7.99 (d, *J* = 8.3 Hz, 1H), δ 7.65 (d, *J* = 8.3 Hz, 2H), δ 3.88 (s, 2H), δ 2.01 (s, 3H), δ 1.57 (d, *J* = 8.4 Hz, 9H), δ 1.20 (s, 3H). $C_{17}H_{24}N_2$. Purity:94.7%

6.2.7 ^{1}H NMR data for memantine derivatives 2a-l

Memantine HCl: ^{1}H NMR (300 MHz, DMSO-d_6) δ 7.85 (s, 3H), δ 2.12 (s, 1H), δ 1.58 (d, *J* = 3.1 Hz, 2H), δ 1.47 – 1.31 (m, 4H), δ 1.26 (s, 4H), δ 1.09 (q, *J* = 12.7 Hz, 2H), δ 0.82 (s, 6H).

***N*-(3,5-Dimethyladamantan-1-yl)benzamide (2a):** Yield: 0.29 g, 73%; Mp: 94-97°C. The product was obtained as a yellow solid and was purified using EtOAc/MeOH (5:1). ^{1}H NMR (300 MHz, DMSO-d_6) δ 7.79 – 7.68 (m, 2H), δ 7.60 (d, *J* = 4.8 Hz, 1H), δ 7.47 – 7.35 (m, 3H), δ 2.12 – 2.07 (m, 1H), δ 1.88 (t, *J* = 4.0 Hz, 2H), δ 1.70 (t, *J* = 4.3 Hz, 4H), δ 1.39 – 1.18 (m, 4H), δ 1.12 (d, *J* = 4.8 Hz, 2H), δ 0.82 (d, *J* = 4.7 Hz, 6H). $C_{19}H_{25}NO$. Purity:98%

***N*-Benzyl-3,5-dimethyladamantan-1-amine (2b):** Yield: 0.20 g, 55%; Mp: 190-192°C. The product was obtained as a dark brown/red solid and was purified using EtOAc/MeOH (5:1). ^{1}H NMR (300 MHz, DMSO-d_6) δ 8.57 (s, 1H), δ 7.51 – 7.38 (m, 5H), δ 4.10 (d, *J* = 12.8 Hz, 2H), δ 2.20 (s, 1H), δ 1.75 (d, *J* = 3.2 Hz, 2H), δ 1.57 (s, 4H), δ 1.31 (d, *J* = 2.9 Hz, 4H), δ 1.15 (d, *J* = 7.6 Hz, 2H), δ 0.87 (s, 6H). $C_{19}H_{27}N$. Purity:97%

2-((3,5-Dimethyladamantan-1-yl)amino)-1-phenylethan-1-one (2c): Yield: 0.08 g, 11%; Mp: 158-160°C. The product was obtained as a dark orange solid and was purified using DCM/MeOH (9:1). ^{1}H NMR (300 MHz, DMSO-d_6) δ 8.41 (s, 1H), δ 8.00 (d, *J* = 7.5 Hz, 2H), δ 7.64 (t, *J* = 7.3 Hz, 1H), δ 7.52 (t, *J* = 7.6 Hz, 2H), δ 4.78 (s, 2H), δ 2.12 (s, 1H), δ 1.73 (s, 2H), δ 1.53 (s, 4H), δ 1.31 – 1.20 (m, 4H), δ 1.09 (d, *J* = 9.9 Hz, 2H), δ 0.81 (s, 6H). $C_{20}H_{27}NO$. Purity: 94.5%

***N*-(3,5-Dimethyladamantan-1-yl)-3-nitrobenzamide (2d):** Yield: 0.34 g, 71%; Mp: 106-109°C. The product was obtained as a light orange solid and was purified using EtOAc/MeOH (5:1). ^{1}H NMR (300 MHz, DMSO-d_6) δ 8.58 (br, 1H), δ 8.31 (d, *J* = 8.0 Hz, 1H), δ 8.24 – 8.14 (m, 1H), δ 8.04 (s, 1H), δ 7.76 – 7.64 (m, 1H), δ 2.09 (q, *J* = 10.1 Hz, 1H), δ 1.90 (d, *J* = 9.5 Hz, 2H), δ 1.71 (q, *J* = 11.9 Hz, 4H), δ 1.41 – 1.20 (m, 4H), δ 1.12 (s, 2H), δ 0.82 (s, 6H). $C_{19}H_{24}N_2O_3$. Purity:95.3%

3,5-Dimethyl-*N*-(3-nitrobenzyl)adamantan-1-amine (2e): Yield: 0.31 g, 42%; Mp: 144-147°C. The product was obtained as a brown solid and was purified using EtOAc/MeOH (5:1). ^{1}H NMR (300 MHz, DMSO-d_6) δ 8.37 (s, 1H), δ 8.14 (d, *J* = 7.8 Hz, 1H), δ 7.90 (s, 1H), δ 7.63 (t, *J* = 7.9 Hz, 1H), δ 4.03 (s, 2H), δ 2.13 (s, 1H), δ 1.63 (s, 2H), δ 1.45 (s, 4H), δ 1.35 – 1.12 (m, 4H), δ 1.10 (d, *J* = 4.6 Hz, 2H), δ 0.83 (s, 6H). $C_{19}H_{26}N_2O_2$. Purity:96.1%

***N*-(3,5-Dimethyladamantan-1-yl)-4-nitrobenzamide (2f):** Yield: 0.37 g, 49%; Mp: 164-166°C. The product was obtained as a light brown solid and was purified using EtOAc/MeOH (5:1). ^{1}H NMR (300 MHz, DMSO-d_6) δ 8.24 (d, *J* = 6.8 Hz, 2H), δ 7.95 (d, *J* = 6.8 Hz, 2H), δ 2.09 (d, *J* = 9.7 Hz, 1H), δ 1.88 (s, 2H), δ 1.78 – 1.62 (m, 4H), δ 1.29 (q, *J* = 12.0 Hz, 4H), δ 1.12 (s, 2H), δ 0.82 (s, 6H). $C_{19}H_{24}N_2O_3$. Purity:96.6%

3-Bromo-*N*-(3,5-dimethyladamantan-1-yl)benzamide (2i): Yield: 0.48 g, 68%; Mp: 110-112°C. The product was obtained as a dark yellow/orange solid and was purified using EtOAc/MeOH (5:1).^{1}H NMR (300 MHz, DMSO-d_6) δ 7.94 (d, *J* = 1.8 Hz, 1H), δ 7.74 (d, *J* = 7.6 Hz, 2H), δ 7.70 – 7.60 (m, 1H), δ 7.35 (t, *J* = 7.9 Hz, 1H), δ 2.08 (d, *J* = 3.3 Hz, 1H), δ 1.87 (d, *J* = 3.1 Hz, 2H), δ

1.77 – 1.59 (m, 4H), δ 1.38 – 1.19 (m, 4H), δ 1.10 (s, 2H), δ 0.81 (s, 6H). $C_{19}H_{24}BrNO$. Purity: 97%

***N*-(3-Bromobenzyl)-3,5-dimethyladamantan-1-amine (2j):** Yield: 0.19 g, 42%; Mp: 135-137°C. The product was obtained as a dark yellow solid and was purified using EtOAc/MeOH (5:1). ^{1}H NMR (300 MHz, DMSO-d_6) δ 7.52 (d, *J* = 1.9 Hz, 1H), δ 7.34 (dd, *J* = 7.7, 1.9 Hz, 1H), δ 7.29 (d, *J* = 7.6 Hz, 1H), δ 7.20 (t, *J* = 7.7 Hz, 1H), δ 3.64 (s, 2H), δ 2.04 (d, *J* = 3.4 Hz, 1H), δ 1.42 (d, *J* = 3.1 Hz, 2H), δ 1.30 – 1.16 (m, 8H), δ 1.05 (s, 2H), δ 0.79 (s, 6H). $C_{19}H_{26}BrN$. Purity:95.2%

4-Bromo-*N*-(3,5-dimethyladamantan-1-yl)benzamide (2k): Yield: 0.38 g, 64%; Mp: 127-130°C. The product was obtained as a light yellow solid and was purified using EtOAc/MeOH (5:1). ^{1}H NMR (300 MHz, DMSO-d_6) δ 7.70 (d, *J* = 8.6 Hz, 3H), δ 7.64 – 7.54 (m, 2H), δ 2.09 (s, 1H), δ 1.86 (d, *J* = 3.1 low Hz, 2H), δ 1.76 – 1.60 (m, 4H), δ 1.38 – 1.18 (m, 4H), δ 1.11 (s, 2H), δ 0.81 (s, 6H). $C_{19}H_{24}BrNO$. Purity: 99%

***N*-(4-Bromobenzyl)-3,5-dimethyladamantan-1-amine (2l):** Yield: 0.53 g, 66%; Mp: 182-185°C. The product was obtained as a light yellow solid and was purified using EtOAc/MeOH (5:1). ^{1}H NMR (300 MHz, DMSO-d_6) δ 9.11 (s, 1H), δ 7.66 – 7.56 (m, 2H), δ 7.53 (d, *J* = 8.5 Hz, 2H), δ 4.03 (s, 2H), δ 2.18 (s, 1H), δ 1.78 (d, *J* = 3.1 Hz, 2H), δ 1.60 (t, *J* = 8.1 Hz, 4H), δ 1.29 (d, *J* = 3.0 Hz, 4H), δ 1.22 – 1.04 (m, 2H), δ 0.85 (s, 6H). $C_{19}H_{26}BrN$. Purity: 99%

3-Amino-*N*-(3,5-dimethyladamantan-1-yl)benzamide (2m): Yield: 0.25 g, 92%; Mp: 128-130°C. The product was obtained as a red solid and was purified using hexane/acetone (5:1). ^{1}H NMR (300 MHz, DMSO-d_6) δ 7.28 (s, 1H), δ 6.99 (t, *J* = 7.8, 1H), δ 6.92 – 6.86 (m, 1H), δ 6.82 (d,

J = 7.3 Hz, 1H), δ 6.66 – 6.55 (m, 1H), δ 5.11 (s, 2H), δ 2.11 – 2.02 (m, 1H), δ 1.84 (d, *J* = 3.2 Hz, 2H), δ 1.66 (s, 4H), δ 1.26 (dd, *J* = 19.5, 8.5 Hz, 4H), δ 1.10 (s, 2H), δ 0.80 (s, 6H). $C_{19}H_{26}N_2O$. Purity: 99.6%

4-Amino-*N*-(3,5-dimethyladamantan-1-yl)benzamide (2n): Yield: 0.15 g, 56%; Mp: 90-92°C. The product was obtained as a dark orange solid and was purified using hexane/acetone (5:1). ^{1}H NMR (300 MHz, DMSO-d_6) δ 7.48 (d, *J* = 8.2 Hz, 2H), δ 7.04 (s, 1H) , δ 6.46 (d, *J* = 8.3 Hz, 2H), δ 5.48 (s, 2H), δ 2.11 – 1.99 (m, 1H), δ 1.84 (d, *J* = 10.1 Hz, 2H), δ 1.67 (t, *J* = 8.5 Hz, 4H), δ 1.33 – 1.21 (m, 4H), δ 1.09 (s, 2H), δ 0.80 (s, 6H). $C_{19}H_{26}N_2O$. Purity:99%

***N*-(3-Aminobenzyl)-3,5-dimethyladamantan-1-amine (2o):** Yield: 0.1 g, 40%; Mp: 219-221°C. The product was obtained as a dark brown solid and was purified using hexane/acetone (5:1). ^{1}H NMR (300 MHz, $CDCl_3$) δ 6.97 (t, *J* = 7.7 Hz, 1H), δ 6.57 (d, *J* = 7.3 Hz, 2H), δ 6.48 (d, *J* = 8.0 Hz, 2H), δ 5.09 (s, 2H), δ 3.72 (s, 2H), δ 2.12 (s, 1H), δ 1.64 (s, 2H), δ 1.50 – 1.37 (m, 4H), δ 1.27 (s, 4H), δ 1.10 (s, 2H), δ 0.83 (d, *J* = 2.9 Hz, 6H). $C_{19}H_{28}N_2$. Purity:96.6%

4-Azido-*N*-(3,5-dimethyladamantan-1-yl)benzamide (2s): Yield: 0.08 g, 43%; Mp: 142-145°C. The product was obtained as a beige solid and was purified using DCM/MeOH (5:1). ^{1}H NMR (300 MHz, $CDCl_3$) δ 7.53 (d, *J* = 8.3 Hz, 2H), δ 6.63 (d, *J* = 8.3 Hz, 2H), δ 5.69 (s, 1H), δ 1.97 – 1.90 (m, 2H), δ 1.75 (s, 4H), δ 1.45 – 1.26 (m, 4H), δ 1.16 (t, *J* = 10.5 Hz, 2H), δ 0.90 – 0.83 (m, 6H). $C_{19}H_{24}N_4O$. Purity: 97%

6.2.8 ^{1}H NMR data for rimantadine derivatives 3a-l

Rimantadine HCl: ^{1}H NMR (300 MHz, DMSO-d_6) δ 7.61 (s, 3H), δ 2.74 (q, *J* = 7.0 Hz, 1H), δ 1.94 (s, 3H), δ 1.66 – 1.46 (m, 12H), δ 1.06 (d, *J* = 6.8 Hz, 3H).

***N*-(1-(1-Adamantan-1-yl)ethyl)benzamide (3a):** Yield: 0.31 g, 76%; Mp: 178-180°C. The product was obtained as a light yellow/brown solid and was purified using EtOAc/MeOH (5:1). ^{1}H NMR (300 MHz, DMSO-d_6) δ 7.89 (d, *J* = 9 Hz, 1H), δ 7.83 – 7.76 (m, 2H), δ 7.52 – 7.35 (m, 3H), δ 3.78 (d, *J* = 7.3 Hz, 1H), δ 1.91 (s, 3H), δ 1.67– 1.45 (m, 12H), δ 1.02 (d, *J* = 7.0 Hz, 3H). $C_{19}H_{25}NO$. Purity:96%

1-(Adamantan-1-yl)-*N*-benzylethan-1-amine (3b): Yield: 0.21 g, 57%; Mp: 170-172°C. The product was obtained as a dark brown solid and was purified using EtOAc/MeOH (5:1). ^{1}H NMR (300 MHz, DMSO-d_6) δ 7.47 (d, *J* = 7.2 Hz, 2H), δ 7.41 – 7.30 (m, 3H), δ 4.04 (d, *J* = 7.2 Hz, 2H), δ 2.26 (s, 1H), δ 1.95 – 1.86 (m, 3H), δ 1.67 – 1.53 (m, 10H), δ 1.31 (d, *J* = 12.0 Hz, 3H), δ 1.06 (d, *J* = 6.8 Hz, 3H). $C_{19}H_{27}N$. Purity:98.1%

***N*-(1-(Adamantan-1-yl)ethyl)-3-nitrobenzamide (3d):** Yield: 0.60 g, 80%; Mp: 160-162°C. The product was obtained as a light brown solid and was purified using EtOAc/MeOH (5:1). ^{1}H NMR (300 MHz, DMSO-d_6) δ 8.63 (t, *J* = 1.9 Hz, 1H), δ 8.39 – 8.21 (m, 3H), δ 7.73 (t, *J* = 8.0 Hz, 1H), δ 3.89 – 3.72 (m, 1H), δ 1.91 (s, 3H), δ 1.68 – 1.40 (m, 12H), δ 1.04 (d, *J* = 7.0 Hz, 3H). $C_{19}H_{24}N_2O_3$. Purity:99%

1-(Adamantan-1-yl)-*N*-(4-nitrobenzyl)ethan-1-amine (3e): Yield: 0.50 g, 68%; Mp: 184-186°C. The product was obtained as a dark brown solid and was purified using EtOAc/MeOH (5:1). ^{1}H

NMR (300 MHz, DMSO-d_6) δ 8.21 (br, 1H), 8.04 (dd, *J* = 8.2, 2.3 Hz, 2H), δ 7.77 (d, *J* = 7.6 Hz, 1H), δ 7.56 (t, *J* = 7.9 Hz, 1H), δ 3.96 – 3.64 (m, 2H), δ 1.98 – 1.85 (m, 5H), δ 1.59 (q, *J* = 10.9 Hz, 10H), δ 1.45 – 1.34 (d, 2H), δ 0.88 (d, *J* = 6.4 Hz, 3H). $C_{19}H_{26}N_2O_2$. Purity:95.1%

***N*-(1-(Adamantan-1-yl)ethyl)-4-nitrobenzamide (3f):** Yield: 0.49 g, 66%; Mp: 169-170°C. The product was obtained as a light brown solid and was purified using EtOAc/MeOH (5:1). ^{1}H NMR (300 MHz, DMSO-d_6) δ 8.26 (d, *J* = 9 Hz, 2H), δ 8.03 (d, *J* = 9 Hz, 2H), δ 3.79 (dd, *J* = 9.2, 6.8 Hz, 1H), δ 1.91 (s, 3H), δ 1.65 – 1.45 (m, 12H), δ 1.03 (d, *J* = 7.1 Hz, 3H). $C_{19}H_{24}N_2O_3$. Purity:94.8%

1-(Adamantan-1-yl)-*N*-(4-nitrobenzyl)ethan-1-amine (3g): Yield: 0.41 g, 56%; Mp: 194-196°C. The product was obtained as a brown solid and was purified using EtOAc/MeOH (5:1). ^{1}H NMR (300 MHz, DMSO-d_6) δ 8.22 – 8.09 (m, 2H), δ 7.60 (d, *J* = 8.4 Hz, 2H), δ 3.94 – 3.66 (m, 2H), δ 1.94 – 1.88 (m, 4H), δ 1.65 – 1.51 (m, 10H), δ 1.45 – 1.35 (m, 3H), δ 0.87 (d, *J* = 6.5 Hz, 3H). $C_{19}H_{26}N_2O_2$. Purity:95.3%

2-((1-(Adamantan-1-yl)ethyl)amino)-1-(4-nitrophenyl)ethan-1-one (3h): Yield: 0.16 g, 33%; Mp: 161-164°C. The product was obtained as an orange solid and was purified using DCM/MeOH (9:1). ^{1}H NMR (300 MHz, $CDCl_3$) δ 8.67 (d, *J* = 8.9 Hz, 2H), δ 8.35 (d, *J* = 8.5 Hz, 2H), δ 5.86 (s, 2H), δ 3.90 (d, *J* = 7.2 Hz, 1H), δ 3.15 – 3.12 (m, 1H), δ 1.63 (s, 5H), δ 1.44 (q, *J* = 7.3 Hz, 13H). $C_{20}H_{26}N_2O_3$. Purity:99%

***N*-(1-(Adamantan-1-yl)ethyl)-3-bromobenzamide (3i):** Yield: 0.30 g, 78%; Mp: 170-172°C. The product was obtained as a beige solid and was purified using EtOAc/MeOH (5:1). ^{1}H NMR (300 MHz, DMSO-d_6) δ 8.01 (d, *J* = 8.6 Hz, 2H), δ 7.81 (d, *J* = 7.8 Hz, 1H), δ 7.68 (d, *J* = 7.8 Hz, 1H), δ 7.39 (t, *J* = 7.9 Hz, 1H), δ 3.77 (p, *J* = 7.3 Hz, 1H), δ 1.91 (s, 3H), δ 1.64 – 1.55 (m, 12H), δ 1.02 (d, *J* = 6.9 Hz, 3H). $C_{19}H_{24}BrNO$. Purity: 96.3%

***N*-(1-(Adamantan-1-yl)ethyl)-4-bromobenzamide (3k):** Yield: 0.25 g, 65%; Mp: 201-203°C. The product was obtained as a beige solid and was purified using EtOAc/MeOH (5:1). ^{1}H NMR (300 MHz, DMSO-d_6) δ 7.97 (d, *J* = 9 Hz, 1H), δ 7.76 (d, *J* = 8.2 Hz, 2H), δ 7.63 (d, *J* = 8.2 Hz, 2H), δ 3.76 (d, *J* = 6.9 Hz, 1H), δ 1.90 (s, 3H), δ 1.65 – 1.55 (m, 12H), δ 1.01 (d, *J* = 6.9 Hz, 3H). $C_{19}H_{24}BrNO$. Purity: 96.5%

1-(Adamantan-1-yl)-*N*-(4-bromobenzyl)ethan-1-amine (3l): Yield: 0.45 g, 56%; Mp: 188-190°C. The product was obtained as a dark brown solid and was purified using EtOAc/MeOH (5:1). ^{1}H NMR (300 MHz, DMSO-d_6) δ 7.69 – 7.57 (m, 1H), δ 7.44 (d, *J* = 8.3 Hz, 2H), δ 7.27 (d, *J* = 8.3 Hz, 2H), δ 3.81 – 3.45 (m, 2H), δ 2.79 (q, *J* = 6.7 Hz, 1H), δ 1.97 – 1.85 (m, 3H), δ 1.67 – 1.44 (m, 10H), δ 1.36 (dq, *J* = 12.2, 2.6 Hz, 2H), δ 0.85 (d, *J* = 6.5 Hz, 3H). $C_{19}H_{26}BrN$. Purity:94.8%

***N*-(1-(Adamantan-1-yl)ethyl)-3-aminobenzamide (3m):** Yield: 0.21 g, 77%; Mp: 128-130°C. The product was obtained as a light brown solid and was purified using hexane/acetone (5:1). ^{1}H NMR (300 MHz, DMSO-d_6) δ 7.61 (d, *J* = 9 Hz, 1H), δ 7.02 (t, *J* = 7.7 Hz, 1H), δ 6.99 – 6.85 (m, 2H), δ 6.63 (ddd, *J* = 8.0, 2.6, 1.0 Hz, 1H), δ 5.15 (s, 2H), δ 3.81 – 3.65 (m, 1H), δ 1.90 (s, 3H), δ 1.52 (dt, *J* = 11.4 Hz, 12H), δ 0.98 (d, *J* = 6.9 Hz, 3H). $C_{19}H_{26}N_2O$. Purity: 99%

***N*-(1-(Adamantan-1-yl)ethyl)-4-aminobenzamide (3n):** Yield: 0.22 g, 81%; Mp: 106-109°C. The product was obtained as a brown solid and was purified using hexane/acetone (5:1). ^{1}H NMR (300 MHz, DMSO-d_6) δ 7.59 – 7.49 (m, 2H), δ 7.33 (d, J = 9.5 Hz, 1H), δ 6.54 – 6.45 (m, 2H), δ 5.50 (s, 2H), δ 3.82 – 3.66 (m, 1H), δ 1.89 (s, 3H), δ 1.64 – 1.55 (m, 12H), δ 0.97 (d, J = 7.0 Hz, 3H). $C_{29}H_{26}N_2O$. Purity:99%

3-(((1-(Adamantan-1-yl)ethyl)amino)methyl)aniline (3o): Yield: 0.12 g, 48%; Mp: 165-168°C. The product was obtained as a dark brown solid and was purified using hexane/acetone (5:1). ^{1}H NMR (300 MHz, DMSO-d_6) δ 6.95 (t, J = 7.5 Hz, 1H), δ 6.58 – 6.32 (m, 4H), δ 5.01 (s, 2H), δ 3.66 (d, J = 12.1 Hz, 2H), δ 2.11 (s, 1H), δ 1.91 (s, 3H), δ 1.58 (t, J = 10.2 Hz, 9H), δ 1.38 (d, J = 11.9 Hz, 3H), δ 0.96 (d, J = 6.7 Hz, 3H). $C_{19}H_{28}N_2$. Purity:96.2%

6.3 Biological Assays

6.3.1 Thioflavin-T (ThT) monitoring of Aβ$_{40/42}$ aggregation kinetics.[146,148]

The ability of synthesized compounds to inhibit and/or modulate Aβ aggregation kinetics was determined using a ThT-based fluorescence assay. The assays were conducted using black, clear-bottom, Costar 384-well plates with 30 seconds of linear shaking at 730 cpm every 5 minutes at 37 °C for 24 h. The ThT excitation/emission was measured at 440 nm/490 nm and readings were

taken every 5 minutes using Biotek Synergy H1 microplate reader. Test compounds were prepared in DMSO and further diluted to 10 x in 215mM phosphate buffer at pH 7.4. The Aβ.Hexafluoroisopropanol (HFIP) samples ($A\beta_{40}$ or $A\beta_{42}$ obtained from rPeptide, USA) was dissolved in 1% ammonium hydroxide and sonicated for 5 minutes at room temperate and diluted to 50 μM in 215 mM phosphate buffer. ThT stock solution was prepared with 50 mM glycine and adjusted to pH 7.4 to give a 15 μM solution. Plating sequence was as follows:

- ThT background: 44 μL ThT, 35 μL buffer, 1 μL DMSO
- Aβ control: 44 μL ThT, 27 μL buffer, 1 μL DMSO
- Compound screening: 44 μL ThT, 20 μL buffer

Then 8 μL of 10x compound dilutions (concentrations tested: 1, 5 and 25 μM) were added and end point reading was measured to determine ThT-interference before finally adding 8 μL of $A\beta_{40}$ or $A\beta_{42}$ stock solutions (5 μM final). Plates were sealed with a transparent plate film prior to initiating the assay. The relative fluorescence intensity units (RFU) were corrected for ThT-interference before processing the aggregation kinetic plots and inhibition percentages. Data presented was mean of triplicate reading of at least 2 independent experiments.

6.3.2 Transmission Electron microscopy (TEM)

80 μL of 215 mM phosphate buffer, 20 μL of 10 x test compound dilutions (250 μM – prepared in the same way as for the Aβ kinetic assay) and 100 μL of $A\beta_{40}$ or $A\beta_{42}$ stock solution (50 μM) were added to a clear Costar, round-bottom 96-well plate. 2 μL of DMSO and 18 μL of phosphate buffer was added to the control wells. The final Aβ:test compound ratio was 1:1 at 25 μM. Plate was incubated on a Fisher scientific plate incubator at 37 °C with constant shaking at 730

cpm for 24 h. TEM grids were prepared by adding 20 μL of incubated test compound and Aβ mixture to the 400 mesh, formvar-coated copper grids using eppendorf pipette. The grids were air-dried in fume hood for a few hours before the buffer salts were washed by adding two drops of ultra-pure water (UPW) followed by quickly removing the water by small pieces of filter papers. The grids were air-dried and negatively stained by adding a drop of 2% phosphotungstic acid (PTA) and immediately dried using small pieces of filter paper. The grids were air-dried for at least 24 hours prior to scanning. The images were produced using a Philips CM 10 transmission electron microscope at 60kV (Department of Biology, University of Waterloo) by a 14-megapixel AMT camera.

6.3.3 Computational Chemistry

The molecular docking studies were conducted using the computational software Discovery Studio Client v17.1.0.16143 (Structure-Based-Design software), from BIOVIA Inc. San Diego, USA. The X-ray crystal structure of Aβ dimer and fibrils were obtained from RCSB Protein Data Bank (PDB id: 2LMN) and were prepared for docking study by adding hydrogens and by assigning CHARMm force field using the *macromolecules* module in the software. The ligand molecules were constructed using the *Build Fragment* tool and energy minimized using *Steepest descent* and S*mart minimizer* algorithms with 500 max steps. Ligand binding site was defined by selecting a 15 Å sphere radius for both Aβ dimer and fibrils. Molecular docking experiments were carried out using the *receptor-ligand interactions* module of the software. The CDOCKER algorithm was chosen to produce the top ten binding modes of the compounds bound using CHARMm force field ranked based on the CDOCKER energies and CDOCKER interaction energies in kcal/mol. Then

the quality of docking was evaluated by studying the types of polar and nonpolar interactions observed.

References

(1) Toodayan, N. (2016) Professor Alois Alzheimer (1864–1915): Lest we forget. *J. Clin. Neurosci. 31*, 47–55.

(2) Guzior, N., Wieckowska, A., Panek, D., and Malawska, B. (2015) Recent development of multifunctional agents as potential drug candidates for the treatment of Alzheimer's disease. *Curr. Med. Chem. 22*, 373–404.

(3) Kumar, A., Singh, A., and Ekavali. (2015) A review on Alzheimer's disease pathophysiology and its management: An update. *Pharmacol. Reports 67*, 195–203.

(4) Korolev, I. O. (2014) Alzheimer ' s disease : a clinical and basic science review. *MSRJ, 4,* 24–33.

(5) Smetanin, P., Kobak, P., Briante, C., Stiff, D., Sherman, G., and Ahmad, S. (2009) Rising tide : the impact of dementia in Canada 2008 to 2038. *RiskAnalytica. 1,* 1-345.

(6) Ahmad, S., Briante, C., Kobak, P., Sherman, G., Smetanin, P. (2010) Rising tide : the impact of dementia on canadian society. executive summary. *Alzheimer Soc. Canada, 1,* 1-66.

(7) Wong, S. L., Gilmour, H., and Ramage-morin, P. L. (2016) Alzheimer ' s disease and other dementias in Canada. *Statistics Canada, 27,* 11-16.

(8) Karch, C. M., and Goate, A. M. (2015) Alzheimer's disease risk genes and mechanisms of disease pathogenesis. *Biol. Psychiatry 77*, 43–51.

(9) Querfurth, H. W., and LaFerla, F. M. (2010) Alzheimer's disease. *N. Engl. J. Med. 362*, 329–344.

(10) Blennow, K., Leon, M. J. De, and Zetterberg, H. (2006) Alzheimer ' s disease *368*, 387–403.

(11) Lansdall, C. J. (2014) Review An effective treatment for Alzheimer ' s disease must consider both amyloid and tau *7*, 1–11.

(12) Citron, M. (2010) Alzheimer's disease: strategies for disease modification. *Nat. Rev. Drug Discov. 9*, 387–398.

(13) Herrmann, N., Chau, S. A., Kircanski, I., and Lanctôt, K. L. (2011) Current and emerging drug treatment options for Alzheimer's disease: a systematic review. *Drugs 71*, 2031–2065.

(14) Scott, L. J., and Goa, K. L. (2000) Galantamine: a review of its use in Alzheimer's disease. *Drugs 60*, 1095–1122.

(15) Geldenhuys, W. J., and Darvesh, A. S. (2015) Pharmacotherapy of Alzheimer's disease: current and future trends. *Expert Rev. Neurother. 15*, 3–5.

(16) Huang, Y., and Mucke, L. (2012) Alzheimer mechanisms and therapeutic strategies. *Cell 148*, 1204–1222.

(17) Glenner, G. G., and Wong, C. W. (1984) Alzheimer's disease: Initial report of the purification and characterization of a novel cerebrovascular amyloid protein. *Biochem. Biophys. Res. Commun. 120*, 885–890.

(18) Masters, C. L., and Selkoe, D. J. (2012) Biochemistry of amyloid β-protein and amyloid deposits in Alzheimer disease. *Cold Spring Harb. Perspect. Med. 2*, 1–24.

(19) Nelson, P. T., Braak, H., and Markesbery, W. R. (2009) Neuropathology and cognitive impairment in Alzheimer disease: a complex but coherent relationship. *J. Neuropathol. Exp. Neurol. 68*, 1–29.

(20) Karran, E., Mercken, M., and Strooper, B. De. (2011) The amyloid cascade hypothesis for Alzheimer's disease: an appraisal for the development of therapeutics. *Nat. Rev. Drug Discov. 10*, 698–712.

(21) Prasansuklab, A., and Tencomnao, T. (2013) Amyloidosis in Alzheimer's disease: the toxicity of amyloid beta (Aβ), mechanisms of its accumulation and implications of medicinal plants for therapy. *Evidence-based Complement. Altern. Med. 2013*, 1-10.

(22) Vinters, H. V. (2015) Emerging concepts in Alzheimer's disease. *Annu. Rev. Pathol. Mech. Dis. 10*, 291–319.

(23) Teich, A. F., and Arancio, O. (2012) Is the amyloid hypothesis of Alzheimer's disease therapeutically relevant? *Biochem. J. 446*, 165–177.

(24) Nixon, R. a. (2007) Autophagy, amyloidogenesis and Alzheimer disease. *J. Cell Sci. 120*, 4081–4091.

(25) McKhann, G. M., Knopman, D. S., Chertkow, H., Hyman, B. T., Jack, C. R., Kawas, C. H., Klunk, W. E., Koroshetz, W. J., Manly, J. J., Mayeux, R., Mohs, R. C., Morris, J. C., Rossor, M. N., Scheltens, P., Carrillo, M. C., Thies, B., Weintraub, S., and Phelps, C. H. (2011) The diagnosis of dementia due to Alzheimer's disease: recommendations from the national institute on aging-Alzheimer's association workgroups on diagnostic guidelines for Alzheimer's disease. *Alzheimer's Dement. 7*, 263–269.

(26) Haass, C., and Selkoe, D. J. (2007) Soluble protein oligomers in neurodegeneration: lessons from the Alzheimer's amyloid beta-peptide. *Nat. Rev. Mol. Cell Biol. 8*, 101–112.

(27) Multhaup, G., Huber, O., Buée, L., and Galas, M. C. (2015) Amyloid precursor protein (APP) metabolites APP intracellular fragment (AICD), Aβ42, and Tau in nuclear roles. *J. Biol. Chem. 290*, 23515–23522.

(28) Nhan, H. S., Chiang, K., and Koo, E. H. (2015) The multifaceted nature of amyloid precursor protein and its proteolytic fragments: friends and foes. *Acta Neuropathol. 129*, 1–19.

(29) Zheng, H., and Koo, E. H. (2006) The amyloid precursor protein: beyond amyloid. *Mol. Neurodegener. 1*, 5-16.

(30) Choi, S. H., Kim, Y. H., Hebisch, M., Sliwinski, C., Lee, S., D'Avanzo, C., Chen, H., Hooli, B., Asselin, C., Muffat, J., Klee, J. B., Zhang, C., Wainger, B. J., Peitz, M., Kovacs, D. M., Woolf, C. J., Wagner, S. L., Tanzi, R. E., and Kim, D. Y. (2014) A three-dimensional human neural cell culture model of Alzheimer's disease. *Nature 515*, 274–278.

(31) Bruggink, K. a, Müller, M., Kuiperij, H. B., and Verbeek, M. M. (2012) Methods for analysis of amyloid-β aggregates. *J. Alzheimers. Dis. 28*, 735–758.

(32) Neve, R. L., McPhie, D. L., and Chen, Y. (2000) Alzheimer's disease: a dysfunction of the amyloid precursor protein. *Brain Res 886*, 54–66.

(33) Castello, M. a., and Soriano, S. (2014) On the origin of Alzheimer's disease. trials and tribulations of the amyloid hypothesis. *Ageing Res. Rev. 13*, 10–12.

(34) Zhao, Y., Bhattacharjee, S., Jones, B. M., Hill, J. M., Clement, C., Sambamurti, K., Dua, P., and Lukiw, W. J. (2015) Beta-Amyloid Precursor Protein (βAPP) Processing in Alzheimer's disease (AD) and age-related macular degeneration (AMD). *Mol. Neurobiol. 52*, 533–544.

(35) De Strooper, B., and Karran, E. (2016) The cellular phase of Alzheimer's disease. *Cell 164*, 603–615.

(36) Eisele, Y. S., and Duyckaerts, C. (2016) Propagation of Aß pathology: hypotheses, discoveries, and yet unresolved questions from experimental and human brain studies. *Acta Neuropathol. 131*, 5–25.

(37) Allinson, T. M., Parkin, E. T., Turner, a J., and Hooper, N. M. (2003) ADAMs family members as amyloid precursor protein a-secretases. *J. Neurosci. Res 74*, 342–352.

(38) Zhang, Y., Thompson, R., Zhang, H., and Xu, H. (2011) APP processing in Alzheimer ' s disease. *Brain. 1*, 1–13.

(39) Zhu, Y., Mori, T., and Mattson, M. P. (2012) SAPP-α modulates β-secretase activity and amyloid-β generation. *Nat Commun. 3*, 1–20.

(40) Chasseigneaux, S., and Allinquant, B. (2012) Functions of Aβ, sAPPα and sAPPβ: similarities and differences. *J. Neurochem. 120*, 99–108.

(41) Agostinho, P., Pliássova, A., Oliveira, C. R., and Cunha, R. a. (2015) Localization and trafficking of amyloid-β protein precursor and secretases: impact on Alzheimer's disease. *J. Alzheimer's Dis. 45*, 329–347.

(42) Jonsson, T., Atwal, J. K., Steinberg, S., Snaedal, J., Jonsson, P. V., Bjornsson, S., Stefansson, H., Sulem, P., Gudbjartsson, D., Maloney, J., Hoyte, K., Gustafson, A., Liu, Y., Lu, Y., Bhangale, T., Graham, R. R., Huttenlocher, J., Bjornsdottir, G., Andreassen, O. A., Jönsson, E. G., Palotie, A., Behrens, T. W., Magnusson, O. T., Kong, A., Thorsteinsdottir, U., Watts, R. J., and Stefansson, K. (2012) A mutation in APP protects against Alzheimer's disease and age-related cognitive decline. *Nature 488*, 96–99.

(43) Catania, C., Sotiropoulos, I., Silva, R., Onofri, C., Breen, K. C., Sousa, N., and Almeida, O. F. X. (2009) The amyloidogenic potential and behavioral correlates of stress. *Mol. Psychiatry 14*, 95–105.

(44) Demars, M. P., Hollands, C., Zhao, K. Da, and Lazarov, O. (2013) Soluble amyloid precursor protein-α rescues age-linked decline in neural progenitor cell proliferation. *Neurobiol. Aging 34*, 2431–2440.

(45) Nalivaeva, N. N., and Turner, A. J. (2013) The amyloid precursor protein: a biochemical enigma in brain development, function and disease. *FEBS Lett. 587*, 2046–2054.

(46) Chang, Y., Tesco, G., Jeong, W. J., Lindsley, L., Eckman, E. a., Eckman, C. B., Tanzi, R. E., and Guénette, S. Y. (2003) Generation of the beta-amyloid peptide and the amyloid precursor protein c-terminal fragment γ are potentiated by FE65L1. *J. Biol. Chem. 278*, 51100–51107.

(47) Müller, T., Meyer, H. E., Egensperger, R., and Marcus, K. (2008) The amyloid precursor protein intracellular domain (AICD) as modulator of gene expression, apoptosis, and cytoskeletal dynamics-relevance for Alzheimer's disease. *Prog. Neurobiol. 85*, 393–406.

(48) Zolezzi, J. M., Bastías-Candia, S., Santos, M. J., and Inestrosa, N. C. (2014) Alzheimer's disease: relevant molecular and physiopathological events affecting amyloid-ß brain balance and the putative role of PPARs. *Front. Aging Neurosci. 6*, 1–12.

(49) Serpell, L. C. (2000) Alzheimer's amyloid fibrils: structure and assembly. *Biochim. Biophys. Acta - Mol. Basis Dis. 1502*, 16–30.

(50) Greenwald, J., and Riek, R. (2010) Biology of amyloid: Structure, function, and regulation. *Structure 18*, 1244–1260.

(51) Bemporad, F., and Chiti, F. (2012) Protein misfolded oligomers: experimental approaches, mechanism of formation, and structure-toxicity relationships. *Chem. Biol. 19*, 315–327.

(52) Sorrentino, P., Iuliano, A., Polverino, A., Jacini, F., and Sorrentino, G. (2014) The dark sides of amyloid in Alzheimer's disease pathogenesis. *FEBS Lett. 588*, 641–652.

(53) Klein, W. L. (2002) Aβ toxicity in Alzheimer's disease: globular oligomers (ADDLs) as new vaccine and drug targets. *Neurochem. Int. 41*, 345–352.

(54) Inouye, H., Gleason, K. a., Zhang, D., Decatur, S. M., and Kirschner, D. a. (2010) Differential effects of Phe19 and Phe20 on fibril formation by amyloidogenic peptide Aβ16-22 (Ac-KLVFFAE-NH2). *Proteins Struct. Funct. Bioinforma. 78*, 2306–2321.

(55) Tycko, R. (2004) Progress towards a molecular-level structural understanding of amyloid fibrils. *Curr. Opin. Struct. Biol. 14*, 96–103.

(56) Arosio, P., Knowles, T. P. J., and Linse, S. (2015) On the lag phase in amyloid fibril formation. *Phys. Chem. Chem. Phys. 17*, 7606–7618.

(57) Wang, D. S., Dickson, D. W., and Malter, J. S. (2006) Beta-amyloid degradation and Alzheimer's disease. *J. Biomed. Biotechnol. 5*, 1-12.

(58) Wildsmith, K. R., Holley, M., Savage, J. C., Skerrett, R., and Landreth, G. E. (2013) Evidence for impaired amyloid β clearance in Alzheimer's disease. *Alzheimers. Res. Ther. 5*, 1–6.

(59) Zlokovic, B. V. (2004) Clearing amyloid through the blood-brain barrier. *J. Neurochem. 89*, 807–811.

(60) Shi, D. Y., Bierhaus, A., Nawroth, P. P., and Stern, D. M. (2009) RAGE and Alzheimer's disease: a progression factor for amyloid-β- induced cellular perturbation? *J. Alzheimer's Dis. 16*, 833–843.

(61) Cai, Z., Liu, N., Wang, C., Qin, B., Zhou, Y., Xiao, M., Chang, L., Yan, L. J., and Zhao, B. (2016) Role of RAGE in Alzheimer's disease. *Cell. Mol. Neurobiol. 36*, 483–495.

(62) Mukherjee, A., and Hersh, L. B. (2002) Regulation of amyloid beta-peptide levels by enzymatic degradation. *J. Alzheimers. Dis. 4*, 341–348.

(63) Miners, J. S., Barua, N., Kehoe, P. G., Gill, S., and Love, S. (2011) Aβ-degrading enzymes: potential for treatment of Alzheimer disease. *J. Neuropathol. Exp. Neurol. 70*, 944–959.

(64) Watt, N. T., Whitehouse, I. J., and Hooper, N. M. (2011) The role of zinc in Alzheimer's disease. *Int. J. Alzheimers. Dis. 2011*, 1–10.

(65) Carrillo-Mora, P., Luna, R., Colín-Barenque, L., n-Barenque, L., Carrillo-Mora, P., Luna, R., and n-Barenque, L. (2014) Amyloid beta: multiple mechanisms of toxicity and only some protective effects? *Oxid. Med. Cell. Longev. 2014*, 1–15.

(66) Wang, X., Wang, W., Li, L., Perry, G., Lee, H., and Zhu, X. (2014) Oxidative stress and mitochondrial dysfunction in Alzheimer's disease. *Biochim. Biophys. Acta 1842*, 1240–1247.

(67) Grimm, A., Friedland, K., and Eckert, A. (2015) Mitochondrial dysfunction: the missing link between aging and sporadic Alzheimer's disease. *Biogerontology 17*, 281–296.

(68) Patten, D. a, Germain, M., Kelly, M. a, and Slack, R. S. (2010) Reactive oxygen species: stuck in the middle of neurodegeneration. *J. Alzheimers. Dis. 20 Suppl 2*, S357–S367.

(69) Manczak, M. (2006) Mitochondria are a direct site of Aβ accumulation in Alzheimer's disease neurons: implications for free radical generation and oxidative damage in disease progression. *Hum. Mol. Genet. 15*, 1437–1449.

(70) Wang, X., Su, B., Siedlak, S. L., Moreira, P. I., Fujioka, H., Wang, Y., Casadesus, G., and Zhu, X. (2008) Amyloid-beta overproduction causes abnormal mitochondrial dynamics via differential modulation of mitochondrial fission/fusion proteins. *Proc. Natl. Acad. Sci. U. S. A. 105*, 19318–19323.

(71) Caspersen, C. (2005) Mitochondrial Aβ : a potential focal point for neuronal metabolic dysfunction in Alzheimer's disease. *FASEB J. 19*, 2040–2041.

(72) Johri, A., and Beal, M. F. (2012) Mitochondrial dysfunction in neurodegenerative diseases. *J. Pharmacol. Exp. Ther. 342*, 619–630.

(73) Perry, G., Cash, A. D., and Smith, M. a. (2002) Alzheimer disease and oxidative stress. *J. Biomed. Biotechnol. 2*, 120–123.

(74) Smith, D. G., Cappai, R., and Barnham, K. J. (2007) The redox chemistry of the Alzheimer's disease amyloid β peptide. *Biochim. Biophys. Acta - Biomembr. 1768*, 1976–1990.

(75) Heppner, F. L., Ransohoff, R. M., and Becher, B. (2015) Immune attack: the role of inflammation in Alzheimer disease. *Nat. Rev. Neurosci. 16*, 358–372.

(76) Minter, M. R., Taylor, J. M., and Crack, P. J. (2016) The contribution of neuroinflammation to amyloid toxicity in Alzheimer's disease. *J. Neurochem. 136*, 457–474.

(77) Mosher, K. I., and Wyss-Coray, T. (2014) Microglial dysfunction in brain aging and Alzheimer's disease. *Biochem. Pharmacol. 88*, 594–604.

(78) Streit, W. J., Mrak, R. E., and Griffin, W. S. T. (2004) Microglia and neuroinflammation: a pathological perspective. *J. Neuroinflammation 1*, 1–4.

(79) Shankar, G. M., Li, S., Mehta, T. H., Garcia-Munoz, A., Shepardson, N. E., Smith, I., Brett, F. M., Farrell, M. a, Rowan, M. J., Lemere, C. a, Regan, C. M., Walsh, D. M., Sabatini, B. L., and Selkoe, D. J. (2008) Amyloid-beta protein dimers isolated directly from Alzheimer's brains impair synaptic plasticity and memory. *Nat. Med. 14*, 837–842.

(80) Selkoe, D. J. (2008) Soluble oligomers of the amyloid β-protein impair synaptic plasticity and behavior. *Behav. Brain Res. 192*, 106–113.

(81) Ferreira, I. L., Bajouco, L. M., Mota, S. I., Auberson, Y. P., Oliveira, C. R., and Rego, a. C. (2012) Amyloid beta peptide 1-42 disturbs intracellular calcium homeostasis through activation of GluN2B-containing N-methyl-d-aspartate receptors in cortical cultures. *Cell Calcium 51*, 95–106.

(82) Verdier, Y., Zarándi, M., and Penke, B. (2004) Amyloid β-peptide interactions with neuronal and glial cell plasma membrane: Binding sites and implications for Alzheimer's disease. *J. Pept. Sci. 10*, 229–248.

(83) Spilsbury, A., Miwa, S., Attems, J., and Saretzki, G. (2015) The role of telomerase protein TERT in Alzheimer's disease and in tau-related pathology in vitro. *J. Neurosci. 35*, 1659–74.

(84) Panossian, L. ., Porter, V. ., Valenzuela, H. ., Zhu, X., Reback, E., Masterman, D., Cummings, J. ., and Effros, R. . (2003) Telomere shortening in T cells correlates with Alzheimer's disease status. *Neurobiol. Aging 24*, 77–84.

(85) Thomas, P., O' Callaghan, N. J., and Fenech, M. (2008) Telomere length in white blood cells, buccal cells and brain tissue and its variation with ageing and Alzheimer's disease. *Mech. Ageing Dev. 129*, 183–190.

(86) Mattson, M. P. (2000) Emerging neuroprotective strategies for Alzheimer's disease: dietary restriction, telomerase activation, and stem cell therapy. *Exp. Gerontol. 35*, 489–502.

(87) Lukens, J. N., Van Deerlin, V., Clark, C. M., Xie, S. X., and Johnson, F. B. (2009) Comparisons of telomere lengths in peripheral blood and cerebellum in Alzheimer's disease. *Alzheimer's Dement. 5*, 463–469.

(88) Bishop, G. M., and Robinson, S. R. (2004) Physiological roles of amyloid-beta and implications for its removal in Alzheimer's disease. *Drugs Aging 21*, 621–630.

(89) Pearson, H., and Peers, C. (2006) Physiological roles for amyloid β peptides. *J. Physiol. 575*, 5–10.

(90) Morley, J. E., Farr, S. a., Banks, W. a., Johnson, S. N., Yamada, K. a., and Xu, L. (2010) A physiological role for amyloid-β protein: enhancement of learning and memory. *J. Alzheimer's Dis. 19*, 441–449.

(91) Rajasekhar, K., Chakrabarti, M., and Govindaraju, T. (2015) Function and toxicity of amyloid beta and recent therapeutic interventions targeting amyloid beta in Alzheimer's disease. *Chem. Commun. 51*, 13434–13450.

(92) Ma, R., Xiong, N., Huang, C., Tang, Q., Hu, B., Xiang, J., and Li, G. (2009) Erythropoietin protects PC12 cells from β-amyloid25-35-induced apoptosis via PI3K/Akt signaling pathway. *Neuropharmacology 56*, 1027–1034.

(93) Maynard, C. J., Bush, A. I., Masters, C. L., Cappai, R., and Li, Q.-X. (2005) Metals and amyloid-beta in Alzheimer's disease. *Int. J. Exp. Pathol. 86*, 147–159.

(94) Atwood, C. S., Obrenovich, M. E., Liu, T., Chan, H., Perry, G., Smith, M. a., and Martins, R. N. (2003) Amyloid-β: A chameleon walking in two worlds: a review of the trophic and toxic properties of amyloid-β. *Brain Res. Rev. 43*, 1–16.

(95) Butterfield, D. A., Drake, J., Pocernich. Chava, and Castegna, A. (2001) Evidence of oxidative damage in Alzheimer ' s disease brain : central role for amyloid β -peptide. *Trends Mol. Med. 7*, 548–554.

(96) Kontush, a, Berndt, C., Weber, W., Akopyan, V., Arlt, S., Schippling, S., and Beisiegel, U. (2001) Amyloid-beta is an antioxidant for lipoproteins in cerebrospinal fluid and plasma. *Free Radic Biol Med 30*, 119–128.

(97) Gibson, G. E., Zhang, H., Sheu, K. F. R., and Park, L. C. H. (2000) Differential alterations in antioxidant capacity in cells from Alzheimer patients. *Biochim. Biophys. Acta - Mol. Basis Dis. 1502*, 319–329.

(98) Hampel, H., Schneider, L. S., Giacobini, E., Kivipelto, M., Sindi, S., Dubois, B., Broich, K., Nisticò, R., Aisen, P. S., and Lista, S. (2015) Advances in the therapy of Alzheimer's disease: targeting amyloid beta and tau and perspectives for the future. *Expert Rev. Neurother. 15*, 83–105.

(99) McGhee, D. J. M., Ritchie, C. W., Zajicek, J. P., Counsell, C. E., Rascol, O., Lefebvre, C., Eisinga, A., McDonald, S., Paul, N., Schwarzschild, M., Ascherio, A., Beal, M., Cudkowicz, M., Curhan, G., Hare, J., Folstein, M., Folstein, S., McHugh, P., Morris, J., Goetz, C., Poewe, W., Rascol, O., Sampaio, C., Stebbins, G., Counsell, C., Green, R., Schneider, L., Amato, D., Beelen, A., Wilcock, G., Swabb, E., Fowler, J., Volkow, N., Logan, J., Wang, G., MacGregor, R., Schyler, D., D, R., Karran, E., Hardy, J., Schwartz, D., Lellouch, J., Hollis, S., Campbell, F., Shults, C., Oakes, D., Kieburtz, K., Beal, M., Haas, R., Plumb, S., White, I., Horton, N., Carpenter, J., Pocock, S., McGhee, D., Parker, A., Fielding, S., Zajicek, J., and Counsell, C. (2016) A review of clinical trial designs used to detect a disease-modifying effect of drug therapy in Alzheimer's disease and Parkinson's disease. *BMC Neurol. 16*, 1-16.

(100) Goure, W. F., Krafft, G. a, Jerecic, J., and Hefti, F. (2014) Targeting the proper amyloid-beta neuronal toxins: a path forward for Alzheimer's disease immunotherapeutics. *Alzheimers. Res. Ther. 6*, 1-15.

(101) Hernandez-Rodriguez, M., Correa-Basurto, J., Martinez-Ramos, F., Padilla-Martinez, I. I., Benitez-Cardoza, C. G., Mera-Jimenez, E., and Rosales-Hernandez, M. C. (2014) Design of multi-target compounds as AChE, BACE1, and amyloid-Beta 1-42 oligomerization inhibitors: In silico and in vitro studies. *J. Alzheimer's Dis. 41*, 1073–1085.

(102) Vassar, R. (2014) BACE1 inhibitor drugs in clinical trials for Alzheimer's disease. *Alzheimers. Res. Ther. 6*, 1-14.

(103) Vassar, R., Kovacs, D. M., Yan, R., and Wong, P. C. (2009) The secretase enzyme BACE in health and Alzheimer's disease: regulation, cell Biology, function, and therapeutic potential. *J. Neurosci. 29*, 12787–12794.

(104) Wang, X.-F., Liu, D.-X., Liang, Y., Xing, L.-L., Zhao, W.-H., Qin, X.-X., Shang, D.-S., Li, B., Fang, W.-G., Cao, L., Zhao, W.-D., Chen, Y.-H., Scheltens, P., Blennow, K., Breteler, M., Strooper, B. De, Frisoni, G., Salloway, S., Attems, J., Yamaguchi, H., Saido, T., Thal, D., Greenberg, S., Gurol, M., Rosand, J., Smith, E., Deane, R., Wu, Z., Sagare, A., Davis, J., Yan, S. Du, Hamm, K., Tarasoff-Conway, J., Carare, R., Osorio, R., Glodzik, L., Butler, T., Fieremans, E., Austin, S., Santhanam, A., Katusic, Z., Kitazume, S., Tachida, Y., Kato, M., Yamaguchi, Y., Honda, T., Hashimoto, Y., Thinakaran, G., Koo, E., Zhang, Y., Thompson, R., Zhang, H., Xu, H., Walsh, D., Selkoe, D., Mattson, M., Cheng, B., Culwell, A., Esch, F., Lieberburg, I., Rydel, R., Ring, S., Weyer, S., Kilian, S., Waldron, E., Pietrzik, C., Filippov, M., Turk, V., Stoka, V., Turk, D., Gauthier, S., Kaur, G., Mi, W., Tizon, B., Levy, E., Hansson, S., Andreasson, U., Wall, M., Skoog, I., Andreasen, N., Wallin, A., Bai, Y., Markham, K., Chen, F., Weerasekera, R., Watts, J., Horne, P., Sastre, M., Calero, M., Pawlik, M., Mathews, P., Kumar, A., Danilov, V., Selenica, M., Wang, X., Ostergaard-Pedersen, L., Westlind-Danielsson, A., Grubb, A., Tizon, B., Ribe, E., Mi, W., Troy, C., Levy, E., Liu, Y., Chu, A., Chakroun, I., Islam, U., Blais, A., Yamada, T., Mukaiyama, I., Miyake, N., Igari, J., Shen, C., Chen, Y., Liu, H., Zhang, K., Zhang, T., Lin, A., Tong, Y., Zhou, W., Fung, V., Christensen, M., Qing, H., Sun, X., Cai, H., Wang, Y., McCarthy, D., Wen, H., Borchelt, D., Price, D., Strooper, B. De, Farzan, M., Schnitzler, C., Vasilieva, N., Leung, D., Choe, H., Qing, H., Zhou, W., Christensen, M., Sun, X., Tong, Y., Song, W., Koh, Y., Arnim, C. Von, Hyman, B., Tanzi, R., Tesco, G., Jorissen, E., Prox, J., Bernreuther, C., Weber, S., Schwanbeck, R., Serneels, L., Kuhn, P., Wang, H., Dislich, B., Colombo, A., Zeitschel, U., Ellwart, J., Lee, H., Shin, H., Park, S., Kim, H., Lee, W., Rhim, B., Peng, Y., Hu, Y., Xu, S., Feng, N., Wang, L., Wang, X., Zhao, Y., Calon, F., Julien, C., Winkler, J., Petasis, N., Lukiw, W., Wolf, B., Wertkin, A., Jolly, Y., Yasuda, R., Wolfe, B., Konrad, R., Deng, A., Irizarry, M., Nitsch, R., Growdon, J., Rebeck, G., Lukasiuk, K., Pirttila, T., Pitkanen, A., Palsdottir, A., Snorradottir, A., Thorsteinsson, L., Butler, J., Sharif, U., Ali, M., McKibbin, M., Thompson, J., Gale, R., Sant'Anna, R., Navarro, S., Ventura, S., Paraoan, L., Foguel, D., Kaeser, S., Herzig, M., Coomaraswamy, J., Kilger, E., Selenica, M., Winkler, D., Mi, W., Pawlik, M., Sastre, M., Jung, S., Radvinsky, D., Klein, A., Goodman, Y., Mattson, M., Smith-Swintosky, V., Pettigrew, L., Craddock, S., Culwell, A., Rydel, R., Mattson, M., Martinez-Vargas, M., Soto-Nunez, M., Tabla-Ramon, E., Solis, B., Gonzalez-Rivera, R., Perez-Arredondo, A., Pawlik, M., Sastre, M., Calero, M., Mathews, P., Schmidt, S., Nixon, R., Sun, B., Zhou, Y., Halabisky, B., Lo, I., Cho, S., Mueller-Steiner, S., Vassar, R., Bennett, B., Babu-Khan, S., Kahn, S., Mendiaz, E., Denis, P., Yan, R., Vassar, R., Tamagno, E., Guglielmotto, M., Monteleone, D., Vercelli, A., Tabaton, M., Gong, B., Pan, Y., Vempati, P., Zhao, W., Knable, L., Ho, L., Singh, A., and Pati, U. (2016) Cystatin c shifts APP processing from Amyloid-β production towards non-amyloidgenic pathway in brain endothelial cells. *PLoS One 11*, 1–16.

(105) Hoey, S. E., Buonocore, F., Cox, C. J., Hammond, V. J., Perkinton, M. S., and Williams, R. J. (2013) AMPA receptor activation promotes non-amyloidogenic amyloid precursor protein processing and suppresses neuronal amyloid-β production. *PLoS One 8*, 1-11.

(106) Bieschke, J., Herbst, M., Wiglenda, T., Friedrich, R. P., Boeddrich, A., Schiele, F., Kleckers, D., Lopez del Amo, J. M., Grüning, B. a, Wang, Q., Schmidt, M. R., Lurz, R., Anwyl, R., Schnoegl, S., Fändrich, M., Frank, R. F., Reif, B., Günther, S., Walsh, D. M., and Wanker, E. E. (2011) Small-molecule conversion of toxic oligomers to nontoxic β-sheet–rich amyloid fibrils. *Nat. Chem. Biol. 8*, 93–101.

(107) Mohamed, T., and P.N. Rao, P. (2011) Alzheimer's disease: emerging trends in small molecule therapies. *Curr. Med. Chem. 18*, 4299–4320.

(108) Churches, Q. I., Caine, J., Cavanagh, K., Epa, V. C., Waddington, L., Tranberg, C. E., Meyer, A. G., Varghese, J. N., Streltsov, V., and Duggan, P. J. (2014) Naturally occurring polyphenolic inhibitors of amyloid beta aggregation. *Bioorganic Med. Chem. Lett. 24*, 3108–3112.

(109) Frid, P., Anisimov, S. V., and Popovic, N. (2007) Congo red and protein aggregation in neurodegenerative diseases. *Brain Res. Rev. 53*, 135–160.

(110) ManKatryna Cisek, Grace L. Cooper, Carol J. Huseby, and J. K. (2014) Structure and mechanism of action of tau aggregation inhibitors. *Curr. Alzheimer Res. 11*, 997–1003.

(111) Yang, F., Lim, G. P., Begum, A. N., Ubeda, O. J., Simmons, M. R., Ambegaokar, S. S., Chen, P., Kayed, R., Glabe, C. G., Frautschy, S. a., and Cole, G. M. (2005) Curcumin inhibits formation of amyloid Beta oligomers and fibrils, binds plaques, and reduces amyloid in vivo. *J. Biol. Chem. 280*, 5892–5901.

(112) Landau, M., Sawaya, M. R., Faull, K. F., Laganowsky, A., Jiang, L., Sievers, S. a., Liu, J., Barrio, J. R., and Eisenberg, D. (2011) Towards a pharmacophore for amyloid. *PLoS Biol. 9*, 25–38.

(113) Feng, Y., Yang, S. G., Du, X. T., Zhang, X., Sun, X. X., Zhao, M., Sun, G. Y., and Liu, R. T. (2009) Ellagic acid promotes Aβ42 fibrillization and inhibits Aβ42-induced neurotoxicity. *Biochem. Biophys. Res. Commun. 390*, 1250–1254.

(114) Planchard, M. S., Samel, M. a., Kumar, A., and Rangachari, V. (2012) The natural product betulinic acid rapidly promotes amyloid-β fibril formation at the expense of soluble oligomers. *ACS Chem. Neurosci. 3*, 900–908.

(115) Wisniewski, T., and Goñi, F. (2014) Immunotherapy for Alzheimer's disease. *Biochem. Pharmacol. 88*, 499–507.

(116) Gelinas, D. S., DaSilva, K., Fenili, D., St George-Hyslop, P., and McLaurin, J. (2004) Immunotherapy for Alzheimer's disease. *Proc. Natl. Acad. Sci. U. S. A. 101*, 14657–14662.

(117) Tayeb, H. O., Murray, E. D., Price, B. H., and Tarazi, F. I. (2013) Bapineuzumab and solanezumab for Alzheimer's disease: is the "amyloid cascade hypothesis" still alive? *Expert Opin. Biol. Ther. 13*, 1075–1084.

(118) Cuajungco, M. P., Fagét, K. Y., Huang, X., Tanzi, R. E., and Bush, A. I. (2006) Metal chelation as a potential therapy for Alzheimer's disease. *Ann. N. Y. Acad. Sci. 920*, 292–304.

(119) Cherny, R. a., Atwood, C. S., Xilinas, M. E., Gray, D. N., Jones, W. D., McLean, C. a., Barnham, K. J., Volitakis, I., Fraser, F. W., Kim, Y. S., Huang, X., Goldstein, L. E., Moir, R. D., Lim, J. T., Beyreuther, K., Zheng, H., Tanzi, R. E., Masters, C. L., and Bush, A. I. (2001) Treatment

with a copper-zinc chelator markedly and rapidly inhibits β-amyloid accumulation in Alzheimer's disease transgenic mice. *Neuron 30,* 665–676.

(120) White, A. R., Barnham, K. J., and Bush, A. I. (2006) Metal homeostasis in Alzheimer's disease. *Expert Rev. Neurother. 6,* 711–722.

(121) Francis, P. T., Palmer, a M., Snape, M., and Wilcock, G. K. (1999) The cholinergic hypothesis of Alzheimer's disease: a review of progress. *J. Neurol. Neurosurg. Psychiatry 66,* 137–147.

(122) Martorana, A., Esposito, Z., and Koch, G. (2010) Beyond the cholinergic hypothesis: do current drugs work in Alzheimer's disease? *CNS Neurosci. Ther. 16,* 235–245.

(123) Rodda, J., and Carter, J. (2012) Cholinesterase inhibitors and memantine for symptomatic treatment of dementia. *BMJ 344,* e2986–e2986.

(124) Iqbal, K., Liu, F., Gong, C.-X., and Grundke-Iqbal, I. (2010) Tau in Alzheimer disease and related tauopathies. *Curr. Alzheimer Res. 7,* 656–664.

(125) Maccioni, R. B., Farías, G., Morales, I., and Navarrete, L. (2010) The revitalized tau hypothesis on Alzheimer's disease. *Arch. Med. Res. 41,* 226–231.

(126) Giacobini, E., and Gold, G. (2013) Alzheimer disease therapy-moving from amyloid-β to tau. *Nat. Rev. Neurol. 9,* 677–686.

(127) Hooper, C., Killick, R., and Lovestone, S. (2008) The GSK3 hypothesis of Alzheimer's disease. *J. Neurochem. 104,* 1433–1439.

(128) Khan, S. S., and Bloom, G. S. (2016) Tau: the center of a signaling nexus in Alzheimer's disease. *Front. Neurosci. 10,* 1–5.

(129) Lee, H.-G., Perry, G., Moreira, P. I., Garrett, M. R., Liu, Q., Zhu, X., Takeda, A., Nunomura, A., and Smith, M. a. (2005) Tau phosphorylation in Alzheimer's disease: pathogen or protector? *Trends Mol. Med. 11,* 164–169.

(130) Schneider, a, and Mandelkow, E. (2008) Tau-based treatment strategies in neurodegenerative diseases. *Neurotherapeutics 5,* 443–457.

(131) Karakaya, T., Fußer, F., Prvulovic, D., and Hampel, H. (2012) Treatment options for tauopathies. *Curr. Treat. Options Neurol. 14,* 126–136.

(132) Ballatore, C., Brunden, K. R., Huryn, D. M., Trojanowski, J. Q., Lee, V. M.-Y., and Smith, A. B. (2012) Microtubule stabilizing agents as potential treatment for Alzheimer's disease and related neurodegenerative tauopathies. *J. Med. Chem. 55,* 8979–8996.

(133) Trojanowski, J. Q. (2013) Tau-focused therapy and tau transmission: implications for Alzheimer's disease and related tauopathies. *Mol. Neurodegener. 8,* 37.

(134) Hynd, M. R., Scott, H. L., and Dodd, P. R. (2004) Glutamate-mediated excitotoxicity and neurodegeneration in Alzheimer's disease. *Neurochem. Int. 45*, 583–595.

(135) Danysz, W., and Parsons, C. G. (2012) Alzheimer's disease, β-amyloid, glutamate, NMDA receptors and memantine - searching for the connections. *Br. J. Pharmacol. 167*, 324–352.

(136) Molinuevo, J. L., Lladó, A., and Rami, L. (2005) Memantine: targeting glutamate excitotoxicity in Alzheimer's disease and other dementias. *Am. J. Alzheimers. Dis. Other Demen. 20*, 77–85.

(137) Huang, Y.-J., Lin, C.-H., Lane, H.-Y., and Tsai, G. E. (2012) NMDA neurotransmission dysfunction in behavioral and psychological symptoms of Alzheimer's disease. *Curr. Neuropharmacol. 10*, 272–285.

(138) Geldenhuys, W. J., Malan, S. F., Bloomquist, J. R., Marchand, A. P., and Van der Schyf, C. J. (2005) Pharmacology and structure-activity relationships of bioactive polycyclic cage compounds: a focus on pentacycloundecane derivatives. *Med. Res. Rev. 25*, 21–48.

(139) Wanka, L., Iqbal, K., and Schreiner, P. R. (2013) The lipophilic bullet hits the targets: medicinal chemistry of adamantane derivatives. *Chem. Rev. 113*, 3516–3604.

(140) De Clercq, E. (2004) Antiviral drugs in current clinical use. *J. Clin. Virol. 30*, 115–133.

(141) Chen, J., and Swope, D. (2007) Pharmacotherapy for Parkinson's disease. *Pharmacother. J. Hum. 27*, 161S–173S.

(142) Suzuki, H., Saito, R., Masuda, H., Oshitani, H., Sato, M., and Sato, I. (2003) Emergence of amantadine-resistant influenza A viruses: epidemiological study. *J. Infect. Chemother. 9*, 195–200.

(143) McKeage, K. (2010) Spotlight on memantine in moderate to severe Alzheimer's disease. *Drugs aging 27*, 177–179.

(144) Mohamed, T., Yeung, J. C. K., Vasefi, M. S., Beazely, M. a, and Rao, P. P. N. (2012) Development and evaluation of multifunctional agents for potential treatment of Alzheimer's disease: application to a pyrimidine-2,4-diamine template. *Bioorg. Med. Chem. Lett. 22*, 4707–4712.

(145) Mohamed, T., Zhao, X., Habib, L. K., Yang, J., and Rao, P. P. N. (2011) Design, synthesis and structure-activity relationship (SAR) studies of 2,4-disubstituted pyrimidine derivatives: dual activity as cholinesterase and Aβ-aggregation inhibitors. *Bioorg. Med. Chem. 19*, 2269–2281.

(146) Mohamed, T., Shakeri, A., Tin, G., and Rao, P. P. N. (2016) Structure–activity relationship studies of isomeric 2,4-diaminoquinazolines on β-amyloid aggregation kinetics. *ACS Med. Chem. Lett. 7*, 502–507.

(147) Zhao, D., Chen, Y., Liu, Q., Zhao, Y., and Li, Y. (2012) Exploring the binding mechanism of thioflavin-T to the beta-amyloid peptide by blind docking method. *Sci. China Chem. 55*, 112–117.

(148) Hortschansky, P., Schroeckh, V., Christopeit, T., Zandomeneghi, G., and Fändrich, M. (2005) The aggregation kinetics of Alzheimer ' s beta-amyloid peptide is controlled by stochastic nucleation. *Protein Sci. 14*, 1753–1759.

Appendix 1: Sample NMR spectra of synthesized derivatives

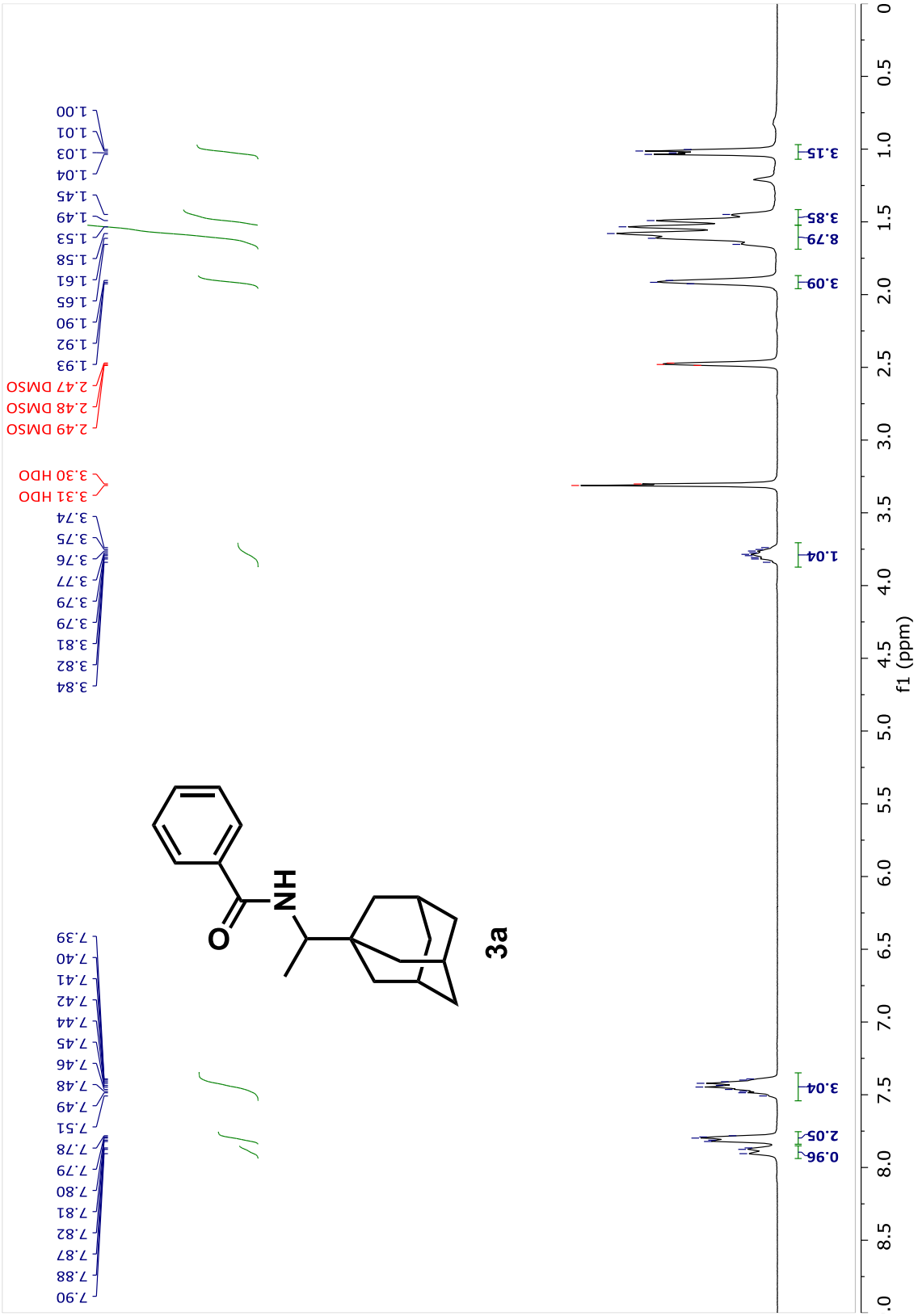

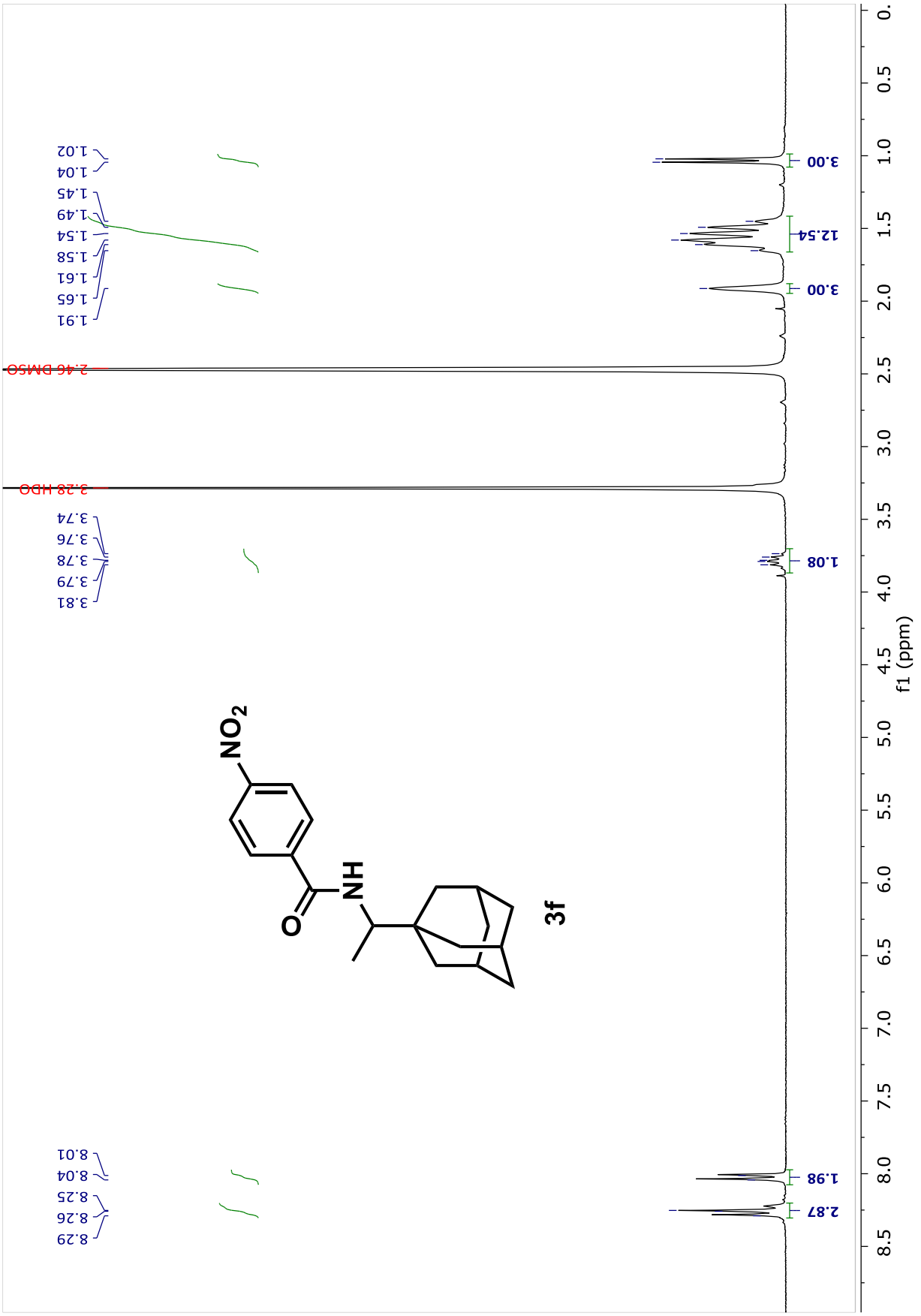
8.29
8.26
8.25
8.04
8.01
3.81
3.79
3.78
3.76
3.74
3.28 HDO
2.46 DMSO
1.91
1.65
1.61
1.58
1.54
1.49
1.45
1.04
1.02
2.87
1.98
1.08
12.54
3.00
3.00
f1 (ppm)
NO2
NH
O
3f

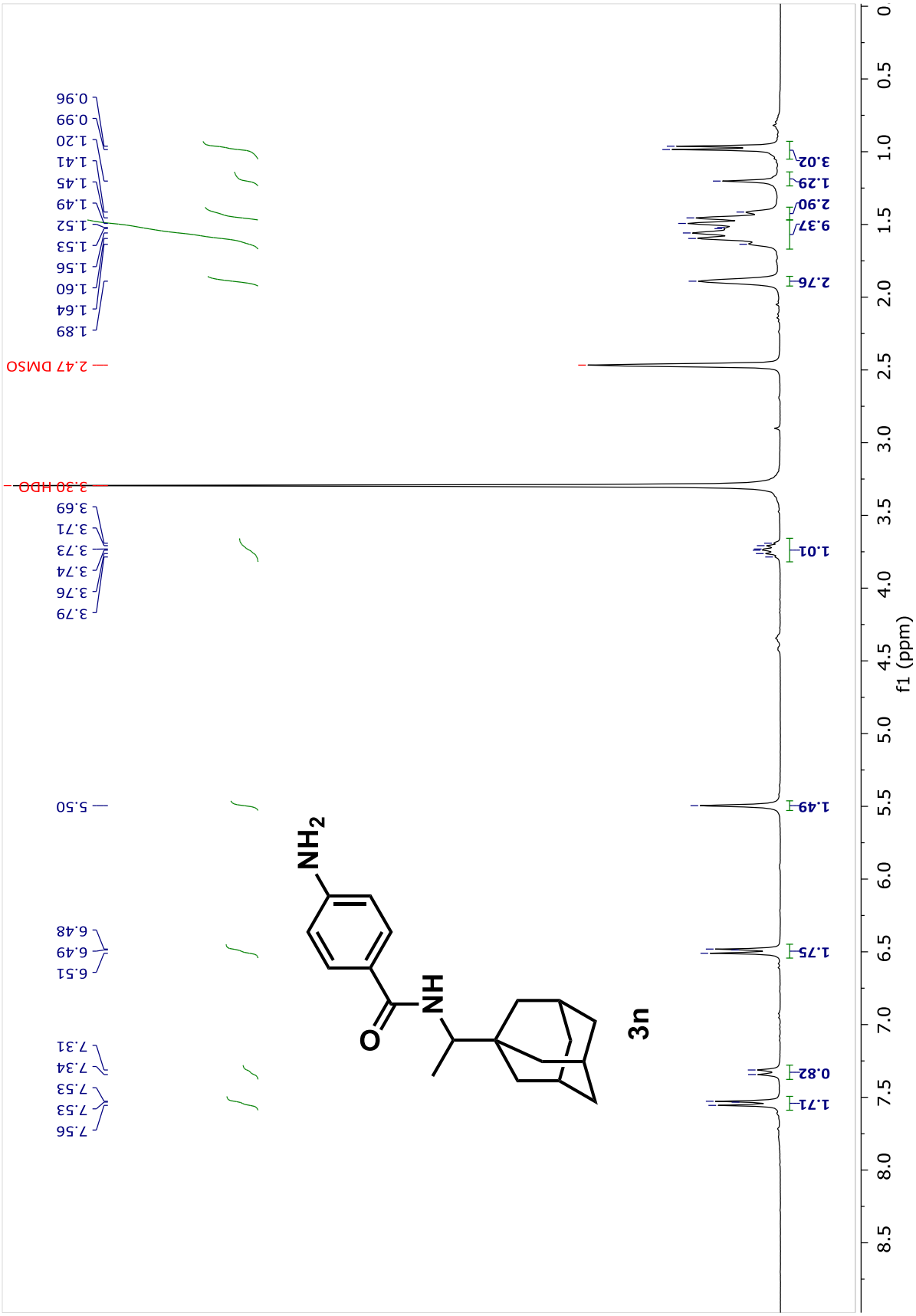
7.56
7.53
7.53
7.34
7.31
6.51
6.49
6.48
5.50
3.79
3.76
3.74
3.73
3.71
3.69
3.30 HDO
2.47 DMSO
1.89
1.64
1.60
1.56
1.53
1.52
1.49
1.45
1.41
1.20
0.99
0.96
1.71
0.82
1.75
1.49
2.76
9.37
2.90
1.29
3.02
1.01
NH2
O
NH
3n
f1 (ppm)

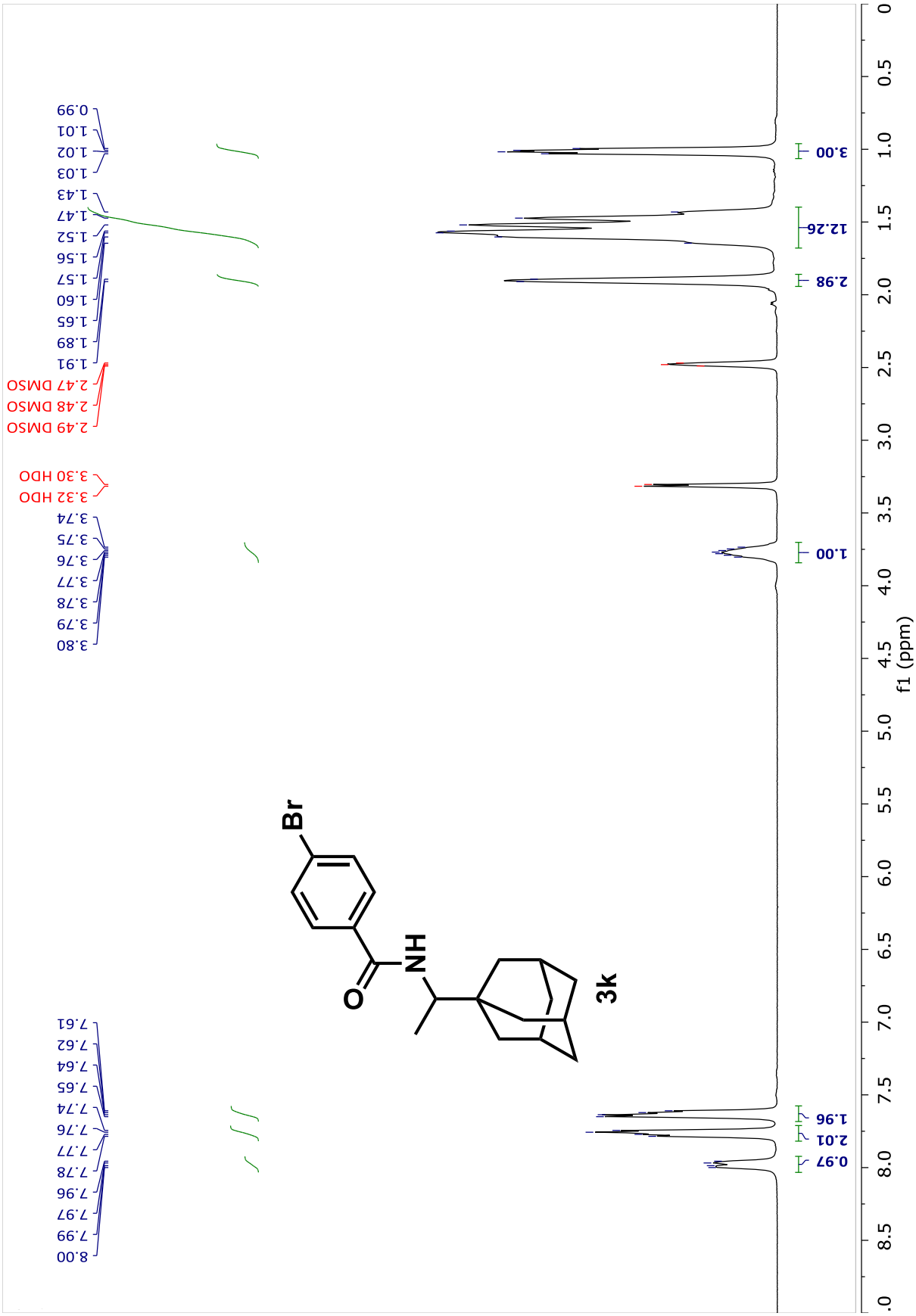
8.00
7.99
7.97
7.96
7.78
7.77
7.76
7.74
7.65
7.64
7.62
7.61
3.80
3.79
3.78
3.77
3.76
3.75
3.74
3.32 HDO
3.30 HDO
2.49 DMSO
2.48 DMSO
2.47 DMSO
1.91
1.89
1.65
1.60
1.57
1.56
1.52
1.47
1.43
1.03
1.02
1.01
0.99
0.97
2.01
1.96
1.00
12.26
3.00
2.98
Br
O
NH
3k
f1 (ppm)

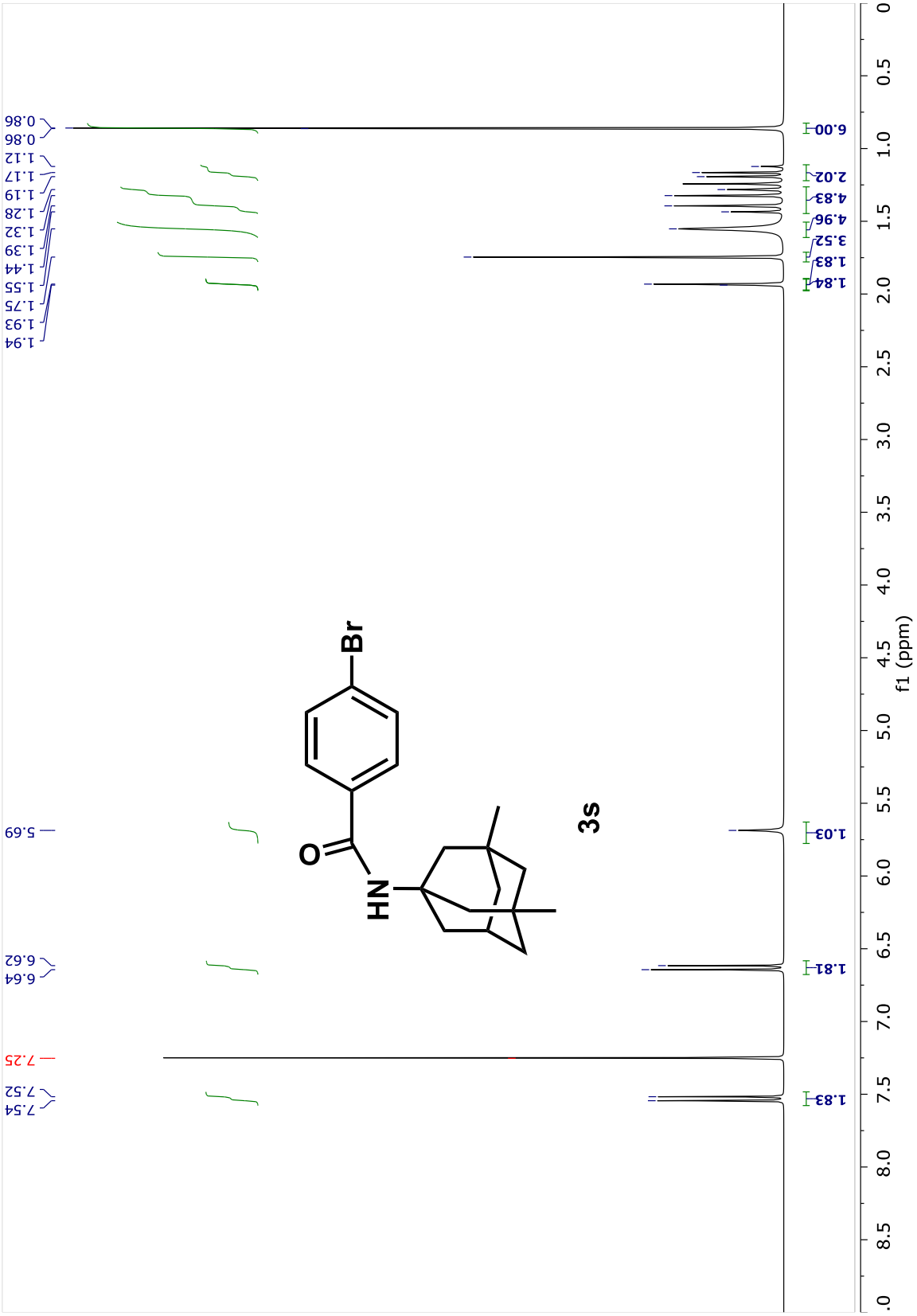
Br
O
HN
3s
f1 (ppm)

Appendix 2: ChE IC_{50} values for a selected number of derivatives.

Compound	AChE(IC_{50} (μM))	BuChE(IC_{50} (μM))
2a	**>50**	**>50**
1f	**17.9**	**>50**
2f	**15.5**	**>50**
3f	**14.5**	**>50**
2b	**15.9**	**16.3**
3n	**7.5**	**27.2**
2n	**7.4**	**>50**
Donepezil	**0.03**	**5.74**

The tested derivatives exhibited moderate inhibition for the AChE with IC_{50} values ranging from 7.4 to >50 μM. Human ChE were used and the assay was conducted using Ellman's method. Results are expressed as an average of triplicate mesuarments of three independent experiments (n = 3).